1991

# Syntheses and structural characterization of zirconium-tin and zirconium-lead binary and ternary systems

Young-Uk Kwon
*Iowa State University*

## INFORMATION TO USERS

This manuscript has been reproduced from the microfilm master. UMI films the text directly from the original or copy submitted. Thus, some thesis and dissertation copies are in typewriter face, while others may be from any type of computer printer.

**The quality of this reproduction is dependent upon the quality of the copy submitted.** Broken or indistinct print, colored or poor quality illustrations and photographs, print bleedthrough, substandard margins, and improper alignment can adversely affect reproduction.

In the unlikely event that the author did not send UMI a complete manuscript and there are missing pages, these will be noted. Also, if unauthorized copyright material had to be removed, a note will indicate the deletion.

Oversize materials (e.g., maps, drawings, charts) are reproduced by sectioning the original, beginning at the upper left-hand corner and continuing from left to right in equal sections with small overlaps. Each original is also photographed in one exposure and is included in reduced form at the back of the book.

Photographs included in the original manuscript have been reproduced xerographically in this copy. Higher quality 6" x 9" black and white photographic prints are available for any photographs or illustrations appearing in this copy for an additional charge. Contact UMI directly to order.

UMI

University Microfilms International
A Bell & Howell Information Company
300 North Zeeb Road, Ann Arbor, MI 48106-1346 USA
313/761-4700 800/521-0600

Order Number 9126209

# Syntheses and structural characterization of zirconium-tin and zirconium-lead binary and ternary systems

Kwon, Young-Uk, Ph.D.

Iowa State University, 1991

U·M·I
300 N. Zeeb Rd.
Ann Arbor, MI 48106

# Syntheses and structural characterization of zirconium-tin and zirconium-lead binary and ternary systems

by

Young-Uk Kwon

A Dissertation Submitted to the
Graduate Faculty in Partial Fulfillment of the
Requirements for the Degree of
DOCTOR OF PHILOSOPHY

Department: Chemistry
Major: Inorganic Chemistry

Approved:

Signature was redacted for privacy.

In Charge of Major Work

Signature was redacted for privacy.

For the Major Department

Signature was redacted for privacy.

For the Graduate College

Iowa State University
Ames, Iowa

1991

TABLE OF CONTENTS

# GENERAL INTRODUCTION

Zirconium and its alloys have been extensively studied in relation to nuclear reactor applications. The low absorption cross section, corrosion resistance, many aspects of the mechanical properties, and relatively low cost of zirconium make it uniquely suitable for this purpose.[1-3] Tin has been known to be an effective additive to zirconium to improve such properties of zirconium alone.[1,2]

Zircaloy-2, an alloy of zirconium with tin (1.2-1.7 wt. %), iron (0.07-0.20), chromium (0.05-0.15), nickel (0.03-0.08), nitrogen (ave. 0.008), and oxygen (ave. 0.17), is commercially produced for nuclear fuel cladding materials. Zircaloy-4, with a slightly different composition, also is used for the same purpose. One of the most popular research subjects on Zircaloy has been the study of phases present or formed after certain types of treatment on these materials.[4,5] Surprisingly, however, there are a few systematic studies done on phase formation and structure[6,7] in the zirconium-tin system which, in general, ought precede the application studies. This apparent lack of knowledge of the basic science has caused many problems in studying the applications of zirconium and Zircaloy.

Lead is an attractive alternative to tin in Zircaloy or zirconium-tin alloys because of its low absorption cross section even though it has a deleterious effect on corrosion resistance.[8] However, the studies on zirconium-lead system are very scanty and the reported phases are very ill-characterized; only a few aspects of the intermetallic phases

therein are known, yet these are very qualitative. Even a proposed phase diagram is nonexistent. It appears that the difficulties of syntheses in this system play the major role in such observations. Alloys in this system are also known as pyrophoric. One of the phases in this system, $Zr_5Pb_3$, was suggested as a neutron-breeding material in nuclear fusion and was studied for such applicability.[9] Naturally, the results of such research can be misleading because of the lack of basic knowledge of the zirconium-lead system.

Another interesting aspect of these systems is the existence of $Mn_5Si_3$-type phases.[10,11] The $Mn_5Si_3$-type structure (hexagonal; $P6_3/mcm$) is characterized by two types of manganese chains extended along the c-axis of the unit cell; the linear chain of Mn1 atoms (at 1/3, 2/3 and 2/3, 1/3 in the projection along the c-axis; Figure 1) and the chain of face-sharing $Mn_{6/2}Si_{6/2}$ regular trigonal antiprisms (or octahedra) (Figure 2). The Mn1 atoms are surrounded by silicon atoms that form distorted trigonal antiprisms.[12] The center of each trigonal antiprism of Mn2 atoms, vacant in a stoichiometric binary compound, can accommodate a third element interstitially.[13,14]

The strikingly wide range of elements that are found to form stoichiometric interstitial compounds with the $Zr_5Sb_3$ host[15,16] ($Mn_5Si_3$-type) to form $Zr_5Sb_3Z$ stoichiometries has provoked further interest in the possible interstitial compounds of these similar but electronically different host systems ($Zr_5Sn_3$ and $Zr_5Pb_3$). Thereby, one can study the effects of electron count change while maintaining the structure. The range of interstitial elements bound, the stability and physical

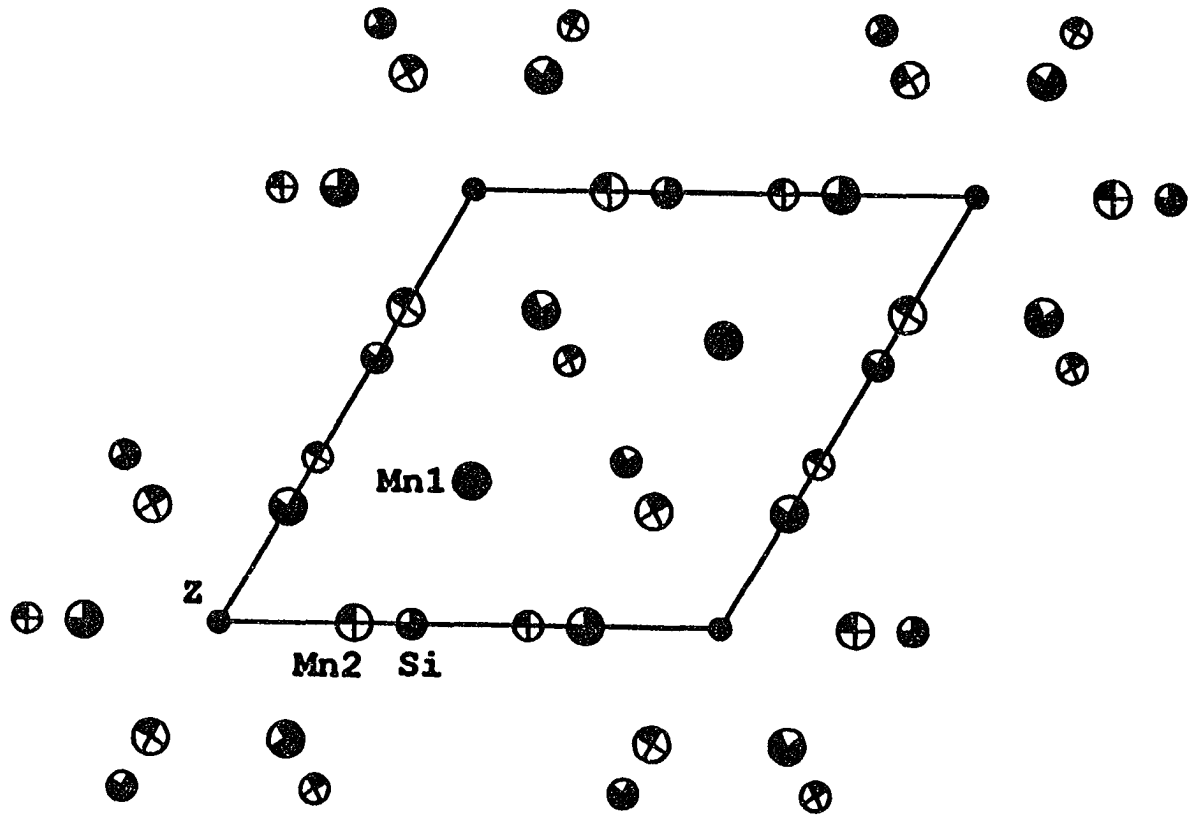


Figure 1. Projection of the stuffed-$Mn_5Si_3$ ($Ti_5Ga_4$)-type structure onto (001). Large circles, manganese; medium circles, silicon; small circles, interstitial site. Atoms are shaded to indicate the height along the c-axis; solid circles are at z = 0 and 1/2.

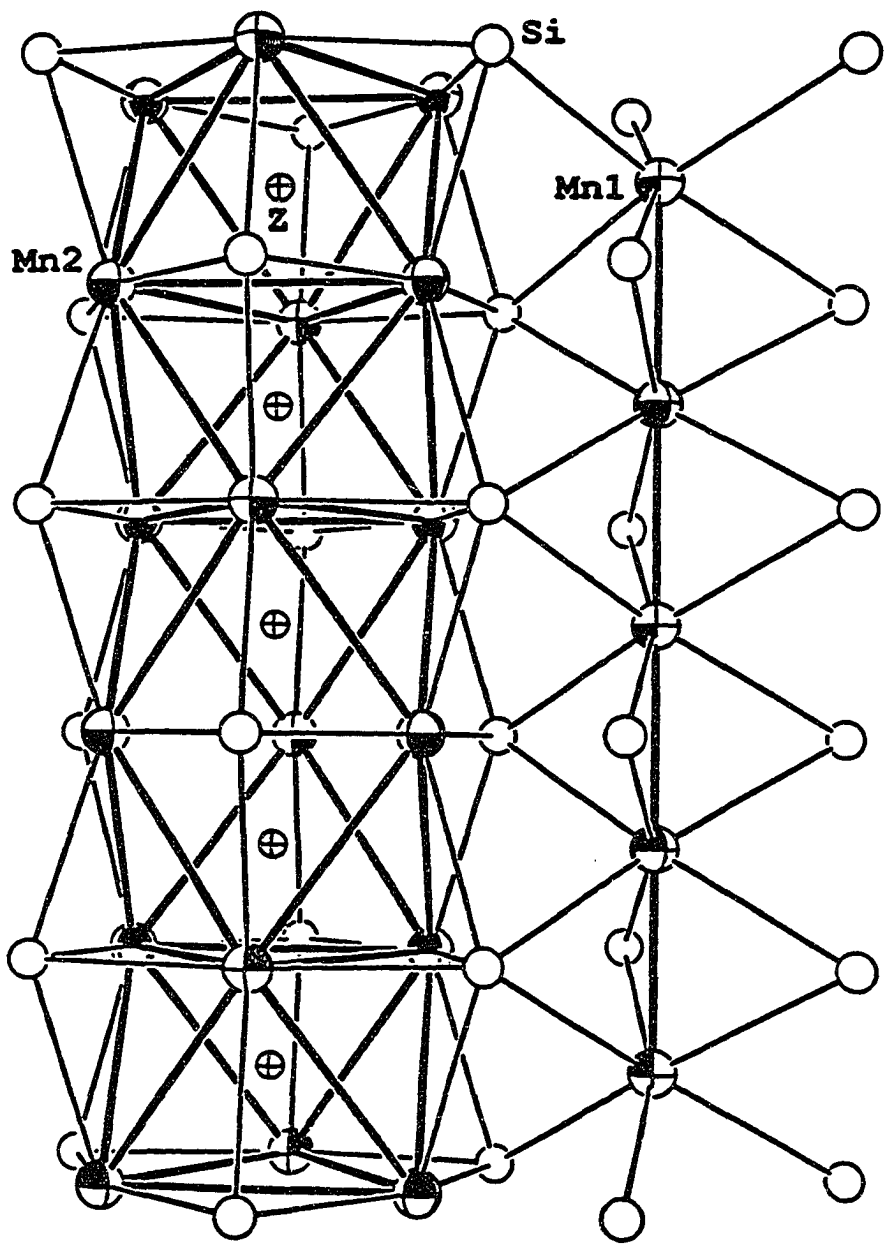


Figure 2. The confacial trigonal antiprismatic (left) and the linear (right) manganese chains viewed perpendicularly to the c-axis (5° tilt) of the stuffed-$Mn_5Si_3$ ($Ti_5Ga_4$)-type structure. The trigonal antiprism and the linear chains have a $\bar{6}$- and a 3-fold axes, respectively. Large circles, manganese; medium circles, silicon; small circles, interstitial site.

properties of so formed interstitial compounds will provide a deeper understanding of the nature of interstitial chemistry.

The study of the binary systems was indispensable to the studies of the ternary systems, especially the interstitial ones. Without a good knowledge of the host, evaluation of the effects of interstitial elements is often vague. Unfortunately, as mentioned earlier, the binary phases were not well characterized. There are controversies on the existence, structure types, or compositions for most of the phases.[17] The binary systems therefore were re-investigated for their phases and structures.

A general outline of the thesis is as follows:
Part I includes the results of the zirconium-tin binary phase studies, especially for the $Zr_5Sn_3$ and $Zr_5Sn_4$ regions - the host and its self-interstitial compound. The common features of the A15 ($Cr_3Si$-type) phases in both systems are highlighted in Part II. The majority of this research has been devoted to the systems in Part III, the interstitial chemistry of $Zr_5Sn_3$ and $Zr_5Pb_3$ hosts. Some of the binary results in zirconium-lead will be presented in Part III because of their relevance to the interstitial compounds that are discussed therein. Some of the attempted interstitial elements among the transition metals led to a different category of phases; $Zr_6Al_2Co$-type and $W_5Si_3$-type derivative phases. These results will be presented in Part IV for their syntheses and structures. The references for the General Introduction, Experimental, and Future Works sections are at the end of the thesis.

# EXPERIMENTAL

## Materials

Zirconium was obtained as reactor-grade strips with a thickness about 20 mil that were fabricated in the Ames Laboratory. Before any reactions, the strips were cut in small pieces of about 50 x 5 mm, and cleaned with a 45 % $HNO_3$, 10 % HF, and 45 % $H_2O$ solution. Because compounds, probably like $ZrF_4.xH_2O$, could remain on the surface of metal after cleaning, an immediate rinse under a flow of distilled water for at least 5 minutes was necessary to guarantee a shiny surface without any impurity spots.

If zirconium powder was necessary, small pieces of strips were hydrogenated to $ZrH_2$, ground into powder, and this powder was dehydrogenated. Zirconium pieces were placed in a clean molybdenum boat which was in turn placed in a silica jacket. The jacket was then connected to a vacuum line via a stopcock and was evacuated to $10^{-5}$ torr. Helium gas was used to purge the line for several times to make it sure that there was no oxygen or water left. After re-evacuation, hydrogen gas was then introduced through a liquid-nitrogen-cooled trap, and the silica jacket and boat were gradually heated up to 650°C. The hydrogen pressure was maintained below 1 atm.. After $H_2$ uptake was finished, the jacket was cooled and evacuated again and then transferred to a dry box, where the $ZrH_x$ (x-2) so formed was ground and passed through a 100-mesh sieve. The powder was replaced in the molybdenum

boat in the silica jacket and was heated slowly while being evacuated. When the temperature reached 700°C and the pressure $10^{-5}$ torr, the reaction was stopped and the resultant zirconium powder was tested by powder diffraction. The lattice constants so obtained agreed well with the literature values within $3\sigma$.[18]

Tin (Baker's analyzed; 99.99 %) had shiny surface upon fusion and was used as received. Lead was obtained as a electrolytic bar (99.9999 %), cold-rolled to sheet (3 mm thick), and stored in a dry box. The black oxidized surface was scraped before use.

The sources and forms of other reagents are included in corresponding parts. Most of them were used as received. Zinc was sublimed in an inverted V-shaped silica tube. One branch of the tube was heated at 1000°C to vaporize zinc, with the other at 450°C to keep the condensed zinc in liquid form. The condensed zinc formed a bar, whose diameter could be controlled by having different diameter silica tubes, when the system was cooled. The surfaces of gallium and indium were scraped before use.

## Furnaces

Resistance furnaces in various shapes, an induction furnace in Dr. H.F. Franzen's group, and an Astro 1000A graphite resistance furnace were used. These have different characteristics and the choice of a furnace depends on the needs of reactions and the materials to be used and formed.

For reactions below 1100°C, resistance furnaces were appropriate. Marshall furnaces, which have very good insulation and, therefore, reasonably small temperature gradients and good temperature stabilities, were used for most of the sintering and annealing reactions. Tubular furnaces with various resistances and diameters were also constructed by connecting two semicylindrical heating elements in series and wrapping the thus-formed tube with insulating materials. Since the insulation of a tubular furnace is generally poorer than that of a Marshall furnace, these were mainly used for low temperature reactions. Exceptions were when vertical reaction tubes were desired. By arranging more than one tubular furnace, temperature gradient and two-zone reactions could be performed in various geometries. Such an example was sublimation and condensation of zinc (see Materials). Lindberg three-zone furnaces were also used when temperature zones were needed.

Temperatures higher than 1100°C were generated by a high-temperature high vacuum furnace, an Astro 1000A graphite resistance unit that had been modified to avoid carbon contaminations and to maintain a high vacuum in the reaction chamber. The furnace was divided longitudinally into two chambers by a gas-tight alumina muffle tube (with O-rings at the ends), and the outside of this tube near the heaters was also protected by a sheet of tantalum wrapped around it. The outside, graphite element chamber was connected to a roughing pump ($\sim 10^{-3}$ torr), while the inner chamber was evacuated by a turbo-molecular pump to a working pressure of $\sim 10^{-6}$-$10^{-7}$ torr. To provide further protection, the welded tantalum reaction containers remained enclosed in a capped

tantalum canister. The tantalum sample containers remained ductile under these conditions. Temperatures were measured by a W-Re thermocouple in the inner chamber that was in contact with the bottom of the tantalum can. The surface of all the containers processed remained completely clean.

Because of its high insulation and high vacuum, quenching reactions cannot be made with this furnace, An alternative to this for quenching reactions is inductive heating. The induction furnace is capable of up to 2000°C. The red radiation of the crucible disappears about five minutes after the power is turned off which would be already an effective quenching. However, if even faster quenching was desired, the evacuated chamber was back-filled with cold nitrogen gas by dipping the end of an inlet hose into liquid nitrogen.

## Containers

Tantalum containers were primarily used. A foot-long, 3/8 in diameter tantalum tube was cut to segments of the desired lengths. The length of the tube depended on the purpose of the reaction to be done. Typical lengths were 4 and 7 cm for annealing/sintering and vapor phase transport reactions, respectively. Segmented tubes were cleaned with a solution of HF, conc. $H_2SO_4$, and $HNO_3$ (20:55:25 v/v), rinsed with water, and dried. One end of each tube was crimped and arc-welded. Later on, zirconium loss to the tantalum container was observed in some systems, and a molybdenum liner of the same length was thereafter placed inside tantalum tubes before crimping. The molybdenum is welded with the

tantalum. Containers thus prepared were pumped in a dry box. Reagents were loaded into each container and the open end of each container was crimped inside the box. The tantalum tubes were then taken out of the box, and the newly crimped ends were arc-welded. The tantalum containers were sealed in an evacuated silica jacket to protect them from air.

High temperature furnaces, both induction and graphite resistance furnaces, did not require the silica jacket since the chambers were under dynamic vacuum. A molybdenum crucible with a cap was also used for the induction heating, especially when volatilization was not appreciable; a sealed tantalum container was used otherwise.

Silica containers were also utilized for some of low temperature reactions. Pnictogens and chalcogens that have high affinity for tantalum were first reacted with zirconium, $Zr_5Sn_3$, or $Zr_5Pb_3$ in silica tubes to reduce their activities before containing them in tantalum tubes.

## Synthetic Techniques

Arc-melting and annealing, powder sintering, vapor phase transport, and flux reaction techniques were employed for most of the syntheses. These will be explained in detail in this section. The choice of the reaction technique depends primarily on the natures of the reagents and, sometimes, of the products.

**Arc-melting**

The very simple principle and direct effect of this technique have been utilized in many solid state compound syntheses. It is a very effective method in that single crystals sometimes are grown, and the possibility of unknown reactions can be very quickly tested. However, the high arc-temperature causes material loss, especially for volatile elements. In general, a lead system cannot be studied with this technique. The same was true for the interstitial systems of $Zr_5Sn_3Z$ where Z was volatile. Even in the Zr-Sn system, excess tin was required to obtain the desired composition after arc-melting. Final compositions were calculated assuming the weight losses were solely from the most volatile element. Usually, a 1 % excess of tin was enough for compositions with ≥ 60 at.% zirconium. When the tin concentration increased, the loss of tin also increased beyond this point and recalculation of the composition of the final product became inaccurate.

Weighed amounts of elements were placed on a copper hearth in an arc-furnace. The chamber was evacuated and purged with argon several times. All following operations were under an argon flow that maintained higher pressure inside the chamber. The arc was generated by touching a zirconium getter with a tungsten electrode. The getter was melted with the arc, and then the arc was moved to the reagent. This process was performed within a minute in most of the cases. To ensure homogeneity of the sample, the arc-melted sample button was turned over, and the above procedure was repeated at least three times. However, the estimated temperature of the arc, 3000°C, and that of water-cooled

copper hearth, <100°C, generated very large temperature gradient within the arc-melted button, and additional homogenization reaction (annealing) was usually required.

Sometimes, the nature of the desired phase required this annealing reaction as an essential part of the synthesis. In this case, the arc-melting reaction was only for creating an intimate mixture of the reagents.

Another problem of this arc-melting technique was the possibility of contamination. Even very small concentrations of impurities in the argon atmosphere would react with the 3000°C melted sample. The zirconium getter was used to reduce such problem. It was melted for about 20 seconds before the arc was moved to sample. After completion of reaction, the arc was moved back to and held at the zirconium getter until the red radiation of the sample was diminished. This procedure seemed to reduce oxygen contamination of samples greatly.

Arc-melting often yields disordered products. The crystal structure refinements of disordered $Zr_5Sb_3Z$ products from arc-melted samples[19] provide good evidence. A peculiar problem of gross sample inhomogeneity associated with high temperature solid solutions was encountered in studying the $Zr_5Sn_3$-$Zr_5Sn_4$ region. The inhomogeneity could only be destroyed by grinding and sintering treatments. Some crystal structure refinements of interstitial compound revealed this problem, that is, mixed or partial occupancies or, in more general term, disorder.

**Powder sintering**

The powder sintering technique was employed as a mild and, therefore, a remedial approach to a rather drastic arc-melting reaction. Most of the systems that had volatile elements were studied with this synthetic method. Since control over the material balance was easier than in the other methods, the unit cell dimensions of single phase products from this type of reaction were taken as representing the ordered stoichiometric compounds.

Reagent powders as elements or compounds were mixed stoichiometrically and pressed into a pellet. The pellet was then sealed in a tantalum tube and sintered. Typical sintering temperatures were between 1000 and 1350°C.

This technique is generally known to produce only polycrystalline products. However, in certain cases, it also produced single crystals. However, such crystal growth was recognized only afterwards and the crystal growth mechanism was not well understood. Furthermore, since the mobility of the elements were limited under most of the sintering conditions, the crystals grown were often not sufficient in size for X-ray analysis.

There are some possible sources of error in this technique, especially when a very light material was to be reacted with a very heavy one. With the typical reaction scale (300-500 mg in total weight), the error associated with balance reading (±1 mg) could reach ±5 to 10 % of the stoichiometry of the starting component. In order to

overcome such problems, light elements were first combined with heavy ones on a larger scale to form compound reagents. Intimate mixing of powders before pelleting also should help reducing errors associated with inevitable material loss during this process.

**Vapor phase transport**

In order to grow single crystals, (chemical) vapor phase transport techniques were tried with many systems, especially the interstitial phases of the $Zr_5Pb_3$ host. This technique is applicable when there is a reversible equilibrium between solid and gaseous phases, the direction of which can be controlled by a subtle change of temperature.[20] Under appropriate conditions, temperature gradients of 50-100°C should transport materials from one temperature zone to the other and often grow single crystals. However, since there are no established thermodynamic data on the chemical species that are present in a given system, a trial and error approach for the materials and reaction conditions to be used is unavoidable. $ZrCl_4$ as transporting agent generally worked better than $ZrI_4$ in crystal growth and material transport. Thermodynamics of these compounds predict that the $ZrI_4$ may work better because it can be decomposed to the elements at lower temperature, ~1300°C;[21] the former would require higher temperature to decompose it to the elements. However, in reality, $ZrCl_4$ was the only successful reagent in crystal growth as well as material transport at 800-1000°C. Moreover, a suitable condition for one system is not necessarily suitable for the others.

Reagent powder(s) and a transporting agent were sealed in a 7-cm long tantalum tube. The reagents were either pre-made phases or stoichiometric mixtures of elements and compounds. The reactions were allowed to proceed in the temperature range of 800-1000°C for 20 days or longer. Except a few cases, a complete material transport was not achieved. This might be because of wrong temperature gradient, a lack of reaction at all between gas and solid, or too short a reaction time. Regardless of these observations, single crystals were often encountered, often at the other end of tube from the bulk. Yields of the crystals were generally very low. Therefore, the single crystals thus grown sometimes did not represent the bulk products.

**Metal fluxes**

The underlying principle of this technique is analogous to crystal growth in conventional solution chemistry, that is, dissolution and concentration of a desired compound in the solvent. The solvent material may or may not be a constituent of the resulting crystals. Several restrictions apply to fluxed reactions of solid state system in this analogy: the high temperature of a fluxed reaction prevents some of the various techniques used in solution crystallization, and the choice of solvent is very limited. The solvent should form melt at the reaction temperature and must be easily separated. A typical method of separation is evaporation of the solvent after the reaction. In this regard, zinc, antimony, bismuth, and lead were the only choices. Cadmium has too high vapor pressure at 1000°C, and the other low

melting elements have too low vapor pressure at 1000°C to be practical. Dissolution of the solvent matrix in acid, i.e., dilute HCl, after reaction was finished would be an alternative.[22] If this technique works, then the choice of solvent could include tin, indium, and gallium. However, the $Zr_5(Sn,Pb)_3Z$ intermetallic compounds are generally unstable to acid, and zirconium forms $ZrOCl_2$ during such a treatment.

Antimony and bismuth were thought to compete with tin or lead in the hosts for zirconium and were not tried. Only zinc for zinc interstitial phases and lead in $Zr_5Pb_4$ syntheses were attempted. The flux media were the constituent elements of the desired compounds. Syntheses of other compounds with flux techniques would have to utilize foreign elements as the flux media, which could make the products complicated by mixed occupancies. A single crystal structure of $Zr_5Sb_3Si$ grown in zinc flux had both zinc and silicon in the interstitial site, and serves as a good example.[19]

Stoichiometric mixtures of reagents with about a 20-fold excess flux material were placed in an alumina crucible that was in turn sealed in an evacuated silica tube. The alumina crucible was located at the center of a vertically standing tubular furnace. The natural temperature gradient of the furnace evaporated and condensed the flux material on a cold spot at the bottom of the silica jacket, leaving crystals of the desired phase in the alumina crucible.

# Analysis

## Guinier powder X-ray diffraction

Guinier powder diffraction was used as the primary characterization method. This method is known to have a high sensitivity and resolving power. From a well crystallized sample, a normal exposure time reveals reflections with > 1 to 2 % of maximum intensity. Powder patterns were obtained for powdered samples fixed on a sample holder by cellophane tape with NBS silicon as an internal standard. An Enraf-Nonius Guinier camera and monochromatic Cu $K\alpha_1$ radiation were used. A Nickel filter was generally unnecessary because the monochrometer is transparent for Cu $K\alpha_1$ radiation only. Powder patterns without a nickel filter have a darker background and, therefore, probably less sensitivity but the time efficiency was greatly enhanced.

The line positions in the powder pattern were calibrated with the known $2\theta$ values of the standard silicon lines. The location of the index line of the film reader on a line in a powder pattern was critical for the accuracy as well as the precision of the lattice parameters calculated. Reading films with the marker at the peak maxima, to the best approximation, yielded the smallest standard deviations and better consistency among different samples of a phase. Previously, placement of the marker at the sharp edge on the right side of a line was a general practice. However, sample lines were sometimes broad, and this caused deviations of the lattice parameters by up to 0.01 Å and larger standard deviations by a factor of 1.5 to 2 compared with the other way.

The calibrated 2θ values of the lines were assigned indices, and lattice parameters were calculated with a least-squares method. In most of the cases, indexing was carried out by matching the 2θ values with those calculated for an assumed crystal structure and lattice parameters.[23] Trial and error methods with the TREOR program[24] were also utilized in indexing some of the superstructures.

**Rietveld powder pattern analysis**

Powder diffractograms for Rietveld refinements[25] were recorded with Dr. H. F. Franzen's Rigaku θ-θ diffractometer. Nickel-filtered Cu Kα radiation was used. The radiation source and detector move and the powder sample is held horizontally throughout the recording. Maximum scan time per step and minimum step size in the 2θ range of 10-90° were the conditions for data recordings. The diffractograms were recorded as numerical intensities for each step of 2θ and were utilized in Rietveld refinements.

An assumed structure type and atom positions were used in the starting models. A Pearson-VII type function was used for the peak profile. The $K\alpha_1/K\alpha_2$ intensity ratio was fixed at 2.0 in the refinements. The refinement generally requires an intuitive approach at the beginning. Background parameters and scale factors were estimated from inspection of the peak intensities and distributions. Variables included 3 or 4 polynomial parameters for background, the scale factor, the shift of zero point, the overall thermal parameter, lattice

parameters, parameters for peak profile, positional and isotropic thermal parameters of the atoms, and multiplicities.

**Single crystal X-ray diffraction**

Candidate single crystals were mounted in thin-wall glass capillaries or on glass fibers. The materials in general were air stable for days and therefore were handled in air. The vapor phase transport reaction products were handled in a crystal-mounting dry box.

Crystals in glass capillaries were fixed with grease. Glass fibers were used when the crystals were too small to be handled in a dry box with gloves. The latter crystals were dipped in n-butylacetate in a watch glass under a microscope. The solvent is moderately volatile and dissolves many types of glue, and most importantly, does not react with the samples. A crystal selected, and sometimes cut, under the solvent was moved to an edge of the watch glass. A glass fiber with glue was wet with the solvent and then the crystal was picked with the fiber immediately. The solvent evaporated within a minute leaving the crystal fixed at the end of the fiber. If crystal re-orientation on the fiber was desired, the sharp edge of a scalpel was wet with the solvent, and this used to dissolve the glue around the crystal. The crystal then could be moved or oriented and eventually re-fixed.

Oscillation and Weissenberg techniques were utilized to select good single crystals. Single crystals thus selected were mounted on a four-circle diffractometer, and data collections were made. Rigaku AFC6R,

CAD4, DATEX, or Syntex $P2_1$ diffractometers were used. The former two have accompanying softwares for structure refinements, TEXSAN[26] and SDP[27], respectively. The data from the last two were processed and refined with the CHES package that consists of programs for block/full matrix refinements (ALLS),[28] Fourier series calculations (FOUR),[29] and empirical absorption correction (ABSN).[30] The TEXSAN and SDP construct orientation matrices with reflections found from random search while with the CHES reflections were chosen from rotation photographs at various angle settings. The lattice types and parameters so obtained were inspected for their standard deviations before proceeding to data collection. Psi-scans for empirical absorption corrections followed data collection.

The reflection data thus obtained were processed with Lorentz-polarization corrections, a decay correction, and an empirical absorption correction using psi-scan data. Observed data for $I/\sigma_I>3$ and $F/\sigma_F>6$ were averaged in the proper Laue group (or point group in the case of a noncentrosymmetric space group).

Starting models were built by direct methods in SHELXS-86[31] or from isomorphous examples. Least-squares, full matrix refinements were performed. The structure factors were calculated using neutral atom scattering factors with anomalous dispersions for heavy atoms (Z>10).[32] Refinements included the scale factor, positional and anisotropic thermal parameters of atoms, their multiplicities, and a secondary extinction coefficient if applicable. Multiplicity refinements were sometimes replaced by refinements of the proportions of two atoms at a

site such that the site was fully occupied by these two atoms. A numerical absorption correction (DIFABS)[33] was applied when the empirical absorption correction resulted in an unacceptable refinement.

**Electron microscopy and microprobe analysis**

A JEOL JSM-840 scanning electron microscope and a KEVEX EDX system were used for elemental analyses. Since a quantitative EDX analysis needs a flat and smooth surface on the sample, only arc-melted samples that had been polished were suitable for the purpose. Sintered samples have pores, and the surface cannot be polished. An arc-melted button, annealed or as-cast, was broken, and a piece of the sample that had a flat face was fixed in a ~1 cm long copper tube with epoxy. The sample surface was then polished with series of sandpapers. The final polishing was, in general, done with ash on a cloth. However, some samples were so ductile that fine leather had to replace the ash in the final polish. The polished sample surface was on the same level as the end of the copper tube holder. Epoxy between these was covered by silver paste to conduct electricity.

Samples were inspected in the compositional (back scattering) and topological modes to determine where to look for elemental analyses. The known bulk compositions were taken for standards to reduce the matrix effect in the analyses. However, there were cases in which an estimation of the bulk composition was impossible, as in the zirconium-lead system, and the pure elements were used for standards.

# PART I. THE ZIRCONIUM-TIN SYSTEM; WITH PARTICULAR ATTENTION TO THE $Zr_5Sn_3$-$Zr_5Sn_4$ REGION AND $Zr_4Sn$

# THE ZIRCONIUM-TIN SYSTEM; WITH PARTICULAR ATTENTION TO THE $Zr_5Sn_3$-$Zr_5Sn_4$ REGION AND $Zr_4Sn$[1]

Young-Uk Kwon and John D. Corbett

From the Department of Chemistry,

Iowa State University, Ames, IA 50011

Published in Chemistry of Materials 1990, 2, 27.

## ABSTRACT

The stoichiometric phases $Zr_5Sn_3$ and $Zr_5Sn_4$ (both $P6_3/mcm$, a=8.4560(7), c=5.779(1) Å and a=8.7656(7), c=5.937(1) Å, respectively) are obtained in high yield from powder sintering reactions of Zr and $ZrSn_2$ at 1000°C. Arc-melted samples over the same composition range give generally complex and diffuse Guinier powder patterns indicative of continuous distributions of compositions between the maximum melting $\sim Zr_5Sn_{3.3}$ ($Zr_5Sn_3$'') and either $Zr_5Sn_3$ or $\sim Zr_5Sn_4$. The arc-melted samples do not improve significantly on annealing at 1000-1100°C, although the line phases are recovered if the samples are first ground and pelleted. We propose a phase diagram for this region in which the limiting phase fields $Zr_5Sn_3$ and $Zr_5Sn_4$ merge at high temperature and exhibit a common melting maximum. The overall behavior doubtlessly derives from the close structural relationship between $Zr_5Sn_3$ and $Zr_5Sn_4$, the latter ($Ti_5Ga_4$-type) being an interstitial tin derivative of the former ($Mn_5Si_3$-type). The structure of a single crystal that grew from arc-melted $Zr_5Sn_3$ was shown to have the intermediate composition $Zr_5Sn_{3.18}$, consistent with the proposed relationships and structures (a=8.5036(9), c=5.820(1) Å, $R/R_w$ = 1.7/2.0 %). The zirconium-richest compound in this system is a line phase with a composition between $Zr_{4.0}Sn$ and $Zr_{4.1}Sn$. The compound shows weak superstructure reflections that require a doubled cell (a=11.252(1) Å) and a more complex structure than the assigned A15-type. $Zr_4Sn$ slowly decomposes to α-Zr(Sn) and $Zr_5Sn_3$ at 820°C.

# INTRODUCTION

The zirconium-rich region of the system zirconium-tin is important because of, among others, the utility of Zircaloy as fuel cladding in pressurized water reactors.[2] Nonetheless, the Zr-Sn phase diagram summary published in 1983 by Abriata, Bolcich, and Arias[3] was listed as provisional because the compositions, even the existence, of some binary phases were in doubt. The most conflicting results concerned the very questionable "$Zr_5Sn_3$", a compound that is particularly important relative to our subsequent studies of the extensive interstitial chemistry that is exhibited by this and structurally related compounds.[4-6] Clarification of the system in the region around $Zr_5Sn_3$ has therefore been the cornerstone of our re-examination of the compositions, structures and phase relationships of binary compounds in the Zr-Sn system.

The principal source of information on the overall phase relationships for Zr-Sn is the 1953 study by McPherson and Hansen,[7] who employed mainly micrographic analysis supplemented by thermal analysis and X-ray diffraction on both as-cast and annealed samples. Westinghouse "Grade 3" crystal bar zirconium was used to prepare most of the compositions of concern here, and the authors several times noted the presence of impurity phases therefrom in their products. Their study encountered unusual experimental difficulties with samples in the neighborhood of $Zr_5Sn_3$, in part because they found these to be exceedingly unstable toward air and/or moisture, such that freshly

polished surfaces began to discolor in a matter of minutes and whole ingots disintegrated to powder in weeks. Notwithstanding, they deduced that a composition near $Zr_5Sn_{3.37}$ (40 a/o Sn) melted congruently at about 1988°C, while as-cast samples closer to the ideal composition $Zr_5Sn_3$ also contained the eutectic with β-Zr. Although the former composition is close to that of $Zr_3Sn_2$, the compound was instead described as $Zr_5Sn_{3.4}$ with the $Mn_5Si_3$ structure based on unpublished work by Pietrokowsky.[8] At about the same time, Nowotny and Schachner[9] reported that a phase with a composition in the range $Zr_5Sn_{2.5}$-$Zr_5Sn_{3.0}$ and with a possibly related structure was formed in powder sintering reactions. However, this result has been subsequently discounted because of the presence of 3.3 a/o C, N and O impurities in their zirconium and the effects that interstitial atoms are known or suspected to have on the stability of many phases with the $Mn_5Si_3$-type structure (Nowotny phases[10]).

A different conclusion was reached by Gran and Andersson,[11] who used X-ray powder and single crystal diffraction to study comparable compositions after the high purity elements had been arc-melted and then annealed at 900°C for two months. They reported that the composition $Zr_5Sn_{2.5}$ gave a single phase with the $Mn_5Si_3$ structure, as verified by single crystal X-ray diffraction. This they designated as $Zr_5Sn_3'$ since the lines of a second, isostructural phase appeared in the pattern close to those of the first when the tin content was increased to that of $Zr_5Sn_{3.0}$. The latter phase had larger lattice constants and was labeled $Zr_5Sn_3''$. The latter plus a compound they called ZrSn (possibly $Zr_5Sn_4$)

were both obtained at the composition $Zr_5Sn_{3.5}$. The presence of an apparent two-phase region $Zr_5Sn_3'$-$Zr_5Sn_3''$ has contributed obvious difficulties to the description of the phase relationships,[12] and the most recent assessment[3] omitted the results of this investigation with the speculation that the effects arose from sample inhomogeneities.

Our efforts have focussed particularly on clarifying this "$Zr_5Sn_3$" region. The investigation has also included examination of the closely-related $Zr_5Sn_4$ with a stuffed ($Ti_5Ga_4$-type) version of the $Zr_5Sn_3$ ($Mn_5Si_3$-type) structure[13] that was left out of the recent compilation because of the lack of verification and a concern about the effect of impurities.

We have also examined the composition of a phase near $Zr_4Sn$ ($Cr_3Si$-type, A15). Both $Zr_4Sn$ and $Zr_3Sn$ appear in the literature, although assignments of the latter are generally based on the ideal stoichiometry for the structure type rather than an experimental study. McPherson and Hansen[7] located this phase near 20 a/o tin by microscopy on annealed samples, although small amounts of β-Zr and $Zr_5Sn_3$ remained. A similar conclusion was reached by Luo et al.[14] but no limits were placed on the composition. On the other hand, Naik and Banerjee[15] found that a $Zr_4Sn$ stoichiometry consisted of α-zirconium and the A15 phase after annealing at 1040°C. The face-centered tetragonal cell ascribed to this phase by McPherson and Hansen (a=7.645, c=12.461 Å) has not been reported since, and all other investigators have cited the cubic A15 ($Pm\bar{3}n$) structure.

# EXPERIMENTAL

## Materials

The zirconium metal used in all experiments was reactor-grade, crystal-bar material that had principal impurities, in ppm atomic, of Fe 680, Ni 350, Hf 100 (by spark source mass spectrometry) and O 220, C 190 (by vacuum fusion). The metal was cold-rolled to sheet, cut into strips and cleaned with a solution of conc. $HNO_3$ and HF in $H_2O$ (55:25:20 v/v). Powdered zirconium was produced through a sequence of hydrogenation, grinding, and dehydrogenation treatments of the strips. Details of the handling of the zirconium materials and of the Guinier X-ray powder diffraction methods have been given previously.[16] No impurities were evident on fusion of the tin chunks employed (Baker's Analyzed: 99.99%). All powdered reactants were handled only in a glove box. The binary phases other than $Zr_5Sn_3$ and $Zr_5Sn_4$ appear to be stable in air for weeks, and no special handling precautions were taken unless there was a particular concern about contamination before analyses by such means as single crystal X-ray diffraction or energy dispersive X-ray (EDX) methods.

## Syntheses

Arc-melting, annealing, and powder sintering techniques were employed. The first was carried out under argon flow in a Centorr 5SA single-arc furnace on a water-cooled copper hearth. Zirconium was

melted first as a getter. The resultant buttons were turned over and remelted at least three times in an effort to ensure homogeneity. Tin is not very volatile above the alloys, especially those in the proximity of $Zr_5Sn_3$, the highest melting compound in the system,[3] and only 1% excess tin was necessary to obtain the desired composition with the assumption that any weight loss arose solely from tin volatilization. Annealing treatments of the arc-melted buttons were carried out in sealed Ta tubes,[17] and these were in turn jacketed within evacuated fused silica containers for treatment in resistance-heated furnaces at 1100°C and below. Induction heating of the Ta containers was employed at 1600°C and 1700°C (±~100°).

Powder sintering reactions were also utilized. Since tin is relatively soft, the compound $ZrSn_2$,[9] which can be easily ground into a powder, was employed as a reagent. Stoichiometric amounts of powdered zirconium and tin granules were loaded into a tantalum tube, this was welded, and the contents were allowed to react at 800°C for about a week. The Guinier powder pattern calculated[18] for $ZrSn_2$ according to its reported structure type and atom coordinates[19,20] accounted for the positions and intensities of all lines very well, and the lattice parameters refined from indexed data agreed well with the literature values (see Results). Intermediate compositions were then prepared from intimate mixtures of powdered Zr and $ZrSn_2$ that were manually pressed into pellets within the glove box with the aid of a 7-mm die set and subsequently sealed in Ta tubes for reaction.

## SEM studies

Photomicrographs and elemental analyses of some as-cast samples were obtained using a JEOL JSM-840 scanning electron microscope and a KEVEX EDX system. Samples were dry polished with a sequence of very fine sandpapers and then ash.

## X-ray diffraction

Powder patterns were obtained on samples mounted between pieces of cellophane tape. An Enraf-Nonius Guinier camera, Cu $K\alpha_1$ radiation ($\lambda$=1.54056 Å), and NBS (NIST) silicon as an internal standard were employed for this purpose. The known $2\theta$ values of the standard lines were fitted to a quadratic in their position on the film, and lattice constants of the sample then calculated by least-squares fit to indexed $2\theta$ values.

Single crystal X-ray diffraction analysis of a well-shaped hexagonal rod that grew from the top of an as-cast button of the nominal composition $Zr_5Sn_{3.0}$ was carried out at room temperature with the aid of a four-circle DATEX diffractometer and monochromatized Mo $K\alpha$ radiation. Programs for data averaging, absorption correction, Fourier synthesis and least-square refinement and the source of the scattering factors have been referenced previously.[21] Some details of the diffraction data collection and refinement are listed in Table 1.

The diffractometer data exhibited systematic absences of hhl (l=2n) reflections. The space group of the $Zr_5Sn_3$ ($Mn_5Si_3$) structure, $P6_3/mcm$,

Table 1. Data collection and refinement parameters for $Zr_5Sn_{3.18}$

| | |
|---|---|
| Space group | $P6_3/mcm$ (no. 193) |
| Z | 2 |
| Lattice dimensions: a, c (Å) | 8.5036(9), 5.820(1) |
| Crystal dimens., mm | 0.01 x 0.01 x 0.1 |
| 2θ (max), deg | 60 |
| Reflections in octants | ±h,k,l |
| measured | 1169[a] |
| observed | 1147 |
| independent | 248 |
| $R_{ave}$, % | 1.8 |
| $R^b$, % | 1.7 |
| $R_w{}^b$ % | 2.0 |
| Second ext. coeff ($10^{-4}$) | 7.3(5) |
| Absorption coeff μ ($cm^{-1}$, Mo Kα) | 168.0 |
| Range of transm coeff | 0.127-0.229 |
| No of parameters | 48 |
| No of variables | 17 |

[a]Systematic absences excluded

[b]$R=\Sigma||Fo| - |Fc||/\Sigma|Fo|$; $R_w=[\Sigma\omega(|Fo| - |Fc|)^2/\Sigma\omega(Fo)^2]^{1/2}$, $\omega=1/\sigma F^2$.

has the highest possible symmetry meeting those conditions and was assumed based on experience. A Fourier map computed after several cycles of least-squares refinement (R=9.1%) starting with the positional parameters of $Mn_5Si_3$ showed a residual electron density at the origin of the unit cell (the center of the zirconium octahedra that are condensed into confacial chains). A tin atom was then included at this position, and its occupancy, along with all other variables, was ultimately refined to 0.180(3), corresponding to the overall composition $Zr_5Sn_{3.18}$. The occupancies of all other atoms but Zr1 were also refined to confirm that all other positions in the host lattice were fully occupied to standard deviations of less than 0.7%. The largest residual in the final difference map computed after convergence (R=0.017, $R_w$=0.020 %) was ~0.2 e/Å$^3$ near Sn1. The refined positional and anisotropic thermal parameters and some important distances are given in Tables 2 and 3, respectively.

Table 2. Positional and thermal parameters of atoms in $Zr_5Sn_{3.18}$

| atom | x | y | z | $B_{11}$[a] | $B_{22}$ | $B_{33}$ | $B_{12}$ |
|---|---|---|---|---|---|---|---|
| Zr1 | 1/3 | 2/3 | 0 | 0.82(2) | 0.82(2) | 0.92(3) | 0.41(1) |
| Zr2 | 0.25228(8) | 0 | 1/4 | 1.67(3) | 0.84(3) | 1.73(3) | 0.42(2) |
| Sn1 | 0.60922(5) | 0 | 1/4 | 0.95(2) | 0.74(2) | 1.19(2) | 0.37(1) |
| Sn2[b] | 0 | 0 | 0 | 0.7(1) | 0.7(1) | 0.9(1) | 0.32(5) |

[a]The form of the anisotropic displacement parameter is:

$\exp[-1/4(B_{11}h^2a^{*2} + B_{22}k^2b^{*2} + B_{33}l^2c^{*2} + 2B_{12}hka^*b^*)]$.

[b]Refined occupancy = 0.181(3).

Table 3. Important bond lengths (Å) in $Zr_5Sn_{3.18}$

| | | | | | |
|---|---|---|---|---|---|
| **Intrachain** | | | | | |
| Zr1 - Zr1 | 2.910(1) | Zr1 - Sn1 | 3.001(0) | Sn1 - Sn1 | 4.417(1) |
| Zr2 - Zr2[a] | 3.716(1) | Zr2 - Sn1[a] | 2.918(0) | Sn1 - Sn2 | 3.628(0) |
| Zr2 - Zr2 | 3.615(1) | Zr2 - Sn1 | 3.139(1) | Sn2 - Sn2 | 2.910(1) |
| | | Zr2 - Sn2[b] | 2.592(1) | | |
| **Interchain** | | | | | |
| Zr1 - Zr1 | 4.910(1) | Zr2 - Sn1[c] | 3.035(1) | | |
| Zr1 - Zr2 | 3.547(1) | Sn1 - Sn1 | 3.452(1) | | |
| Zr2 - Zr2 | 5.120(1) | | | | |

[a]Normal to $\vec{c}$.

[b]Interstitial atom.

[c]Exo bond between confacial chains.

# RESULTS AND DISCUSSION

## The $Zr_4Sn$ Phase (A15-type)

Samples in this region were prepared by arc-melting followed by annealing at 1000°C for seven days; the second step is important for a respectable yield. As before,[7] we were not able to prepare samples that were free of both β-zirconium and $Zr_5Sn_3$, although these were in the best cases less than about 5% each. Products of vapor phase transport reactions (using $ZrX_4$) or fluxed reactions utilizing zinc gave other phases even when starting with $Zr_4Sn$, while sintering Zr and $ZrSn_2$ powders at 1000°-1300°C always left substantial amounts of β-Zr and $Zr_5Sn_3$. Annealing $Zr_4Sn$ at 820°C for 10 days gave significant decomposition to α-Zr and $Zr_5Sn_3$, as noted before.[13] This reaction may be a factor in the anomalously low volume fractions of product observed on decomposition of α-Zr(Sn) solutions.[3,22]

According to our studies, the composition of this phase lies between $Zr_{4.0}Sn$ and $Zr_{4.1}Sn$ and is a line phase at 1000°C judging from the lattice constant invariability. Whether the stoichiometry is structurally fixed at precisely 4:1 cannot be determined without a more definitive evaluation of the structure. Two obvious structural possibilities based on the A15 structure type are either vacancies ($Zr_3Sn_{0.75}$) or zirconium substitutions on the tin site ($Zr_3(Sn_{0.8}Zr_{0.2})$). A single crystal, diffraction analysis of $Nb_4Ge$, which has the same conflict between structure type and composition,

established that it is $Nb_3(Ge_{0.8}Nb_{0.2})$,[23] and the same seems likely for $Zr_4Sn$. The measured density of an annealed sample with an overall $Zr_4Sn$ composition that contained ~5 % $Zr_5Sn_3$ was 7.10(2) g/cm$^3$, closer to that calculated for the substitutional (7.22 g/cm$^3$) than for the (less likely) vacancy model (6.77g/cm$^3$). Additional, qualitative support for the substitutional model comes from a comparison of the two calculated[10] powder pattern intensity distributions with that estimated visually from the experimental pattern.

We also observe clear evidence for a superstructure, meaning that the real structure must be more complex. Doubling the exposure time for Guinier photographs reveals four more very weak but clear and reproducible reflections in addition to the 11 associated with the A15 cell (for $\theta < 39°$, Cu $K\alpha_1$ radiation). The pattern can be indexed with a cubic cell twice as large, viz. 11.252(1) Å vs 5.6254(7) Å for the A15 subcell.[24] A lower symmetry is thereby required. The larger cell probably arises from substitutional ordering considering the evidently fixed composition of the phase and the character of tin solutions in $\alpha$-, $\beta$-zirconium. However, our efforts to account for all of the lines and their intensities by modifying the parent structure have so far been unsuccessful. On the other hand, the reflections earlier attributed to a larger tetragonal cell[7,25] can all, with some allowance for probable uncertainties, be matched with our results plus two possible lines from $\alpha$-zirconium.

## $ZrSn_2$

A phase with a composition near ZrSn was estimated in the original study of this system following an electrolytic separation and chemical analysis.[7] A few years later, Hansen and Aderko[26] attributed this phase to $ZrSn_2$ in the $TiSi_2$ structure based on an interim study of the latter.[9] We performed some sintering reactions around the ZrSn composition and found no evidence for an equiatomic phase.

## The $Zr_5Sn_3$-$Zr_5Sn_4$ Region

Much experience has been acquired in recent years regarding $A_5B_3$ phases with the $Mn_5Si_3$ structure in which a variety of interstitial atoms may be incorporated into the center of a chain of confacial $A_{6/2}$ octahedra. Changes in the hexagonal lattice parameters are usually very sensitive, qualitative indicators of this event, including for systems like $Zr_5Sb_{3+x}$ in which more of the main-group element can serve as a self-interstitial.[4-6,16] Therefore, the formation of a partial tin interstitial in the component with the larger cell, $Zr_5Sn_3''$, seemed like a reasonable postulate regarding Gran and Andersson's report[11] that two $Mn_5Si_3$-type phases with different sets of lattice parameters were present after arc melting and annealing. This is particularly reasonable since the subsequently discovered $Zr_5Sn_4$[13] ($Ti_5Ga_4$-type) is in fact the even larger result of the full occupancy of the interstitial site in $Zr_5Sn_3$ by tin. However, the reason why apparently biphasic products had been obtained earlier was not clear.

Our effort to resolve these problems and to identify the equilibrium conditions have led to the investigation of numerous reactions of the types listed in Table 4 for compositions between $Zr_5Sn_{2.7}$ and $Zr_5Sn_4$ (33.3 and 44.4 a/o Sn). The notation of Gran and Andersson, $Zr_5Sn_3'$ and $Zr_5Sn_3''$ for the smaller and larger lattice constant components, respectively, in arc-melted products is retained for the time being. The Guinier-based lattice parameters determined for all of the line phases in the Zr-Sn system are listed in Table 5. The proposed phase relationships in Figure 1 build on those published for the other regions;[3] the new portions will be explained and justified in the following text.

The results in Table 4 show that the nature of the products depends very much on the synthetic conditions, as already implied by various reports. Appropriate powder sintering reactions for about two weeks at 1000°C produce well-defined line phases with stoichiometries $Zr_5Sn_3$ and $Zr_5Sn_4$ (to within ±0.3 a/o) and, for neighboring compositions, well established separations into these two phases or $Zr_4Sn$ (Table 4, no. 1-5). Our lattice parameters for the stoichiometric phases, Table 5, agree reasonably well with the earlier report for sintered $Zr_5Sn_3$ (a=8.445, c=5.785 Å, Debye-Scherrer data)[9] and $Zr_5Sn_4$ (a=8.759, c=5.916 Å).[13]

The arc-melting reactions with or without subsequent annealing give a variety of results. As-cast samples of compositions like $Zr_5Sn_{2.5}$ that are deficient in tin relative to $Zr_5Sn_3$ provide sharp powder

Table 4. Typical reuslts from the reaction of $Zr_5Sn_3$ compositions

| reaction | composition, | conditions[b] | | results[c] | hexagonal phase, Å[d] | |
|---|---|---|---|---|---|---|
| | $Zr_5Sn_n$[a] | | (°C, time) | | a | c |
| 1 | 2.70 | ST | 1000 2 w | $Zr_5Sn_3$ + $Zr_4Sn$ | 8.4553(7) | 5.7844(9) |
| 2 | 3.00 | ST | 1000 2 w | $Zr_5Sn_3$ | 8.4547(7) | 5.7805(9) |
| 3 | 3.00 | ST | 1100 9 d | $Zr_5Sn_3$ | 8.4572(7) | 5.778(1) |
| 4 | 3.50 | ST | 1000 2 w | $Zr_5Sn_3$ + $Zr_5Sn_4$ | | |
| 5 | 4.00 | ST | 1000 11 d | $Zr_5Sn_4$ | 8.7656(7) | 5.937(1) |
| 6 | 2.50 | AM | | $Zr_5Sn_3'$ (100%) (sharp pattern) | 8.4752(5) | 5.7897(7) |
| | | AN | 1150 10 d | $Zr_5Sn_3'$ (70%) + $Zr_4Sn$ (30%) | 8.4596(5) | 5.7740(7) |
| 7 | 2.82 | AM,AN | 1000 1 w | $Zr_5Sn_3'$ (90%) + $Zr_4Sn$ (10%) | 8.4561(6) | 5.7798(7) |
| 8 | 2.99 | AM | | $Zr_5Sn_3'$ (diffuse) + $Zr_5Sn_3''$ | (8.5074(7) | 5.8211(7))[e] |
| | | AN | 1100 6 d | $Zr_5Sn_3'$ (diffuse) + $Zr_5Sn_3''$ + $Zr_4Sn$ | | |
| 9 | 3.08 | AM,AN | 1600 4 h | $Zr_5Sn_{3.1}$[f] (sharp) | 8.488(1) | 5.806(2) |
| 10 | 3.26 | AM | | $Zr_5Sn_{3.3}$[f] (sharp pattern, "single" phase) | 8.5442(6) | 5.8440(7) |
| | | AN | 1000 15 d | $Zr_5Sn_{3.3}$ + $Zr_5Sn_3'$ (<20%) (separate and diffuse) | | |

| | | | | | | | |
|---|---|---|---|---|---|---|---|
| 11 | $3.4_5$ | AM | | | $Zr_5Sn_{\sim 3.4}$ | 8.573(1) | 5.862(1) |
| | | AN | 1000 | 11 d | $Zr_5Sn_{\sim 3.4}$ + $Zr_5Sn_4$ (very diffuse) | | |
| 12 | 3.7 | AM | | | (very diffuse) | | |
| | | AN | 1100 | 11 d | $Zr_5Sn_3'$ (~5%) + $Zr_5Sn_4$ (very diffuse) | | |
| 13 | 3.7 | AM,AN | 1300 | 4 h | $Zr_5Sn_3'$ + $Zr_5Sn_{4-x}$ (both diffuse) | | |
| 14 | 4.0 | AM | | | (very diffuse) | | |
| | | AN | 1700 | 1 h | $Zr_5Sn_{4-x}$ (sharp) + $ZrSn_2$ (~5%) | 8.7418(7) | 5.926(1) |
| 15 | 4.0 | AM,AN | 1000 | 3 d | $Zr_5Sn_4$ (sharp) + $Zr_5Sn_3$ (<5%) + $ZrSn_2$ (~5%) | | |

[a] ±~0.03 up to n=3.3.

[b] AM: arc-melting; AN: annealing; ST: sintering; °C.

[c] Notations for arc-melted products follow Gran and Andersson; $Zr_5Sn_3''$ has the larger cell, $Zr_5Sn_3' = Zr_5Sn_3$. Yields are estimated from the powder pattern intensities.

[d] Space group $P6_3/mcm$.

[e] Data for $Zr_5Sn_3''$, see text.

[f] Approximate composition based on a sharp pattern for an apparently well-defined product.

Table 5. Structure types and lattice constants of binary zirconium-tin compounds[a]

| compound | structure type | space group | lattice constants (Å) |
|---|---|---|---|
| $Zr_4Sn$ | $Cr_3Si$ (A15) | $Pm\bar{3}n$ | a=5.6254(7) |
| $Zr_5Sn_3$ | $Mn_5Si_3$ | $P6_3/mcm$ | a=8.4560(7) |
| | | | c=5.779(1) |
| $Zr_5Sn_4$ | $Ti_5Ga_4$ | $P6_3/mcm$ | a=8.7656(7) |
| | | | c=5.937(1) |
| $ZrSn_2$ | $TiSi_2$ | Fddd | a=9.577(1) |
| | | | b=5.6434(6) |
| | | | c=9.9287(9) |

[a]Room temperature data for equilibrium phases synthesized at 1000°C.

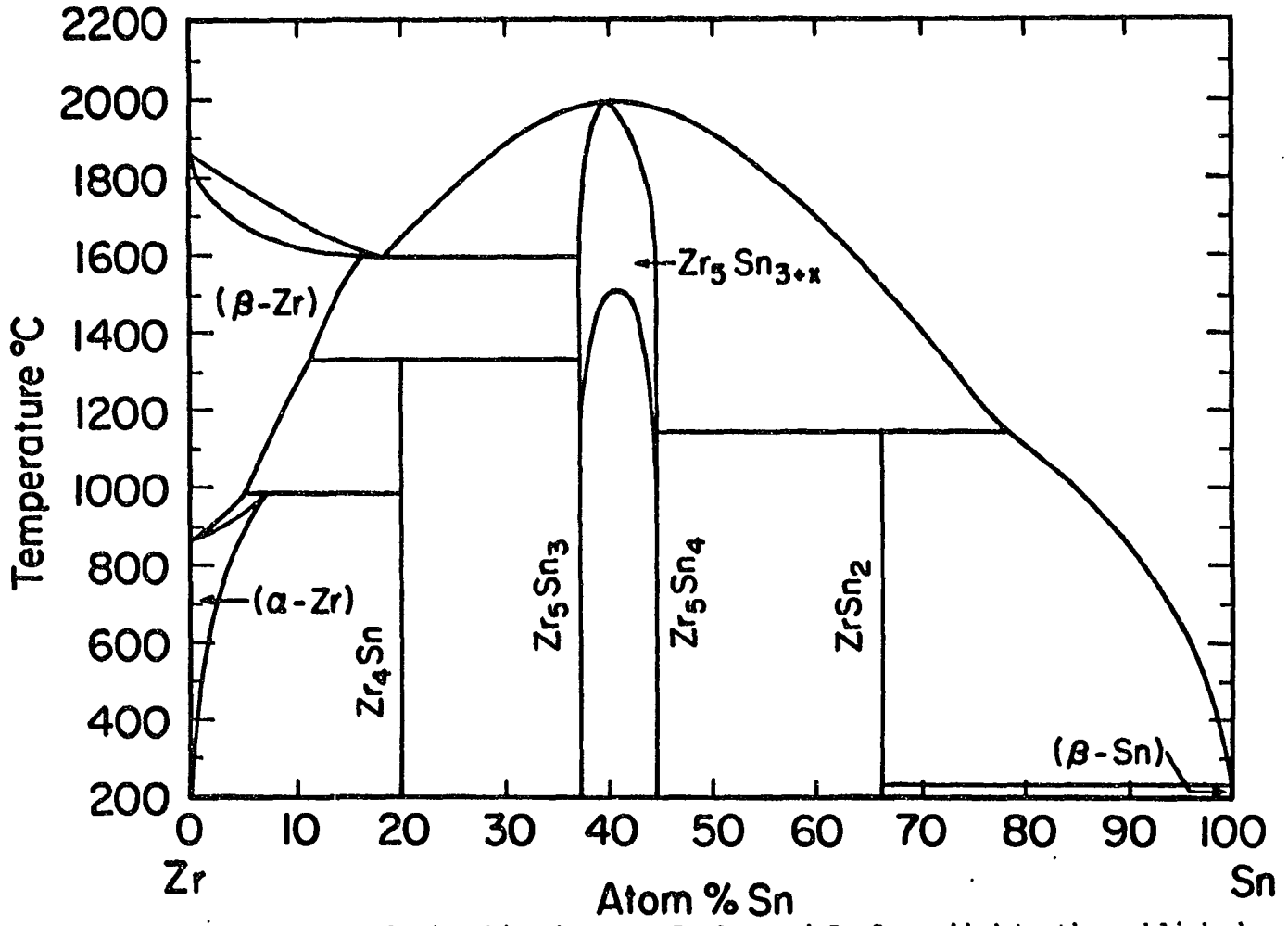


Figure 1. The proposed phase relationships between $Zr_5Sn_3$ and $Zr_5Sn_4$ added to the published, provisional diagram but with fixed point data omitted.[3] The actual solidus and liquidus boundaries in the central region have not been determined except for that of the melting maximum.

patterns. However, these show only $Zr_5Sn_3$, and $Zr_4Sn$ is seen only after annealing at 1000-1150°C. The absence of β-zirconium from the accompanying eutectic[3] in the as-cast product is unusual. However, this fixed point is reported to be near 19.1 a/o Sn and 1592°C and therefore to have substantially the same composition as the nominal $Zr_4Sn$ that forms peritectoidally near 1327°C (Figure 1).

We suggest that crystal growth following substantial transformation of the intimate β-Zr-$Zr_5Sn_3$ eutectic mixture into $Zr_4Sn$ during the rapid cooling of the button is insufficient for this product to be seen by X-rays. More significant in these observations is the fact that the dimensions of the $Zr_5Sn_3$ cell obtained from tin-poor compositions, $Zr_5Sn_{2.82}$, for example (7 in Table 4; a=8.4561(6), c=5.7798(7) Å), agree well not only with those obtained for sintered $Zr_5Sn_{3.0}$ (8.4560(7), 5.779(1) Å average) but also with data given for $Zr_5Sn_3'$ (8.46, 5.78 Å, respectively).[11] Therefore, $Zr_5Sn_3'$ will hereafter be considered to be the stoichiometric $Zr_5Sn_3$.

In contrast, the products of arc-melting reactions for the nominal composition $Zr_5Sn_3$ and beyond give more complex and frequently more diffuse powder patterns, suggesting fairly broad distributions of products. Typical line profiles for arc-melted samples across the $Zr_5Sn_3$-$Zr_5Sn_4$ region are sketched in Figure 2; the arrows mark the positions of the sharp lines for the corresponding line phases prepared by sintering. Lines in as-cast composition $Zr_5Sn_3$ at first appearance seem to be those of a mixture of $Zr_5Sn_3$ with a dominant and better defined isostructural $Zr_5Sn_3''$. A more detailed examination shows that

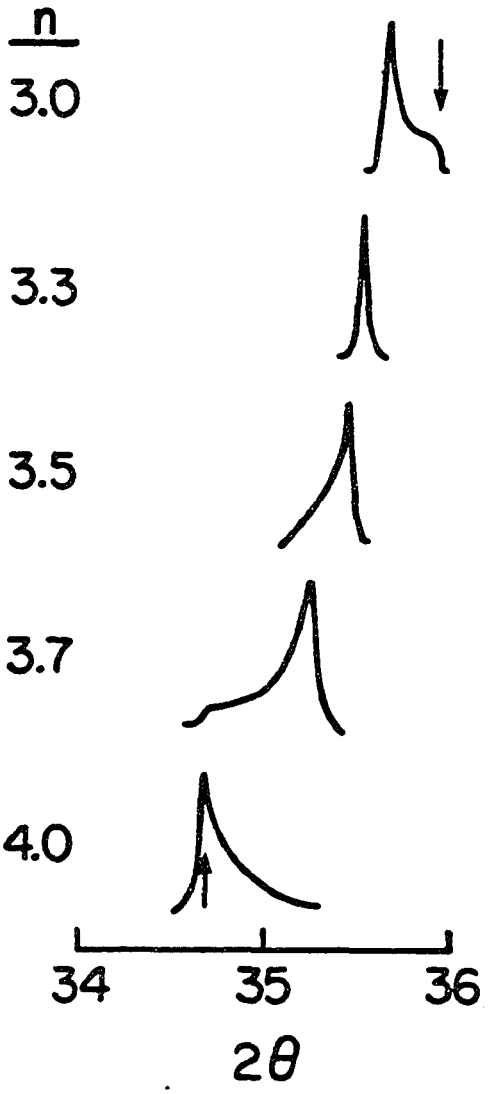


Figure 2. Line profile of (211) reflections in Guinier patterns from arc-melted samples over the composition range $Zr_5Sn_n$, $3.0 \leq n \leq 4.0$. Arrows mark the positions of the (211) line in the stoichiometric end phases obatined by powder sintering.

these actually consist of a strong and fairly sharp $Zr_5Sn_3$'' component paired on the high angle side with a weaker and quite uniform band that terminates in a relatively sharp edge at the $Zr_5Sn_3$ position. Annealing at 1000-1100°C always gives the same mixed pattern but $Zr_4Sn$ is now apparent as well. Annealing an arc-melted $Zr_5Sn_{3.08}$ composition at ~1600°C for a few hours (9 in Table 4) produces a sharp, $Zr_5Sn_3$-like pattern with slightly greater lattice constants, but we are less confident of the composition after this more drastic treatment in a tantalum container. The lattice constants for $Zr_5Sn_3$'' typically fall in the neighborhood of a=8.5074(7), c=5.8211(7) Å, in close proximity to the earlier report, 8.50 Å and 5.81 Å.[11] In contrast to the diffuse pattern obtained for $Zr_5Sn_3$, that for the arc-melted $Zr_5Sn_{3.26}$ shows only very sharp lines that reflect the presence of a single, homogeneous and well-crystallized phase (Figure 2). The expansion in the lattice constants (10 in Table 4) is approximately proportional to the amount of extra tin, a further indication that these structures contain partial tin interstitials. (A similar trend has been documented for the isotypic $Zr_5Sb_{3+x}$ system.[16]) In addition, many needle-like crystals up to 5-mm in length grow from the surface of the buttons near $Zr_5Sn_{3.26}$ during cooling in the arc-furnace, to the extent that the product sometimes resembles a bundle of needles more than a button. Annealing at 1000°C for 15 days is insufficient to attain clean phase separation from these samples, only diffuse $Zr_5Sn_3$ lines, not bands, being added.

Samples still richer in tin give progressively more diffuse patterns when prepared by arc-melting. A $Zr_5Sn_{3.45}$ composition (11 in Table 4)

shows a dominant and somewhat larger cell for $Zr_5Sn_{\sim 3.4}$ plus 30-40% as much intensity distributed in a low angle tail on each line, that is, toward the isostructural $Zr_5Sn_4$. The distribution broadens appreciably during the typical 1000°C anneal. Quenched alloys of $Zr_5Sn_{3.7}$ and $Zr_5Sn_4$ composition provide only diffuse powder lines, corresponding to a wider range of compositions among the crystallites, and only partial separation into $Zr_5Sn_3$ and $Zr_5Sn_4$ is obtained for the former after 11 days at 1100°C. Recognition of $Zr_5Sn_4$ as a new phase would be difficult under these conditions. The inhomogeneity of as-cast $Zr_5Sn_4$ is further demonstrated by the appearance of small amounts of both $Zr_5Sn_3$ and $ZrSn_2$ in the pattern after annealing at 1000°C (14 in Table 4) while a fairly sharp pattern of the substoichiometric phase plus a few lines for $ZrSn_2$ appear after a brief period at 1700°C (±~100°C).

A very contrasting result is achieved if these arc-melted buttons are simply ground, pressed into pellets, and sintered. The macroscopic inhomogeneities that seem evident in the arc-melted samples are clearly removed by the grinding process, and good equilibrium phase separation is obtained. Thus, as-cast compositions $Zr_5Sn_3$ and $Zr_5Sn_{3.5}$ produce sharp patterns of pure $Zr_5Sn_3$ plus, in the latter, $Zr_5Sn_4$ after this procedure followed by 18 days at 1000°C.

## Phase Relationships and Distributions

The foregoing observations generally reflect the presence of sufficient compositional segregation during solidification of liquid alloys in the neighborhood of $Zr_5Sn_3$ and $Zr_5Sn_4$ that homogeneity cannot

be achieved by annealing at 1000-1150°C for up to 15 days (or 900°C for two months[11]). One can construct phase relationships that are consistent with these properties. Those shown in Figure 1 build on the published, provisional Zr-Sn diagram[3] with probable relationships that can be deduced from the present study. It should be noted that none of the solidus or liquidus phase boundaries shown in the center region have been directly determined except for the congruent melting temperature and composition.

Around 1000°C only two line phases are present in the center region, $Zr_5Sn_3$ and $Zr_5Sn_4$, but as the temperature rises appreciably, both broaden toward each other. These must eventually join, and we have drawn one way this might occur considering the close structural relationship between the two phases (below). At even higher temperatures the phase breadth closes up toward the maximum melting point described in the original study,[7] $Zr_5Sn_{\sim 3.3}$ at 1988°C. (The location of this is probably uncertain by up to ±0.1 in the tin coefficient or ±0.7 a/o Sn.) The phase relationships are based particularly on the distinctive powder pattern line profiles of as-cast samples (Figure 2) and the results of annealing that so clearly reflect a distribution of cell dimensions and compositions.

The phase diagram illustrates that $Zr_5Sn_3$, a line phase at lower temperatures, does not melt congruently and thus cannot be obtained as-cast with the usual rapid cooling, as observed. Rather, the first crystals to form have a composition in the neighborhood of $Zr_5Sn_{3.3}$, leaving the remaining liquid richer in zirconium. The lattice constants

that pertain to the moderately sharp diffraction distribution seen for $Zr_5Sn_3$'' (Table 4) as well as to a single crystal studied (below) both suggest that the first macrocrystals have compositions near $Zr_5Sn_{3.2}$. These grow progressively poorer in tin as the button cools until they achieve the fully reduced $Zr_5Sn_3$ plus β-zirconium in the eutectic at ~1592°C, in accord with the powder pattern lineshapes as well as microscopy (below). Furthermore, the existence of a composition gradient within a nominal $Zr_5Sn_3$ sample means that equilibrium can be achieved only by diffusion over some distances. This cannot be accomplished in days to weeks at 1000°C but can in a few hours at 1600-1700°C where diffusion is faster, the solidus region is broad, and neighboring compositions are liquid. However, simply grinding the button to a fine powder followed by sintering of a pressed pellet at 1000°C works equally well since most of the segregation is eliminated.

The line widths in the powder patterns of quenched alloys decrease with increasing tin content and reach a minimum, corresponding to a homogeneous (metastable) phase, near $Zr_5Sn_{3.3}$. With more tin (11 in Table 4) the lines again broaden, but this time to reflect a substantial distribution of larger cells approaching $Zr_5Sn_4$ in size. As-cast products near $Zr_5Sn_{3.7}$ and $Zr_5Sn_4$ give such broad lines as to be relatively useless; annealing these near 1000°C brings about little improvement in the former while the pattern for the latter, though sharp, still indicates inhomogeneity by the presence of small amounts of both $Zr_5Sn_3$ and $ZrSn_2$. A considerable incongruity of the freezing process in the region $Zr_5Sn_{3.5}$-$Zr_5Sn_4$ is manifest.

Table 6. The intensity of $Zr_5Sn_3$'' lines relative to those of the adjoining band that ends at $Zr_5Sn_3$ in the Guinier powder patterns of as-cast buttons with the overall composition $Zr_5Sn_{3.0}$

| | location in button | | |
|---|---|---|---|
| | top | middle | bottom |
| Normal melting | 5 | 3 | 2 |
| Cooler arc | 3 | | 1.5 |
| Single melt | 10 | | 1.5[a] |
| Composition near the center of the crystallites(EDX) | $Zr_5Sn_{3.24}$ | | $Zr_5Sn_{3.14}$ |

[a] $Zr_5Sn_3$'' is more diffuse.

An SEM-EDX study of a button of overall composition $Zr_5Sn_3$ that had been sectioned vertically and polished provided further details. Of additional interest are the changes seen in the diffraction intensity distribution for the $Zr_5Sn_3''$ component relative to the $Zr_5Sn_3$ band as a function of sample location within the button, the relative intensity of the arc, and whether the button has been turned over and remelted, as is customary. These are summarized in Table 6.

Electron microscopy of the top portion showed a parallel array of well-formed blades or rods ~20-50 μm wide and with very little cracking. These were separated by narrow bands of the eutectic. The crystal size and order decreased and the amount of cracking increased downward in the button. The overall appearances were similar to those in Figs. 23 and 24 in ref. 7 except that our crystal sizes and the order were somewhat greater. Broad areas near the top and bottom of the button gave closely concordant compositions of $Zr_5Sn_{3.00}$ and $Zr_5Sn_{2.97}$ (±~0.01), respectively, when the overall composition was used for calibration. Thus, vertical composition gradients appear to be fairly small. In contrast, the center regions of the individual crystals near the top and bottom of the button were significantly higher in tin and somewhat different, $Zr_5Sn_{3.24}$ and $Zr_5Sn_{3.14}$, respectively. The data support the notion that growth of the original crystallites results in radial composition gradients down to $Zr_5Sn_3$ at their boundaries, as reflected in powder pattern line profiles.

The relative intensities of $Zr_5Sn_3''$ (~$Zr_5Sn_{\sim 3.2}$) lines and of the accompanying $Zr_5Sn_3$ band in the powder patterns of samples from

different locations and melting conditions, Table 6, are also informative regarding distributions present within samples. Either a single melt or a hotter arc serve to increase the gradients, particularly at the top of the button.

Whisker crystals often grow from the upper surface of these buttons, presumably in the last stages of solidification, and a single crystal X-ray diffraction study was carried out on a ~10 μm thick sample that grew from the top of a $Zr_5Sn_{3.0}$ composition (Tables 1-3). The lattice constants obtained with the diffractometer, a=8.5036(9), c=5.820(1) Å, are, within the usual accuracy of this method, the same as found by Guinier methods for $Zr_5Sn_3$'' at the same composition, 8.5074(7) and 5.8211(7) Å. The overall composition refinement, $Zr_5Sn_{3.18}$, also provides a reference. Although this crystal presumably grew axially rather than radially, it may still have internal gradients and thus an average composition less than that of the melting maximum. The additional tin beyond that of the host $Zr_5Sn_3$ was found in the usual interstitial site within the confacial octahedral chain.

# CONCLUSIONS

The more unusual results of this investigation - the inhomogeneity of many arc-melted samples, the ineffectiveness of annealing treatments, and the general nature of the apparent phase relationships in the $Zr_5Sn_3$-$Zr_5Sn_4$ region - can all be regarded as deriving from the close interconnection between the structures of $Zr_5Sn_3$ and $Zr_5Sn_4$. The unusual $Mn_5Si_3$-type structure of $Zr_5Sn_3$ (and many other compounds) affords a well-bonded arrangement with one particularly important feature: chains of zirconium octahedra that share opposite faces and are edge-bridged by tin, viz., $Zr_{6/2}Sn_{6/2}$. This feature adds a particular versatility to the chemistry of the compound in that additional atoms can often be bonded within each of these octahedra, tin in the case of $Zr_5Sn_4$. Although $Zr_5Sn_3$ and $Zr_5Sn_4$ are line phases at lower temperatures, it is not surprising that their close structural relationship leads to a range of nonstoichiometry (solid solution) at higher temperatures that eventually spans the region between them. The maximum melting point of this solution turns out to be about $Zr_5Sn_{3.3}$. Most of the complications arise from these last two features, as already described.

We have seen evidence of related problems in other $A_5B_3$-B systems where this structure type applies. Thus, $Zr_5Sb_{3+x}$ samples can be prepared over the range $0.0 \leq x \leq 0.4$ (but not for x=1, i.e., $Zr_5Sb_4$) by sintering near 1100°C, and this solution exhibits a maximum melting point near $Zr_5Sb_{3.2}$. In this case, $Zr_5Sb_3$ freezes incongruently to

produce $Zr_5Sb_{3.2}$ and a high-temperature polytype of $Zr_5Sb_3$, and their segregation again seems probable on the basis of annealing insufficiencies.[16] Not many other systems are known that contain both $Mn_5Si_3$- and $Ti_5Ga_4$-type members. However, the zirconium-gallium[28,29] and thorium-tin[30] systems would appear to be a likely candidates for similar melting problems.

Finally, the interstitial chemistry of these $A_5B_3$ phases is by no means limited to bonding of up to one additional B element in the host. Both $Zr_5Sb_3$ and $Zr_5Sn_3$ form extensive series of $Zr_5Sb_3Z$ and $Zr_5Sn_3Z$ phases in the same structure with interstitial heteroatoms Z.[4-6] In the case of tin, Z includes all of the elements in the fourth period between Cu and Se as well as B-O and Al-S in the second and third periods, respectively. Most of these ternary phases, the oxide included, are stoichiometric in Z when prepared by sintering and can readily be distinguished from the binaries by their lattice constants. Some novel exceptions in stoichiometry have been found in another system, $La_5Ge_3Z_x$.[31] Nonstoichiometry, B-Z exchange and related complications are often found in these ternary systems under arc-melting conditions, as might be expected.

## REFERENCES


1. The Ames Laboratory-DOE is operated for the U. S. Department of Energy by Iowa State University under Contract No. W-7405-Eng-82. This research was supported by the Office of Basic Energy Sciences, Materials Sciences Division, Washington, D. C.
2. Rahn, F. A Guide to Nuclear Power Technology; Wiley: New York, 1984.
3. Abriata, J. P.; Bolcich, J. C.; Arias, D. Bull. Alloy Phase Diagr. 1983, 4, 147.
4. Corbett, J. D.; Garcia, E.; Kwon, Y.-U.; Guloy, A. Pure and Applied Chem. 1990, 62, 103.
5. Kwon, Y.-U.; Corbett, J. D., Department of Chemistry, Iowa State University, Ames, IA, unpublished research, 1990.
6. Garcia, E.; Corbett, J. D. Inorg. Chem. 1988, 27, 2907.
7. McPherson, D. J.; Hansen, M. Trans. Am. Soc. Met. 1953, 45, 915.
8. Pietrokowsky, P., Jet Propulsion Laboratory, California Institute Technology., U.S. Army, Contract DA-04-495-ORD-18, 1952, unpublished.
9. Nowotny, H.; Schachner, H. Monatsh. Chem. 1953, 84, 169.
10. Nowotny, H.; Benesovsky, F. In "Phase Stability in Metals and Alloys", P. S. Rudman, J. Stringer, and R. I. Jaffee, Eds., McGraw-Hill: New York, 1966; p. 319.
11. Gran, G.; Andersson, S. Acta Chem. Scand. 1960, 14, 956.

12. Kubaschewski-von Goldbeck, O. In "Zirconium: Physico-Chemical Properties of Its Compounds and Alloys", Atomic Energy Review, Special Issue No. 6, Int'l Atomic Energy Agency: Vienna, 1976; p. 121.

13. Rossteutscher, W.; Schubert, K. Z. Metallkd. 1965, 56, 813.

14. Luo, H. L.; Vielhaber, E.; Corenzwit, E. Z. Physik. 1970, 230, 443.

15. Naik, U.; Banerjec, S. Trans. Indian Inst. Met. 1978, 31, 318. The abstract and the summary of this article are contradictory regarding the probable composition of the A15 phase.

16. Garcia, E.; Corbett, J. D. Inorg. Chem. 1988, 27, 2353.

17. Corbett, J. D. Inorg. Synth. 1983, 22, 15.

18. Clark, C. M.; Smith, D. K.; Johnson, G. J. "A FORTRAN IV Program for Calculating X-Ray Diffraction Patterns: Version V"; Department of Geosciences, The Pennsylvania State University, University Park (1973).

19. Laves, F.; Wallbaum, H. J. Z. Kristallogr. 1939, 101, 78.

20. Jeitschko, W. Acta Crystallogr. 1977, B33, 2347.

21. Hwu, S.-J.; Corbett, J. D.; Poeppelmeier, K. R. J. Solid State Chem. 1985, 57, 43.

22. Carpenter, G. J. C.; Ibrahim, E. I.; Watters, J. F. J. Nucl. Mater. 1981, 102, 280.

23. Rasmussen, S. E.; Hazell, R. G. Acta Crystallogr. 1979, B35, 1677.

24. The 2θ values of the superlattice reflections for $Zr_4Sn$ (Cu $K\alpha_1$) and their indices in the larger cell are as follows: 15.740°, 200; 17.580°, 210; 19.348°, 211; 29.748°, 321.

25. Powder Diffraction File, JCPDS, International Centre for Diffraction Data, Swarthmore, PA, 1979, Pattern no. 10-185.

26. Hansen, M.; Anderko, K."Constitution of Binary Alloys", 2nd ed.; McGraw-Hill: New York, 1958; p. 1219.

27. Nowotny, H.; Auer-Welsbach, H.; Bruss, J.; Kohl, A. Monatsh. Chem. 1959, 90, 15.

28. Pötzschke, M.; Schubert, K. Z. Metallkd. 1962, 53, 474.

29. Boller, H.; Parthé, E. Monatsh. Chem. 1963, 94, 25.

30. Cirafici, S.; Palenzona, A.; Manfrinetti, P. J. Less-Common Met. 1983, 90, 49.

31. Guloy, A.; Corbett, J. D., Department of Chemistry, Iowa State University, Ames, IA, unpublished research, 1990.

# PART II. THE A15 PHASES IN THE ZIRCONIUM-TIN AND ZIRCONIUM-LEAD SYSTEMS

# INTRODUCTION

Many authors have reported conflicting results for the phase at 20–25 at. % Sn in the zirconium-tin binary system. McPherson and Hansen discussed a face-centered tetragonal (a=7.645, c=12.461 Å) phase for $Zr_4Sn$ composition.[1] Tanner et al. also reported a different tetragonal phase (a=6.90, c=11.10 Å) for the same composition.[2] A similar but still different tetragonal phase was reported by Nesic et al. in 1970.[3] This phase was found in a 1.2 at. % Sn alloy and was discussed as an impurity-induced phase.

On the other hand, reports after 1960 seem to agree on the structure type of this phase as $Cr_3Si$-type (A15 phase). However, they did not agree on the composition. Gran and Andersson,[4] Rossteutscher and Schubert,[5] and Naik and Banerjee[6] reported that the A15 phase has a $Zr_3Sn$ composition whereas Luo et al. in 1970 reported a quantitative synthesis of the same phase with a $Zr_4Sn$ composition.[7] It appears that the $Zr_3Sn$ assignments were based on the structure type identified by the diffraction pattern rather than on synthetic considerations. The $Zr_4Sn$ composition seemed more likely from all of the above observations.[8] However, this point was subject to confirmation.

The phase stability was another concern in studying this system. Luo et al.[7] observed decomposition of this phase when slowly cooled from 1000°C or quenched from 800°C, while quenching from 1000°C yielded this phase quantitatively. Schubert et al. also reported this as a high temperature phase.[9] However, they did not give any details of the

sample handling. Carpenter et al.[10] reported that the volume fraction of the precipitate of this phase in zirconium-tin alloys upon low temperature aging was an order of magnitude smaller than the reported phase diagram would predict.[1,8] They attributed this observation to either a larger solubility of tin in zirconium than reported or a slow diffusion rate. Their results also could be interpreted as the decomposition of the $Zr_4Sn$ phase at low temperature. In addition, studies on Zircaloy, which contained up to 1.7 wt. % Sn, did not find this phase, in contradiction to that predicted by the reported phase diagram.[11-13] A low temperature instability of this phase was assumed. These problems were studied in the present research.

There is also a report on a A15 phase in zirconium-lead system whose composition had been tentatively determined as $Zr_5Pb$.[14] No further reports were found on this phase. Since the off-stoichiometry of this A15 phase appeared to be related to that in the Zr-Sn system, this phase was also synthesized and studied.

# EXPERIMENTAL

The detailed descriptions of the materials, synthetic techniques, and analytical methods are presented in the General Experimental section. Therefore, this section will only present some details that are pertinent to the subject of the part.

## Materials

Powdered $ZrSn_2$ and $Zr_5Pb_4$ were synthesized for sintering reactions by combining the soft elements with zirconium powder in stoichiometric ratios in sealed tantalum tubes at 800-1000°C. $ZrO_{0.1}$, generously donated by Dr. R. Ziebarth, had been synthesized by reacting zirconium metal with known amount of oxygen. The lattice parameters of this sample matched well with those reported for $ZrO_{0.1}$ composition.[15,16]

## Syntheses

Arc-melting and subsequent annealing reactions in tantalum tubes with molybdenum liners were primarily used for the $Zr_4Sn$ system. The annealing treatment is an essential part of the synthesis because the $Zr_4Sn$ phase undergoes peritectoid decomposition at 1327±20°C.[1] The alternative powder sintering reactions suffered from very sluggish diffusion rates, in contrast to the report by Luo and coworkers.[7] Most of the products from the powder sintering reactions were mixtures of the desired A15 phase and its neighbors ($\alpha$-Zr and $Zr_5Sn_3$).

Arc-melting reactions of Zr-Pb system were not practical because of lead volatilization. Several such reactions ended up with massive lead losses. Naturally, a sintering reaction was the last resort for the synthesis. However, the same problem of slow diffusion rate as in Zr-Sn system was observed. A previous study on the zirconium-rich side also reported slow reaction rates in zirconium-lead system.[17]

## SEM/EDX Studies

Elemental analyses of some samples of $Zr_{4+x}Sn$ and $Zr_{-6}Pb$ were carried out by using a JEOL JSM-840 scanning electron microscope and a KEVEX EDX system. Samples were dry polished with a series of sandpapers. The samples in this study were extremely ductile so that they had to be rubbed with a very smooth and fine leather cloth as the last touch.

## Density Measurement

A standard pycnometric method with distilled water was employed for the density measurement of an arc-melted and annealed button of $Zr_4Sn$. The surface of the sample did not appear to have reacted after about ten minutes in water.

# RESULTS AND DISCUSSION

## Zr-Sn System

### Composition

The controversy on the composition was easily resolved by analyzing two products of $Zr_4Sn$ and $Zr_3Sn$ compositions, each arc-melted and annealed at 1000°C for 7 days. The former showed over 90 % yield of the A15 phase whereas the latter had strong reflections of $Zr_5Sn_3$ plus the major A15 phase in the powder patterns. The composition is $Zr_4Sn$ or close to this.

A natural consequence to the discrepancy between the observed and ideal compositions of this phase is whether this phase has a solid solution or not. Solid solutions of A15 phases are known for many other systems such as Nb–Ge,[18] Nb–Sn,[19] and Nb–In.[20] The phase breadths of these phases are reported between 75 and 80 at. % or more of Nb. The niobium-richest compositions in these correspond to that of $Zr_4Sn$.

A series of compositions $Zr_{4+x}Sn$ (x=-0.2, 0, 0.3, and 0.6) were arc-melted and annealed at 1050°C for 7 days. These samples were analyzed with powder patterns and by SEM/EDX, and the results are listed in Table 1. The powder patterns all showed the A15 phase (a=5.6254(7) Å) as the major phase while the second phases were $Zr_5Sn_3$ for $x \leq 0$ and α-Zr for $x > 0$ samples. The line positions of the A15 phase in all four powder patterns were identical, indicating no lattice parameter change with composition. The intensities of the second phases grew as the

Table 1. Guinier powder pattern and SEM/EDX results of $Zr_{4+x}Sn$ samples

| x | | second phases[a] | | composition of |
|---|---|---|---|---|
| loaded | corrected[b] | XRD[c] | SEM[d] | A15 phase (Zr:Sn)[e] |
| -0.20 | -0.20 | $Zr_5Sn_3$ (15%) | $Zr_5Sn_3$ | 80.9(6):19.1(4) |
| | | | | 80.0(5):20.0(4) |
| 0.00 | 0.02 | $Zr_5Sn_3$ (5%) | $Zr_5Sn_3$ | 80.0(6):20.0(4) |
| 0.30 | 0.25 | α-Zr (5%) | Zr | 80.8(6):19.2(4) |
| | | | | 80.9(6):19.2(4) |
| 0.60 | 0.61 | α-Zr (10%) | Zr | 80.7(6):19.3(4) |

[a]Second phases in addition to the major $Zr_4Sn$ phase.

[b]Corrected for the weight loss during the arc-melting.

[c]Relative intensities with respect to that of $Zr_4Sn$ phase.

[d]Identified visually.

[e]EDX analysis results.

composition moved away from 4:1. All of these results indicate that the composition of the A15 phase does not deviate from 4:1 significantly.

SEM/EDX results agree with those of powder patterns. The compositions of the A15 phase were analyzed by taking the overall composition of x=0.0 sample as standard. Within experimental error limit, the compositions of the A15 phases in all four samples were identical. The A15 phase is, therefore, a line phase and the composition is very close to $Zr_4Sn$. The line phase nature of this compound is a contrast to the solid solutions of the niobium-based A15 phases (above).

The very small amount of $Zr_5Sn_3$ from the powder pattern of x=0.0 sample was almost invisible in SEM and might have originated from the surface of the button (below). Another possibility is incomplete equilibrium. According to the published phase diagram,[1] there is an eutectic point between β-zirconium and $Zr_5Sn_3$ at 19.1 at. % Sn, which is slightly tin poorer than the 4:1 composition, and as-cast $Zr_4Sn$ must contain ~5 % of $Zr_5Sn_3$ in addition to the eutectic mixture. The $Zr_5Sn_3$ tends to form crystallites immediately after arc-melting, and these crystallites might have been retained even after annealing.

## Structure

The A15 phase ($Cr_3Si$-type; $Pm\bar{3}n$) has a cubic unit cell. The structure consists of silicon atoms at 0,0,0 and 1/2, 1/2, 1/2 positions and chains of chromium atoms that are extended to all three directions (Figure 1).

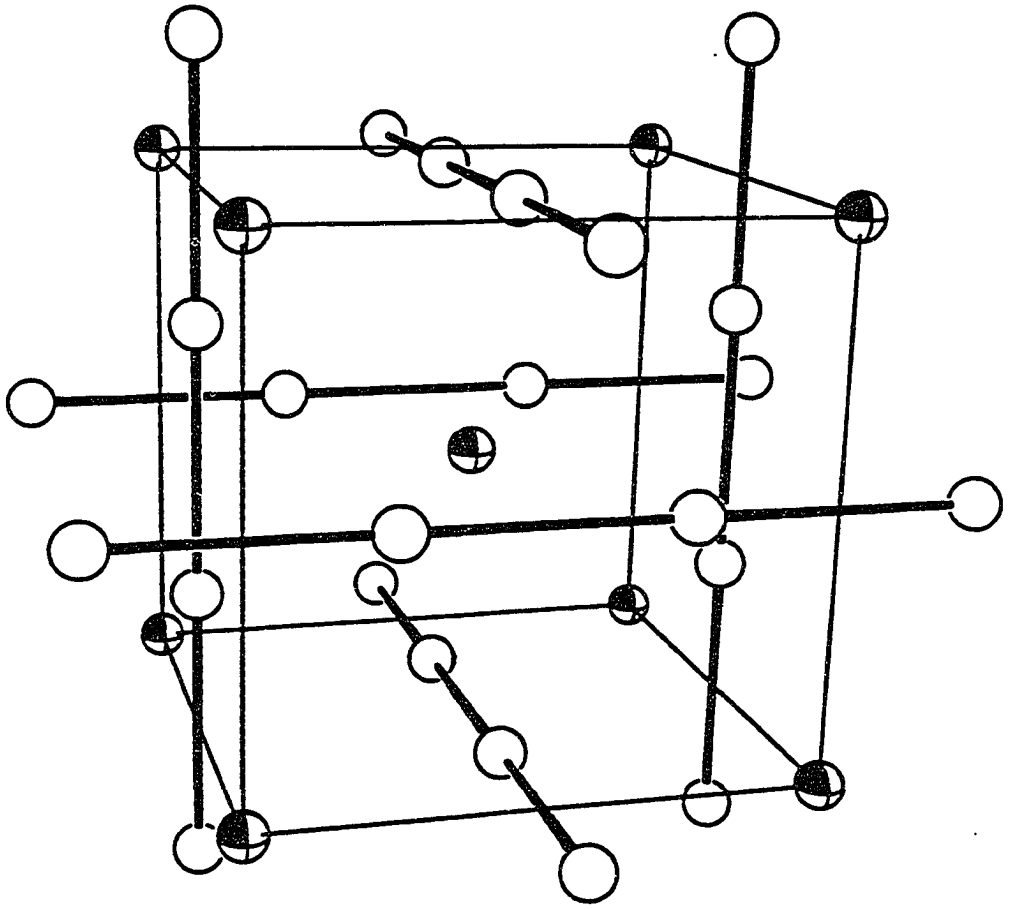

Figure 1. The structure of the A15 ($Cr_3Si$-type) phase. The shaded atoms are silicon and the open atoms are chromium. The chains consist of equally spaced chromium atoms at (1/4, 0, 1/2).

The discrepancy between the experimentally determined composition and that of ideal structure type and the line phase nature of this compound raise further questions about the structure, that is, where does the extra zirconium go and how it is ordered?

Two extreme possibilities for the extra zirconium are substitutional ($Zr_3(Zr_{0.2}Sn_{0.8})$) and vacancy ($Zr_3Sn_{0.75}$) models. The measured density 7.10(2) g/cm$^3$ is closer to that calculated for the former, 7.22 g/cm$^3$, than for the latter, 6.77 g/cm$^3$. Another piece of supporting evidence for the substitutional model was obtained from a comparison of calculated and observed intensity distributions (Table 2). The substitutional model fits better. A single crystal study of $Nb_4Ge$, which had the same conflict of structure type and composition, gave disordered $Nb_3(Nb_{0.2}Ge_{0.8})$ in the A15 structure, paralleling above conclusion.[21]

When the exposure time was doubled for the powder pattern, four additional lines were revealed. Including these, the powder pattern could be indexed with a cubic cell with dimensions double that of the original cubic unit cell ($a'=2a$) ($2\theta$ (Cu $K\alpha_1$) and the indices of these in the supercell are as follows: $15.74_0°$, 200; $17.58_0°$, 210; $19.34_8°$, 211; $29.74_8°$, 321; all < 2 % of $I_{max}$). The indices of the superlattice reflections restrict the structure to primitive cubic cells. However, attempts to account for the line positions and the intensities of these superlattice reflections with variations of the original substitutional A15 structure have not been successful. Since the extra zirconium was

Table 2. Comparison of intensities in observed and calculated powder patterns of $Zr_4Sn$

| $2\theta^a$ | hkl | observed I | calculated I | |
|---|---|---|---|---|
| | | | $Zr_3Sn_{0.75}$ | $Zr_3(Zr_{0.2}Sn_{0.8})$ |
| 14.38 | 200 | 43 | 32.7 | 42.1 |
| 16.10 | 210 | 100 | 100.0 | 100.0 |
| 17.64 | 211 | 98 | 73.4 | 94.5 |
| 25.12 | 222 | 6.6 | 8.8 | 6.7 |
| 26.16 | 320 | 23 | 22.4 | 22.4 |
| 27.16 | 321 | 46 | 38.0 | 49.0 |
| 29.08 | 400 | 13 | 15.3 | 17.4 |
| 32.60 | 420 | 13 | 10.0 | 12.8 |
| 33.46 | 421 | 18 | 18.7 | 18.7 |
| 34.26 | 332 | 11 | 8.3 | 10.7 |
| 39.56 | 520,432 | 12 | 14.7 | 14.7 |
| 40.28 | 521 | 12 | 9.0 | 11.5 |
| 41.64 | 440 | 10 | 7.9 | 9.0 |
| 44.32 | 600,442 | 3.9 | 3.9 | 4.9 |
| 44.98 | 610 | 2.9 | 2.9 | 2.9 |
| 45.60 | 611,532 | 9.0 | 8.1 | 10.0 |

[a]Mo Kα-radiation; PICKER diffractometer.

concluded to be mixed with tin in the tin site, an ordering of these atoms was assumed; the zirconiums in the chain were assumed to be intact in all considerations. However, models based on such assumptions did not match either the diffraction pattern or the determined stoichiometry, or both.

Single crystal growth also has been tried to solve the ordering problems by X-ray structure analysis, however, without success. This might be because of the peritectoid nature of this phase and its extreme sensitivity to foreign elements that prevent the use of flux or vapor phase transport media.

Electron microscopy was also applied to obtain an idea about the possible space groups of the superstructure. However, the hard and brittle nature of this compound did not yield a suitably thin sample for TEM (transmission electron microscope) study.

**Stability**

The reported instability of this phase was, at first, understood as originating from the difference of thermodynamics of α- and β-zirconium relative to this phase. Therefore, the decomposition temperature of the A15 phase was assumed to be at 982°C, the transition point of tin-saturated β- to α-zirconium. However, annealing reactions above and below this temperature both yielded almost the same quantity of A15 phase. In fact, many other publications reported observation of the $Zr_4Sn$ phase as low as 300°C[10,22] as opposed to the few contrary reports. Therefore, the possibility of an intrinsic decomposition at low

temperature was eliminated. Rossteutscher and Schubert,[5] who once reported this phase as a high temperature phase, retracted this idea after observation of this phase after a 650°C annealing.

The powder patterns of many of the stoichiometrically loaded samples showed α-Zr as well as $Zr_5Sn_3$ as second phases. Obviously, this observation violates phase rule. The $Zr_5Sn_3$ was thought to have formed in the arc-melting reaction and to have been retained even after annealing. In order to attain homogeneous A15 samples, annealed buttons of $Zr_4Sn$ composition were ground and pressed into pellets for sintering reactions. Such treatment generally enhances the diffusion rate drastically, as in the $Zr_5Sn_3$-$Zr_5Sn_4$ system.[23] However, surprisingly enough, the resultant powder patterns were always composed of $Zr_4Sn$, α-Zr, and $Zr_5Sn_3$, the last two with considerably greater intensities regardless of what temperature was applied for the sintering.

Internal pressure within the arc-melted button appeared to explain this observation. This postulate assumes that the A15 phase is metastable but is retained because the decomposition into α-zirconium and $Zr_5Sn_3$ increases the sample volume, and this is suppressed by the rigid matrix of the button. Therefore, grinding of the button releases the strain to form more stable Zr and $Zr_5Sn_3$. However, this theory does not explain how A15 phase is formed, even very fractionally, from a powder sintering reactions (see Experimental). Moreover, the calculated atomic volume of $Zr_4Sn$ is negligibly different from that of the appropriate Zr and $Zr_5Sn_3$ mixture.

An interesting observation is that the zirconium in the powder patterns in this system is always in the α-form in the temperature range of 900-1200°C. This is a contradiction to the phase diagram according to which β-zirconium should appear above 982°C. Unsuccessful quenching could account for this observation. However, the diffusion rate of tin in zirconium was reported to be very sluggish,[10,22] and such a possibility did not satisfactorily explain this observation. Impurities were assumed to affect the system. The influence of oxygen, one of the most probable impurities, was studied first.

The compositions $Zr_4SnO_x$ (x=0.1, 0.15, 0.2, and 0.4) were arc-melted and annealed at 1050°C for 7 days. $ZrO_{0.1}$ chips were used as oxygen source. The last two samples showed no $Zr_4Sn$ in their powder patterns, only α-Zr and $Zr_5Sn_3$ phases. The line positions for $Zr_5Sn_3$ corresponded to the pure binary phase, not $Zr_5Sn_3O_x$ (Part III), while the lattice parameters of the α-Zr phase varied with the oxygen content (hexagonal; a=3.2214(8), 3.2411(3), c=5.162(3), 5.1705(4) Å for x=0.1 and 0.4, respectively) and did not match any of the α-Zr dimensions in the binary systems Zr-O or Zr-Sn. This is easy to see since the a-parameter of α-Zr with oxygen changes in the opposite direction to that with tin. The lattice parameters of $ZrO_x$ range over a=3.2326-3.248, c=5.1473-5.172 Å for $0 \leq x \leq 0.1$,[15,16] and those of $ZrSn_x$ are formulated as $a=3.2326 - 0.276x$, $c=5.1473 + 0.284x - 0.064x^2$ for $0 \leq x \leq \sim 0.07$.[24] Therefore, the α-Zr in these must contain both oxygen and tin. However, the effects of these elements on the lattice parameters are so different that estimation of the concentrations of both in α-Zr is

impractical. Roughly, the x=0.4 sample takes more of a Zr-O character and the x=0.1 one, Zr-Sn, judging from the lattice parameter trends.

The powder patterns of x ≤0.15 samples showed three phases; $Zr_4Sn$, α-Zr, and $Zr_5Sn_3$. The intensity of the $Zr_4Sn$ phase was much weaker than in the above, ground and sintered 'pure' binary samples.

Sintering reactions of $Zr_5Sn_3O_y$ (y=0.1 and 0.5) and Zr for $Zr_4SnO_x$ compositions (x=0.033, and 0.167) at 1050°C for 7 days showed similar results. The x=0.167 sample showed only α-Zr and $Zr_5Sn_3$ while the x=0.033 one showed the A15 phase in addition. Therefore, the critical oxygen concentration for the complete decomposition of $Zr_4SnO_x$ lies between x=0.15 and 0.167.

These results imply that the decomposition of A15 phase upon grinding and sintering is, in fact, a ternary phase equilibrium in the Zr-Sn-O (or other impurity) system, not a metastable phase decomposition. The ternary phase equilibrium was attained by homogeneously mixing the surface-bound oxygen with the rest of the sample on grinding. There is a very narrow three phase field of α-Zr(O,Sn)-$Zr_5Sn_3$-$Zr_4Sn$ below x=0.167 in $Zr_4SnO_x$, and beyond this point, there is a two phase region of α-Zr(O,Sn) and $Zr_5Sn_3$. Even though $Zr_5Sn_3$ is capable of bonding interstitial oxygen to form $Zr_5Sn_3O_x$ at 1100°C (see Part III), the oxygen in this ternary system goes into the α-Zr. A similar behavior may be assumed for the other possible impurities. The study of the ternary phase diagram Zr-Sn-Fe observed a similar effect of iron on the stability of this $Zr_4Sn$ phase.[25]

There are two possible ways of oxygen contamination, from the arc-melting process or from exposure of the samples to the air. An arc-melted and annealed button was split into two parts; one part was kept in the dry box and the other in air for 100 hours as finely ground powder before each was pelleted and sintered at 1000°C for 7 days. Their powder patterns were indistinguishable from each other, and both had the same features as the previously mentioned decomposition products. The second possibility was excluded.

An arc-melted button was filed on all the exposed surface, and the center was treated in the same manner as previously (annealed and then ground and sintered). The resultant powder pattern still showed three phases, but the intensities of α-Zr and $Zr_5Sn_3$ were considerably weaker than in the other samples. Therefore, the impurity is introduced during the arc-melting process and especially on the surface of the button.

In light of these results, it is not surprising that the aging products of Zircaloy, which contains 1 at. % of oxygen and other elements, does not have the $Zr_4Sn$ phase even if phase diagram of the Zr-Sn binary system requires its formation.

## Zr-Pb System

The study of this system is very limited by the availability of workable synthetic techniques. Arc-melting is simply not applicable because of the volatility of lead. Sintering reactions suffered from a sluggish diffusion rate. However, it appeared that sintering reactions

were the only possible way, and therefore, this system could not be thoroughly studied.

Sintering reactions of Zr and $Zr_5Pb_4$ powders at 1000°C for 10 days for compositions $Zr_xPb$ (x=4, 5, 6) showed that the x=6 sample had the most (~90 %) of the A15 phase (a=5.6619(4) Å). The powder patterns were identical otherwise; $Zr_5Pb_3$ was the second phase and α-Zr gave very weak lines. The identical lattice parameters of the A15 phase in these powder patterns imply that this is a line phase or it has a very narrow solid solution range, as in the $Zr_4Sn$ case. The composition appears to be close to $Zr_6Pb$.

Despite the volatility problem, arc-melting and annealing reactions were performed for SEM/EDX studies (see General Eexperimental section). The corrected compositions were $Zr_{6.20}Pb$ and $Zr_{5.62}Pb$ for initial compositions $Zr_6Pb$ and $Zr_5Pb$, respectively. The powder patterns of these samples were different from those of sintering reactions, the A15 phase and α-Zr only. The EDX/SEM-determined compositions of the major phases were $Zr_{5.89}Pb$ and $Zr_{5.71}Pb$ for $Zr_{6.20}Pb$ and $Zr_{5.62}Pb$ samples, respectively. The second phase in each sample was lead-richer than the major phase which is a contradiction to the powder pattern result. However, the analysis results are reasonably close to 14.5–14.9 at. % Pb for the major phases in these samples. The composition also agree with the above observations from powder patterns. The A15 phase in Zr-Pb, therefore, is concluded to have about 14.7% of Pb ($Zr_{5.8}Pb$).

Assuming zirconium substitution to lead and no vacancy, the structure becomes $Zr_3(Zr_{0.41}Pb_{0.59})$. No superstructure was found in the powder patterns.

# References


1. McPherson, D. J.; Hansen, M. Trans. Am, Soc. Met. 1953, 45, 915.
2. Tanner, L. E.; Levinson, D. W.; McPherson, D. J. Nucl. Sci. Abstr. 1958, 12, 2332.
3. Nesic, O. M.; Stefanovic, V. M.; Spasic, Z. L. Fizika Suppl. 1970, 2, 31.1.
4. Gran, G.; Andersson, S. Acta Chem. Scand. 1960, 14, 956.
5. Rossteutscher, W.; Schubert, K. Z. Metallkd. 1965, 56, 813.
6. Naik, U.; Banerjee, S. Trans. Indian Inst. Met. 1978, 31, 318.
7. Luo, H. L.; Vielhaber, E.; Corenzwit, E. Z. Physik. 1970, 230, 443.
8. Abriata, J. P.; Bolcich, J. C.; Arias, D. Bull. Alloy Phase Diagr. 1983, 4, 147.
9. Schubert, K.; Anantharaman, T. R.; Ata, H. O. K.; Meissner, H. G.; Pötzschke, M.; Rossteutscher, W.; Stolz, E. Naturwissenschaften 1960, 47, 512.
10. Carpenter, G. J. C.; Ibrahim, E. F.; Watters, J. F. J. Nucl. Mater. 1981, 102, 280.
11. VanderSande, J. B.; Bement, A. L. J. Nucl. Mater. 1974, 52, 115.
12. Vitikainen, E.; Nenonen, P. J. Nucl. Mater. 1978, 78, 362.
13. Versaci, R. A.; Ipohorski, M. J. Nucl. Mater. 1979, 80, 180.
14. Scarborough, J. O.; Betterton, J. O., Jr., U.S. Atomic Energy Committee ORNL-3470, 1963, 26.
15. Seaverson, L. M.; Corbett, J. D. Inorg. Chem. 1983, 22, 3202.
16. Holmberg, B.; Dagerhamn, T. Acta Chem. Scand. 1961, 15, 919.

17. Hansen, M. "Constitution of Binary Alloys", McGraw-Hill; New York, 1958, p. 1121.

18. Jorda, J. L.; Flücker, R.; Müller, J. J. Less-Common Met. 1978, 62, 25.

19. Schadler, H. W.; Osika, L. M.; Salvo, G. P.; DeCarlo, V. J. Trans. Met. Soc. AIME 1964, 230, 1074.

20. Villas, P.; Girgis, K. Z. Metallkd. 1982, 73, 169.

21. Rasmussen, S. E.; Hazell, R. G. Acta Crystallogr. 1979, B35, 1677.

22. Speich, G. R.; Kulin, S. A. "Zirconium and Zirconium Alloys", America Society of Metals: Metals Park, OH, 1953, p. 200.

23. Betterton, J. O., Jr.; Easton, D. S. J. Metals 1961, 13, 86.

24. Kwon, Y.-U.; Corbett, J. C. Chem. Mater. 1990, 2, 27.

25. Tanner, L. E.; Levinson, D. W. Trans. Am. Soc. Met. 1960, 52, 1115.

# PART III. INTERSTITIAL PHASES OF $Zr_5Sn_3$ AND $Zr_5Pb_3$ HOSTS

# INTRODUCTION

Interstitial compounds were originally defined as the compounds of transition metal elements with hydrogen, carbon, and nitrogen atoms that formed without or with minor structural changes to the metals.[1,2] However, this rather restricted 'space-filling' definition of a interstitial compound had to be revised following the findings of carbides of, for example, iron, cobalt, and nickel that were structurally unrelated to their parent materials.[3] Nowadays the accepted definition of an interstitial compound is a compound with non-metal atoms in a lattice of metallic elements without direct bonds between the non-metals so that the latter are surrounded solely by the metallic elements.[4]

A consequence of this definition is that these compounds show good electrical conductivity.[4,5] However, the brittleness, for example, of many compounds in this family indicates that the bonding nature of the interstitial elements is directional rather than more or less isotropic as in metals. Such characteristics of interstitial compounds have been challenges to chemists theoretically and conceptually.[3,6-8]

There have been attempts to understand the bonding nature of these and to synthesize new interstitial compounds for applications. Systematic syntheses and structural characterizations of new interstitial compounds of various host types will help such efforts.

The $Mn_5Si_3$-type compounds are interesting for their possibilities of accommodating interstitial elements.[9,10] (For structural details, see

the General Introduction.) The center of each $Mn_{6/2}Si_{6/2}$ trigonal antiprism of Mn1 atoms is vacant in the stoichiometric binary compound.[11] However, the size of this vacant site is often large enough to accommodate a third interstitial element in the structure. $Zr_5Si_3Z_x$ (Z=B, C, N, O),[12-17] $Zr_5Al_3Z_x$ (Z=C, O)[18,19] are examples of such interstitial derivatives of $Zr_5Si_3$ and $Zr_5Al_3$ (both $Mn_5Si_3$-type), respectively. The stoichiometry of the interstitial element (x) in above formulae may range from 0.0 to 1.0, where these extremes represent stoichiometric binary host and fully occupied interstitial compounds.

Being small in size, the C, N, O interstitials in this structure sometimes have been neglected by previous researchers, and some of the phases that were reported as binary $Mn_5Si_3$-type compounds turn out to have contained interstitial atoms.[12,20,21] The interstitial atoms sometimes play a crucial role in the stabilities of the $Mn_5Si_3$-type structures. The family of compounds called "Nowotny phases" are those in a $Mn_5Si_3$-type structure that are interstitially stabilized and, otherwise, would crystallize in different structure type or not exist.[9] $Nb_5Ga_3$ ($W_5Si_3$-type) with O[21] or C,[22] $La_5Sn_3$ ($W_5Si_3$) with C or O,[12] $Ti_5Ga_3$ ($W_5Si_3$) with O,[23] and $M_5Si_3$-C (M=V, Nb, Ta, Cr, Mo)[9] are such examples. The stabilization effect of an interstitial element appears to be very high in these examples. This could be also the case even when the 'binary' host compounds already occur in the $Mn_5Si_3$-type structure.

Interestingly, the interstitial site capacity of this structure type compounds is not limited to conventional interstitial elements such as

B, C, N, and O. Compounds that have $Ti_5Ga_4$-type ($P6_3/mcm$) structure can be viewed as stuffed $Mn_5Si_3$-type compounds with the same metal or one metalloid (for example, Ga in $Ti_5Ga_4$) occupying the interstitial site.[23,24] $Zr_5Al_4$,[25] $Zr_5Sn_4$,[26,27] $Hf_5Sn_4$,[28] are a few examples of such compounds. Further reports of various interstitial elements in this structures are found in $Ce_5Sn_3Ag$,[29] $R_5Bi_3Cu$ (R=La, Ce, Pr, Nd, Gd and Tb),[30] $(Zr,Hf)_5(Sn,Pb)_3(Ni,Cu)$,[28] and $(Ti,Zr,Hf)_5Sb_3(Ni,Cu,Zn)$.[31]

Recently, Garcia and Corbett reported systematic syntheses and characterization of stoichiometric interstitial compounds of $Zr_5Sb_3Z$, where Z stand for 15 different elements.[32,33] The wide and diverse nature of the interstitial elements in the same chemical environment and in the same crystal structure type are striking. Further studies in this and similar systems are required for better understanding of the bonding in and properties of these interstitial compounds. $Zr_5Sn_3$ has $Mn_5Si_3$-type structure and its crystal dimensions are very close to those of $Zr_5Sb_3$.[27] Therefore, one can study the effect of electron count in the interstitial compounds because of the different number of electrons in the conduction bands of these host compounds. A similar study on $Zr_5Pb_3$ host was considered also interesting since this has an identical electron count to that of $Zr_5Sn_3$ yet the dimensions are larger and any geometric effect is different.[34]

As the first step towards such goals, systematic and synthetic studies were carried out. The stoichiometries and quantitative syntheses of the desired interstitial compounds were the major objectives. Crystal structure refinements were also performed, when

possible, to attain information on the stoichiometries and structural details of these compounds. The results of $Zr_5Sn_3$ and the $Zr_5Pb_3$ host systems are presented separately in the first and second sections, respectively. General comparison within and between each of these systems will be made in the last discussion section. The binary system of the host $Zr_5Sn_3$ and its tin self-interstitial version $Zr_5Sn_4$ were also studied, and these results were discussed in Part 1. The binary compound $Zr_5Pb_3$ and its self-interstitial $Zr_5Pb_4$ are covered in the corresponding section of this part.

# EXPERIMENTAL

## Materials

The source and treatments of the zirconium and tin used in this study are described in Part I of this thesis. Lead was obtained as a metallic bar which was cold rolled to sheet (3 mm) and kept in a dry box. The oxidized surface of lead was scraped off before use. Other materials are listed in Table 1 for their purity, sources, and forms. Except zinc, cadmium, indium, and gallium, most of these elements were used as received. Zinc was sublimed and condensed in an inverted V-shaped evacuated silica tube. The other elements were purified mechanically by scraping the surfaces before use.

## Synthesis

Arc-melting, annealing, sintering, vapor phase transport, and flux reaction techniques were utilized for the syntheses. The arc-melting technique and its problems were discussed in detail in Part I.

Sintering reactions were performed when powdered reagents were available. For those elements that did not come in a powder form were first reacted with zirconium by arc-melting (for Cr, Mn, Fe, Co, Ni, Cu, and Al) or with zirconium powder in a sealed Ta tube (for Ga, Ge, Ag, In, Sb, P, S, As, Se, Te, and Pb) in their appropriate compositions to make brittle and powdery compounds for further reactions. Stoichiometric amounts of these reagents were mixed, and the mixture was

Table 1. Materials used in the syntheses

| material | source | purity | form |
|---|---|---|---|
| B | Aesar | 99.5 % | crystals |
| ZrC | Cerac | | powder |
| ZrN | Cerac | | powder |
| $ZrO_2$ | Hohnson Matthey | | powder |
| Al | United Mineral & Chemical | High Purity | wire |
| Si | Ames Lab. | zone refined | crystal bar |
| P | Aldrich | 99.999 % | lump |
| S | Alfa Products | 99.999 % | powder |
| Ti | Ames Lab | | chip |
| Cr | A.D. Mackay | | chip |
| Mn | A.D. Mackay | 99.9 % | chip |
| Fe | Plastic Metals | 99.9 % | chip |
| Co | Aesar | 99.9+ % | chip |
| Ni | Matheson Coleman & Bell | | sheet |
| Cu | J.T. Baker Chem | 99.99 % | turning |
| Zn | Fisher Scientific | 99.99 % | granule |
| Ga | Johnson Matthey | 99.99 % | granule |
| Ge | Johnson Matthey | 99.999 % | lump |
| As | Aldrich | 99.9999 % | lump |
| Se | American Smelting & Refining | 99.999 % | granule |
| Ag | G. Frederick Smith Chem | Reagent | small granule |
| Cd | Cominco Products | 99.999 % | strip |
| In | Cominco Products | | lump |
| Sb | Allied Chemical & Dye | | lump |
| Te | United Mineral & Chemical | 99.999 % | lump |

pressed into a pellet. The pellet was placed in a sealed Ta tube and heated.

In some of the systems the growth of single crystals was attempted through vapor phase transport reactions. Stoichiometric ratios of reagent powders as in the sintering reactions were loaded in long tantalum tubes with $ZrI_4$, $ZrCl_4$, or $CdI_2$ as transporting agents. Temperature gradients of 50 to 100° were applied to most of the reactions at 800 to 1000°C by using two-zone furnaces.

When one of the component elements has a high enough vapor pressure and forms a melt at the reaction temperature, flux reaction technique is applicable. An excess of the flux material and stoichiometric amounts of other reagents were loaded in an alumina crucible which, in turn, was sealed in an evacuated closed silica tube. The tube was held vertically, and the crucible was placed around the upper part of the tube at the center of a tubular furnace. By setting these in this way, unreacted excess flux material vaporized and condensed at the bottom of the silica tube leaving desired product, sometimes single crystals, in the alumina crucible.

## Analysis

### X-ray diffraction

The details of sample handling for the Guinier powder diffraction and the interpretation are discussed in the General Introduction. Single crystal X-ray diffraction analyses were done with Rigaku AFC6R and CAD4 diffractometers. The data collection and refinement parameters

for each single crystal structure are present in the corresponding sections. For those refinements whose results do not represent the desired bulk phases and, therefcre, are less important, only the refined parameters are given in the tables. The lattice parameters in the tables were calculated from the powder patterns of the bulk products from which the single crystals were obtained except for those that did not represent the bulk; for these the lattice parameters were obtained from the single crystal diffractometers. The R-indices for data averages are for the reflections with $I/\sigma_I > 3$ except for those noted in the corresponding tables.

**SEM/EDX studies**

Photomicrographs and elemental analyses of the samples were obtained by using a JEOL JSM-840 scanning electron microscope and a KEVEX EDX system. Samples were dry-polished with a sequence of very fine sandpapers and then ash.

# RESULTS

The general crystallographic parameters for the $Ti_5Ga_4$-type (interstitial $Mn_5Si_3$-type) structure are listed in Table 2.[11] Most of the parameters are fixed. The refinement results of individual crystal structures are presented in corresponding sections for the variable parameters only.

The temperature gradients of vapor phase transport reactions are denoted with arrows (i.e., 900°⟶850°C). The temperature to the left of the arrow is where the starting materials were placed.

Table 2. General crystallographic Parameters for $Zr_5(Sn, Pb)_3Z$ type structures[a]

| atom | site | position | | | thermal parameters[b] | | | | | |
|---|---|---|---|---|---|---|---|---|---|---|
| Sn(Pb) | 6(g) | x | 0 | 1/4 | $U_{11}$ | $U_{22}$ | $U_{33}$ | $1/2U_{22}$ | 0 | 0 |
| Zr1 | 4(d) | 1/3 | 2/3 | 0 | $U_{11}$ | $U_{11}$ | $U_{33}$ | $1/2U_{11}$ | 0 | 0 |
| Zr2 | 6(g) | x | 0 | 1/4 | $U_{11}$ | $U_{22}$ | $U_{33}$ | $1/2U_{22}$ | 0 | 0 |
| Z | 2(b) | 0 | 0 | 0 | $U_{11}$ | $U_{11}$ | $U_{33}$ | $1/2U_{11}$ | 0 | 0 |

[a]Space Group $P6_3/mcm$ (no. 193).

[b]Sometimes these are replaced by $B_{iso}$.

## Interstitial Compounds of $Zr_5Sn_3Z$

The synthetic conditions and the lattice parameters of the compounds in this system are listed in Table 3. Most of the compounds were stoichiometric except those marked in the table. The details of individual systems follow.

### Second period elements

The nature of these elements and their refractory binary compounds with zirconium hampered the syntheses. Boron and carbon have very high melting points, in contrast to the low melting and boiling points of tin. The same is true for the binary compounds of these elements with zirconium that were used as reagents. Very high temperatures are necessary in order to have enough mobility of the atoms in sintering and annealing reactions. Sometimes long reaction times are also needed. However, under these extreme conditions, tin often vaporizes, and control over the composition is often lost. In general, low temperature sintering is therefore required before a high temperature is applied. By doing this, tin forms intermediates that are more stable than $ZrSn_2$ or the elemental form and can withstand high temperatures.

In many of the cases, the desired phases were obtained as mixed with impurities in the products. However, the unit cell dimensions as well as single crystal structure refinements prove that stoichiometric interstitial phases of these interstitials were synthesized.

**Boron** Powder sintering reaction of Zr, $ZrSn_2$, and amorphous boron (95 %) at 1300°C for 3 days yielded an interstitial phase plus

Table 3. Interstitial compounds of $Zr_5Sn_3Z$[a]

| element | synthetic condition[b] | crystal parameters | | | |
|---|---|---|---|---|---|
| | | a(Å) | c(Å) | V(Å$^3$) | c/a |
| B | S | 8.4936(4) | 5.8029(5) | 362.54(5) | 0.683 |
| C | S | 8.4268(7) | 5.8001(8) | 356.69(8)[c] | 0.688 |
| N | S | 8.4040(8) | 5.7698(8) | 352.91(8)[c] | 0.687 |
| O | S,V | 8.4256(8) | 5.763(1) | 354.31(9)[c] | 0.684 |
| Al | AN | 8.655(1) | 5.871(1) | 380.9(1) | 0.678 |
| Si | S | 8.6072(9) | 5.844(1) | 374.9(1) | 0.679 |
| P | S | 8.5449(5) | 5.9171(7) | 374.16(6) | 0.692 |
| S | S | 8.5065(5) | 5.9646(6) | 373.78(6)[c] | 0.701 |
| Cu | S | 8.6043(5) | 5.8686(8) | 379.27(6) | 0.681 |
| Zn | S | 8.6325(7) | 5.877(1) | 379.28(9) | 0.681 |
| Ga | S | 8.6599(6) | 5.8794(8) | 381.85(7) | 0.679 |
| Ge | S | 8.6397(5) | 5.8661(6) | 379.21(6)[c] | 0.679 |
| As | S | 8.6037(6) | 5.9200(9) | 379.51(8)[c] | 0.688 |
| Se | S | 8.5584(5) | 5.9515(6) | 377.52(6)[c] | 0.695 |
| $Fe_{1/3}Sn_{1/3}$[d] | AM | 8.6063(5) | 5.8639(7) | 376.14(6) | 0.681 |
| $Co_{1/3}Sn_{1/3}$[d] | AM | 8.5934(7) | 5.861(1) | 374.82(9) | 0.682 |
| $Ni_{1/3}Sn_{1/3}$[d] | AM | 8.5812(6) | 5.8577(8) | 373.55(7) | 0.683 |
| $Sn_{0.09}$ | AN | 8.4802(5) | 5.7950(7) | 360.91(6) | |
| $Zr_5Sn_3$[e] | | 8.4560(7) | 5.779(1) | 357.86(9) | 0.683 |
| $Zr_5Sn_4$[e] | | 8.7656(7) | 5.937(1) | 395.06(9) | 0.677 |

[a] stuffed-$Mn_5Si_3$ ($Ti_5Ga_3$-type) (space group $P6_3/mcm$).

[b] S = powder sintering; V = vapor phase transport; AN = annealing after arc-melting; AM = arc-melting.

[c] The data are averages for more than one sample.

[d] Estimated from the loaded compositions.

[e] Reference 27.

$ZrB_2$ and $ZrO_2$ as impurities. The source of oxygen in this product is uncertain. The lattice parameters of this phase (a=8.4936(4), c=5.8029(5) Å) were slightly larger than those of binary $Zr_5Sn_3$. The product pellet was ground and pelleted for a second sintering at 1350°C for 5 days. The powder pattern was identical to the previous one except for the intensity distribution. The $ZrB_2$ and $ZrO_2$ had become much weaker (each 5 % in intensitiy). The lattice parameters of the major phase were virtually unchanged. The expanded lattice parameters from those of the host compound indicate that these contain boron interstitials. No binary $Zr_5Sn_{3+x}$ with this lattice dimension could be synthesized under these reaction conditions (Part I).[27] However, the presence of $ZrB_2$ and $ZrO_2$ obstructs assurance of a stoichiometric compound.

An independent arc-melting reaction of Zr, Sn, and crystalline boron yielded a similar powder pattern as above samples; the lattice parameters were slightly shifted (a=8.484(1), c=5.800(2) Å), and $ZrB_2$ was a trace impurity (< 5 %), but no $ZrO_2$ was seen. However, admitting the uncertainty involved in arc-melted samples, the sintered result can be appropriately considered as representing a boron intersititial phase.

**Carbon** The low mobilities of elements in this system are well exemplified by a sintering reaction at 1000°C for 10 days, a typical and suitable condition for the interstitial phases of other period elements such as copper and gallium (below). $Zr_5Sn_3$ from arc-melting reaction and carbon powders were mixed as reactants. The resultant powder pattern showed unreacted $Zr_5Sn_3$ and $Zr_2SnC$[34] phases, and the carbon

interstitial product could hardly be identified. This might be, in part, because of the stability of $Zr_2SnC$, apparently a low temperature phase, but most obviously it arose because of the slow diffusion rate of carbon or of carbon-bound zirconium.

In contrast to the low temperature reaction, a sintering reaction of Zr, $ZrSn_2$, and ZrC at 1200°C for 1 hour followed by 1500°C for 4 hours in an induction furnace yielded $Zr_5Sn_3C$ phase (a=8.4298(8), c=5.799(1) Å) as the major product (80 %); $Zr_2SnC$ was minor. An even better result was obtained from a sintering reaction at 1350°C for 5 days, single phase $Zr_5Sn_3C$ (a=8.4238(5), c=5.8011(7) Å).

The reduced lattice parameters relative to $Zr_5Sn_3$ as well as the quantitative yield provide support that this is a stoichiometric compound.

Further evidence on the stoichiometry was obtained from an X-ray structure analysis of a single crystal. In order to grow single crystals, the pure $Zr_5Sn_3C$ sample from the above 1500°C sintering reaction was arc-melted. A very small crystal (0.005 x 0.005 x 0.01 mm) from this arc-melted button was picked and data collection was carried out with the CAD4 diffractometer. A slightly different hexagonal unit cell (a=8.435(1), c=5.7898(8) Å) from those of sintered products was obtained from the reflections found in the random search. However, the values match quite very well with those from powder pattern (a=8.435(1), c=5.795(1) Å) of the same sample. The extinction conditions fit the $P6_3/mcm$ space group for the supposed $Mn_5Si_3$ structure type. Refinements with zirconium and tin atoms only proceeded well. A difference Fourier

after completion of anisotropic thermal parameter refinement revealed 4 e/Å$^3$ electron density at the origin. Carbon was then included at the origin and the refinement proceeded to R=2.6 and $R_w$=2.6 %. DIFABS was applied for the last convergence. The multiplicities of atoms were also included with that of Zr1 fixed at full occupancy. The refined composition was $Zr_{3.04(1)}Zr_2Sn_{3.006(9)}C_{1.08(6)}$. Within the standard deviations, the composition is stoichiometric. The occupancy of Zr2 showed a 4$\sigma$ deviation from the stoichiometric value. The data collection and refinement parameters are shown in Table 4.

**Nitrogen** Stoichiometric amounts of Zr, $ZrSn_2$, and ZrN powders were sintered at 1100°C for 2 days and subsequently at 1350°C for 3 days. The powder pattern showed an interstitial phase, ZrN, and Zr. The lattice parameters of the interstitial phase were a=8.4030(7), c=5.7695(7) Å, even smaller than those of carbon interstitial. This product was ground and sintered at 1350°C for 5 days. There was about 10 % ZrN along with $Zr_5Sn_3N$ phase in the powder pattern. The lattice parameters (a=8.4050(8), c=5.7700(8) Å) were virtually unchanged from the previous ones even though the relative intensity of this phase had grown considerably. This should mean that the nitrogen interstitial phase has a fixed composition, and this might be stoichiometric.

**Oxygen** Oxygen was one of the most extensively studied interstitial elements. A sintering reaction of Zr, $ZrSn_2$, and $ZrO_2$ powders at 1350°C for 5 days yielded an interstitial phase (a=8.4257(7), c=5.7611(9) Å) plus many impurity lines. A similar result was obtained

Table 4. Data collection and refinement parameters for $Zr_5Sn_3C$[a]

| atom | occupancy | x | thermal parameters (x $10^3$) | | |
|---|---|---|---|---|---|
| | | | $U_{11}$ | $U_{22}$ | $U_{33}$ |
| Sn | 1.002(3) | 0.6034(1) | 5.9(3) | 4.0(5) | 8.8(4) |
| Zr1 | 1 | 1/3 | 5.4(4) | 5.4(4) | 4.0(6) |
| Zr2 | 1.014(4) | 0.2357(2) | 13.6(6) | 6.1(7) | 13.2(6) |
| C | 1.08(6) | 0 | 0.8(4)[b] | | |

| | |
|---|---|
| lattice parameters (Å) | |
| a | 8.435(1) |
| c | 5.7898(8) |
| crystal size (mm) | 0.005 x 0.005 x0.01 |
| $2\theta_{max}$, ° | 55 |
| octants | ±h,k,l |
| reflections | |
| measured | 953 |
| observed | 676 |
| independent | 139 |
| $R_{ave}$, % | 5.3 |
| R, % | 2.6 |
| $R_w$, % | 2.6 |
| largest peak (e/Å$^3$) | 1.5 (0.36, 0, 0.25) |
| absorption corr. method | 2 psi scans and DIFABS |

[a]Refined composition: $Zr_{3.04(1)}Zr_2Sn_{3.006(9)}C_{1.08(6)}$.

[b]$B_{iso}$.

from a higher temperature and a shorter reaction time, 1650°C and 4 hours, a=8.4333(5), c=5.7661(5) Å. In this case, the second phase was identified as unreacted $ZrO_2$. An arc-melting reaction of this sintered pellet took care of the $ZrO_2$, but Zr was an impurity. The lattice parameters (a=8.4361(6), c=5.7643(7) Å) of the interstitial phase changed only slightly from the previous ones. An X-ray structure refinement on data from a single crystal from an arc-melting reaction of $ZrO_{0.1}$, Zr, Sn, and $ZrO_2$ produced a stoichiometric composition, $Zr_3Zr_{2.00(1)}Sn_{3.01(1)}O_{0.92(3)}$. The data collection and the refinement parameters are listed in Table 5.

As a low temperature approach, stoichiometric amounts of Zr, $ZrSn_2$, and $ZrO_2$ powders were loaded in a 7-cm long Ta tube with $ZrCl_4$ as a transporting agent. After 15 days under a temperature gradient of 900⟶850°C, there was neither material transport nor crystallization. However, the powder pattern clearly showed a smaller $Zr_5Sn_3$ phase (a=8.4255(8), c=5.765(1) Å) as well as $Zr_5Sn_4$ and Zr. The lattice parameters are very close to those of other oxygen interstitial products from high temperature sintering reactions, suggesting that this also is an oxygen interstitial phase.

Comparison of the lattice parameters from different systheses showed that the a-parameters of the oxygen interstitial products vary with synthetic method while the c-parameters are virtually unchanged. The deviation of the a-parameter between the largest and the smallest is 11σ, which might be a significant sign of partial occupation in some of the samples, whereas the c-parameters are virtually the same. Since

Table 5. Data collection and refinement parameters for $Zr_5Sn_3O$[a]

| atoms | occupancy | x | thermal parameters (x $10^3$) | | |
|---|---|---|---|---|---|
| | | | $U_{11}$ | $U_{22}$ | $U_{33}$ |
| Sn | 1.004(5) | 0.60260(6) | 6.9(3) | 5.8(3) | 13.7(4) |
| Zr1 | 0.998(5) | 1/3 | 6.3(4) | 6.3(4) | 7.7(5) |
| Zr2 | 1 | 0.2359(1) | 10.7(4) | 4.5(5) | 15.4(5) |
| O | 0.92(3) | 0 | 4(2)[b] | | |

| | |
|---|---|
| lattice parameters (Å) | |
| a | 8.4361(6) |
| c | 5.7643(7) |
| diffractometer | Datex |
| $2\theta_{max}$, ° | 55 |
| octants | ±h,k,l |
| reflections | |
| measured | 953 |
| observed | 792 |
| independent | 163 |
| $R_{ave}$, % | 3.0 |
| R, % | 1.8 |
| $R_w$, % | 2.3 |
| largest peak (e/Å$^3$) | 0.3 (0.56, 0.125, 0) |
| second. ext. coeff. (x $10^{-7}$) | 120(10) |
| absorption correction | 2 psi scans |

[a]Refined composition: $Zr_3Zr_{2.00(1)}Sn_{3.01(1)}O_{0.92(3)}$.

[b]$B_{iso}$.

oxygen only shrinks the structure, the smaller ones must be for the more nearly stoichiometric interstitial phase.

As for the possibility of a substoichiometric oxide phase, Zr, $ZrO_{0.1}$, and Sn for the compositions $Zr_5Sn_3O_x$ (x=0.1 and 0.5) were arc-melted. The powder patterns of the as-casts showed single phases with expanded unit cell dimensions over $Zr_5Sn_3$, indicating tin as well as possibly oxygen interstitials (see Part 1). However, after grinding and sintering at 1100°C for 7 days, the x=0.1 sample showed a single phase of a reduced unit cell dimension (a=8.4540(7), c=5.7700(9) Å) from that of binary and the as-cast. The x=0.5 sample, after being ground and sintered at 1100°C for 7 days, showed some unidentified lines in addition to an interstitial phase whose dimensions (a=8.4338(6), c=5.7603(8) Å) were very close to those of larger oxygen phases from the above short sintering reaction and arc-melting reaction products. The 1650°C sintered product, therefore, can be regarded as a substoichiometric oxygen interstitial phase. The results of substoichiometric compounds imply that the $Zr_5Sn_3$ host has a capacity range for oxygen content at temperature as low as 1100°C.

**Thrid period elements**

The relatively low melting points of these elements compared with those of the previous section allow some variety of synthetic techniques. Powder sintering, arc-melting, and annealing reactions were utilized as well as direct vaporization of these elements when applicable. However, in some cases the reaction between the

interstitial reagent and the container Ta became a serious problem in synthesizing stoichiometric compounds. This problem is particularly encountered with pnictides and chalcogenides. The consistency of the lattice parameters and the yields from different reaction approaches should provide some evidence of the stoichiometries of the phases synthesized.

**Aluminum** Arc-melting reactions of the elements yielded an interstitial phase and $Zr_4Al_3$ as second phase (~15 %). Annealing these buttons at 1000°C for about 10 days was enough to obtain single phase $Zr_5Sn_3Al$ (a=8.655(1), c=5.871(1) Å). The lattice parameter expansion upon annealing was large but reproducible. This was probably due to enhanced ordering upon annealing. The expanded lattice parameters are comparable to those of zinc and gallium interstitial compounds whose atomic sizes are close to that of aluminum (below; Table 3). These and the reproducible lattice parameters support that the annealed samples can be considered as stoichiometric aluminum interstitials.

A single crystal was picked from a crushed arc-melted button, and a data collection was made with the CAD4 diffractometer. The lattice parameters from the diffractometer were a=8.599, c=5.848 Å, close to those from the powder pattern. Systematic extinction conditions from the reflection list confirmed the $P6_3/mcm$ space group. The refinement converged with anisotropic thermal parameters of all atoms (R=4.2, $R_w$=6.3 %) (Table 6). However, the stoichiometry of the single crystal was refined as $Zr_{2.99(1)}Zr_2Sn_{2.98(2)}Al_{1.12(2)}$ when the occupancy of Zr1 was fixed at unity. If a partial tin interstitial and full occupancy of

Table 6. Refinement parameters of $Zr_5Sn_3Al$[a]

| atom | occupancy | x | thermal parameters (x $10^3$) | | |
|---|---|---|---|---|---|
| | | | $U_{11}$ | $U_{22}$ | $U_{33}$ |
| Sn | 0.996(4) | 0.6127(1) | 8.2(3) | 3.9(4) | 4.0(4) |
| Zr1 | 1 | 1/3 | 4.3(3) | 4.3(3) | 1.2(7) |
| Zr2 | 0.993(6) | 0.2657(2) | 14.1(6) | 4.8(5) | 6.9(6) |
| Al | 1.12(2) | 0 | 5(1) | 5(1) | 3(2) |

[a]Refined composition: $Zr_{2.99(1)}Zr_2Sn_{2.98(2)}Al_{1.12(2)}$.

the site are to be assumed, the interstitial is 4.7(8) % tin and 95.3(8) % aluminum. Except for the aluminum occupancy of the interstitial site, the host structure is well defined as stoichiometric. The aluminum occupancy deviates from the ideal value by only 6σ which may be insignificant, in which case the phase can be considered as stoichiometric. However, the lattice parameters are smaller than those of annealed samples by 22σ and 16σ for a and c parameters, respectively, implying some vacancies as well as tin substitution. In this case, the of the interstitial site has less aluminum and more tin. This explanation is more likely since the lattice dimension expansion upon annealing cannot be explained by the first possibility, that is, a stoichiometric aluminum interstitial phase.

Overall, the single crystal analysis does not provide strong evidence for a stoichiometric aluminum interstitial phase. Nevertheless, throughout this study, it was evident that essentially no aluminum was substituting into the host structure even during the arc-melting and that the host composition remained stoichiometric. These make it more probable for the annealed sample to be considered as stoichiometric.

Since powder sintering reactions generally produce more reliable results, sintering reactions of Zr, $ZrSn_2$, and $ZrAl_2$ powders were carried out at 1100°C for 7 to 10 days. Surprisingly enough, none of the sintering reactions yielded only the interstitial phase. Instead, there were two $Mn_5Si_3$-type phases in the powder patterns; one smaller than the binary $Zr_5Sn_3$ and one larger than the arc-melted and annealed

$Zr_5Sn_3Al$ (above) phase. The smaller phase could be understood as a solid solution between $Zr_5Al_3$ and $Zr_5Sn_3$. The former is known to have $Mn_5Si_3$-type structure at high temperature,[18] and there are reports of solid solutions of this phase with $Zr_5Si_3$[35] and $Zr_5Sb_3$.[36] The larger phase also may be understood as a mixed interstitial of Al and Sn in the $Zr_5Sn_3$ host. Following the result of the above single crystal refinement, however, the tin lattice site appears to be occupied exclusively by tin. There must be a third phase to balance the equations; however, none was observed in the powder pattern, probably because of the very small amount.

The results of the sintering reactions appeared to be incompleted, however, why such reactions for aluminum interstitial only was slow was not clear. Probably the diffusion was slowed by the presence of the solid solutions mentioned above.

**Silicon** This phase was quantitatively synthesized by a sintering reaction of stoichiometric mixture of Zr, $ZrSn_2$, and Si powders at 1000°C for 6 days. The unit cell dimensions (a=8.6072(9), c=5.844(1) Å) lie betwen those with aluminum and phosphorus interstitials.

$Zr_5Si_3$ is also known as a $Mn_5Si_3$-type compound, but only above 1745°C.[12,37] Therefore, it is unlikely to form a solid solution with $Zr_5Sn_3$ at around 1000°C.

**Phosphorus** The first synthesis of this phase was made by reaction of powdered $Zr_5Sn_3$ with excess phosphorus (Zr:P = 1:1) in a Ta tube at 1000°C for 9 days. An interstitial phase with an expanded lattice (a=8.5554(5), c=5.9173(8) Å) relative to the binary was formed

along with ZrP as the major phase. The Ta tube was attacked by the phosphorus. The product powder was pelleted and fired at 1000°C for additional 10 days. The intensity distribution between these two phases had reversed, but the line positions of the interstitial phase had not changed at all. However, since much of zirconium had been used to form ZrP, there must have been excess tin in the sample, some of which might have occupied the interstitial site. The lattice parameters could not be taken for those of a stoichiometric phase.

A better and cleaner yield of the interstitial phase was obtained when the stoichiometic mixture of $Zr_5Sn_3$ and P was first fired at 500°C for 6 days in a closed silica tube before the mixture was pelleted and sintered at 1100°C for 13 days. The amount of the second phase (ZrP) was much less (~5 %). However, the unit cell dimensions (a=8.5449(5), c=5.9171(7) Å) were smaller than the previous ones.

A similar result was obtained after a sintering reaction of Zr, $ZrSn_2$, and ZrP powders at 1300°C for 8 days. The lattice parameters were a=8.5355(4), c=5.9118(6) Å, even smaller than the previous sample. Phosphorus loss to Ta tube in the course of the reaction appears to be responsible for the inconsistency of the lattice parameters and the yields of these reactions. The results from the second reaction are tentatively taken as representing the stoichiometric compound because of the cleanest yield.

Sulfur The same techniques as in the phosphorus case were utilized. Direct reaction of $Zr_5Sn_3$ and excess sulfur at 1000°C for 7 days in a tantalum tube yielded an interstitial phase (a=8.5041(7),

c=5.9586(9) Å) as well as the major product $Zr_3S_2$. When $Zr_5Sn_3$ was reacted with a stoichiometric amount of sulfur at 500°C for 6 days before the mixture was pelleted and sintered at 1100°C for 13 days, the yield of the interstitial phase became quantitative (a=8.5054(6), c=5.9638(7) Å).

A sintering reaction of a pellet of Zr, $ZrSn_2$, and $ZrS_2$ powders at 1350°C for 5 days yielded essentially the same result as above (a=8.5076(3), c=5.9653(5) Å). In contrast to the phosphorus case, the lattice parameters were highly consistent regardless the synthetic route. The constant lattice dimensions and the quantitative yields of the three different reaction products suggest that a stoichiometric $Zr_5Sn_3S$ phase has been synthesized.

Garcia has reported a single crystal structure refinement of $Zr_5Sb_3S_{0.7}$ from an arc-melted source,[38] implying that substoichiometric sulfur interstitial phase may be existing in the analogous $Zr_5Sn_3$-S system. Because of this possibility and the well defined lattice dimensions of the stoichiometric phase, the possibility of substoichiometric sulfur phase was studied in detail.

Powdered $Zr_5Sn_3$ from a powder sintering reaction was loaded in a silica tube with a stoichiometric amount of sulfur and reacted at 600°C for 4 days. The homogeneous-looking product powder was split into three parts, and each part was mixed with appropriate amounts of Zr and $ZrSn_2$ to make compositions $Zr_5Sn_3S_x$ (x=1/3, 1/2, and 2/3). Each mixture was pelleted and sintered at 1050°C for a week. The powder pattern of the

x = 2/3 sample showed a single phase (a=8.504(1), c=5.868(2) Å) with line positions that were shifted from those of the stoichiometric phase. The x = 1/2 sample showed an impurity $Mn_5Si_3$-type phase (< 5% intensity) in addition to an interstitial phase (a=8.5039(7), c=5.847(1) Å) whose lines were further shifted from those of the x = 2/3 sample. The line positions of this sample were preserved in x = 1/3 sample (a=8.5047(7), c=5.846(1) Å), but the intensity of the second phase grew (~15 %). The second phases in these samples were identical in line positions and they matched with those of binary $Zr_5Sn_3$. Thermodynamics of solid solution requires this $Zr_5Sn_3$-like phase be an interstitial phase even though the lattice dimensions are indistinguishable from those of binary $Zr_5Sn_3$; a very small amount of sulfur interstitial must be the explanation. The lattice parameters are plotted as functions of the loaded sulfur concentration (Figure 1). It is very clear that there is a solid solution between half and full occupations of sulfur in the interstitial site. Below half occupation, there is a two phase region between $Zr_5Sn_3$ and $Zr_5Sn_3S_{0.5}$ and an another solid solution at the low extreme concentration of sulfur. However, the latter has not been explored in this study.

An interesting observation in Figure 1 is that the a-parameters do not change as the sulfur concentration changes within the experimental error limit, but the c-parameter increases parabolically. An explanation is that a sulfur atom in an interstitital site requires certain dimension along a and c axes. As the sulfur concentration increases, S-S repulsion increases between adjacent octahedra, and this

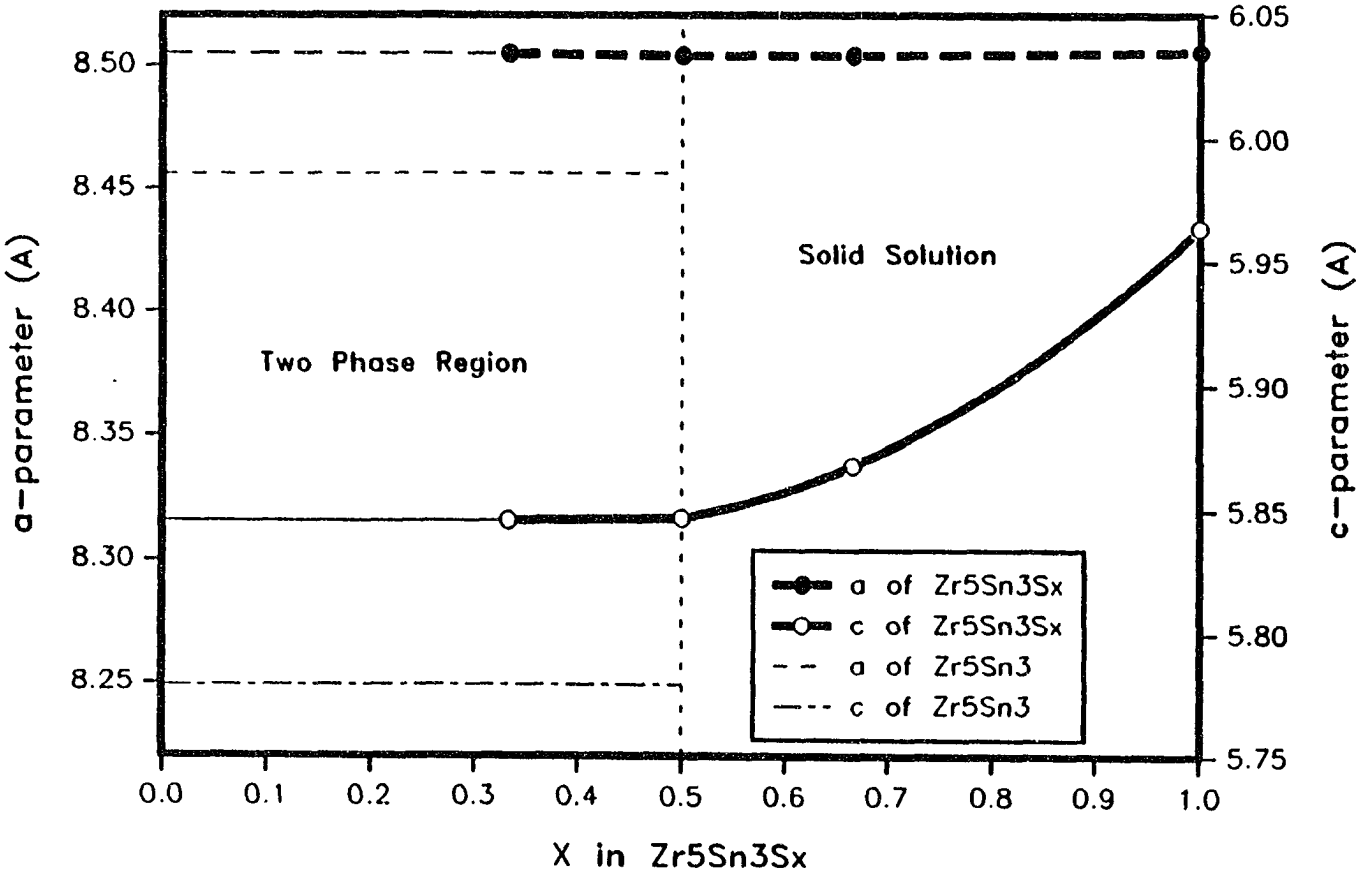


Figure 1. The unit cell parameter change of $Zr_5Sn_3S_x$ as a function of the sulfur content (x). The upper lines are for the a-parameter (left axis) and the lower lines are for the c-parameter (right axis). The lines were extended to x ~ 0 to show the biphasic region between ~0 < x < 1/2. The lattice parameters of the second phase (see text) shown with the narrow lines approximate those of $Zr_5Sn_3$ (x = 0) from comparison of the line positions in the powder patterns.

requires expansion in the c-axis, while the a-dimension is not influenced. In the ideal ordered case, the x=1/2 phase should have alternating S interstitials along the c-axis, the direction the confacial octahedron array, and in this case, there is no strain caused by sulfur-sulfur contact. This is probably why the solid solution limit is near half interstitial. However, the powder patterns of all these substoichiometric phases showed broadening of all the lines that have l ≠ 0 indices. The broadening is more severe when the l index is large. This means that there is a macroscopic distribution of cells with different c-parameters. Thus, even in the sample of x = 1/2, there are some sulfur-sulfur contact. No superstructure was found in the powder patterns.

**Fourth period elements**

In this section, the results of the reactions of the elements from copper to selenium will be discussed. These were the only ones in this period that showed convicing evidence of stoichiometric interstitial phases. The other elements in the same period will be covered in the following section.

Basically, the types of synthetic approaches were the same as in the previous section since the nature of the elements in this period follows that of their next smaller congeners, respectively. In addition, flux and vapor phase transport reactions were attempted in the syntheses.

Copper The copper interstitial of $Zr_5Sn_3$ host was first reported by Rieger et al. in 1965.[28] They synthesized this phase by sintering

under unspecified conditions. However, the quoted lattice dimensions (a=8.75, c=5.90 Å) lack one digit for each parameter compared with those for other phases in the same paper. Moreover, their values are considerably larger than those for other interstitial compounds in the same period (see Table 3) and are rather close to those of $Zr_5Sn_4$ (a=8.7418(7), c=5.926(1) Å), suggesting a possibility of a poor synthesis and misassignment of the product.

Quantitative synthesis of this phase was achieved through sintering reactions. In order to have copper in a powdered reagent, the compounds $Zr_2Cu$ or $Zr_2Cu_3$ were synthesized by arc-melting reactions, and each product was ground to a powder. Conditions of 1000°C and about 10 days were enough to get ternary interstitial phases of copper without any impurities. However, there is a discrepancy between the lattice parameters of the two products from different reactions under the same conditions (a=8.6249(7), c=5.877(1) and a=8.6043(5), c=5.8686(8) Å). The discrepancy must reflect the difference in the interstitial copper content. The larger one presumably is fully occupied, and the latter is partially defective. The latter was examined with a Rietveld refinement analysis. The refinement was unsuccessful because of the couplings between the scale factor, the multiplicities and the thermal parameters of Zr1 and Cu. However, the refinement had a tendency to have partial copper occupancy, < 90 %, implying that the former was closer to the stoichiometric compound.

This phase was also attempted with an isothermal vapor phase transport (mineralizing) reaction starting with Zr, $ZrSn_2$, and CuI at

1000°C for 30 days. The homogeneous-looking black powder product was a single phase in the powder pattern, and gave even larger unit cell dimensions (a=8.636(1), c=5.887(1) Å) than those from above powder sinterings. However, this was considered a partially tin mixed phase. Even though partial tin interstitial at 1000°C did not occur in the binary system, it could be justified by following evidences: First, the reaction was loaded without counting the $ZrI_3$ that would form. The product interstitial phase was forced to be zirconium deficient or tin (and copper) rich. Second, the phases with interstitials of iron, cobalt, and nickel were found to contain partial tin mixed with these elements in the interstitial sites (below). Copper, being next to nickel, may have the same tendency. However, this group of elements as interstitials exhibit a distinction, that is, the copper phase could be synthesized at 1000°C whereas the others were found to be unstable below ~1300°C. The assumed partial tin interstitial phases of copper could be explained in terms of a transition between iron-nickel and the stoichiometric main group interstitial phases.

Zinc Neither arc-melting nor powder sintering was appropriate for this system. Zinc is very volatile, and the synthesis of Zr-Zn binary compounds as reagents for sintering reactions was unsuccessful in this research even though there are some known phases in this system. Another possibility lay with the volatility of zinc in the synthesis.

The interstitial phase of zinc was easily synthesized by reacting $Zr_5Sn_3$ powder with excess zinc at 1000°C for 9 days in a tantalum tube. There were always lines of elemental zinc mixed with those of zinc

interstitial phase (a=8.6325(7), c=5.877(1) Å) in the powder patterns, suggesting that excessive zinc did not upset the material balance by reacting with zirconium or tin.

An attempted crystal growth by a flux reaction of premade $Zr_5Sn_3Zn$ powder and excess zinc in an alumina crucible and a silica tube at 1000°C for 7 days gave some single crystals. However, the structure refinement of this crystal revealed that this was ZrSi in the CrB structure type.

**Gallium** Arc-melting reaction of galliums may present a danger of loss this element as the vapor pressure of gallium is higher than that of tin. Nevertheless, an arc-melting reaction was performed in order to grow single crystals. The corrected composition was $Zr_5Sn_3Ga_{0.99}$ assuming only gallium was lost. The powder pattern showed a single interstitial phase of a=8.599(1), c=5.852(1) Å without any impurity. A large crystal was picked from the crushed button, and data collection was performed with the CAD4 diffractometer. The cell dimensions for this crystal (a=8.595(1), c=5.846(1) Å) are very close to those from the powder pattern. Systematic extinctions and the unit cell dimensions were in accord with the $Mn_5Si_3$ structure type. The refinement converged to $Zr_{3.012(8)}Zr_2Sn_{3.02(1)}Ga_{0.840(5)}$ ($R=2.7$, $R_w=3.7$ %) (Table 7). The structure refinement revealed the very common effect of arc-melting on the single crystals grown, as in the aluminum case. The Zr and Sn atoms are all well behaved with full occupancies and fairly isotropic thermal parameters. However, only 84% of the interstititial site appeared to be

Table 7. Refinement parameters for $Zr_5Sn_3Ga$[a] from arc-melting

| atom | occupancy | x | thermal parameters (x $10^3$) | | |
|---|---|---|---|---|---|
| | | | $U_{11}$ | $U_{22}$ | $U_{33}$ |
| Sn | 1.005(3) | 0.61133(8) | 4.5(2) | 1.9(3) | 3.4(3) |
| Zr1 | 1 | 1/3 | 1.9(3) | 1.9(3) | 1.8(6) |
| Zr2 | 1.008(3) | 0.2634(1) | 8.2(4) | 2.9(4) | 4.4(4) |
| Ga | 0.840(5) | 0 | 4.4(6) | 4.4(6) | 7(1) |

[a]Refined composition: $Zr_{3.012(8)}Zr_2Sn_{3.02(1)}Ga_{0.840(5)}$.

filled by gallium. If partial tin substitution is assumed, the overall occupancy on the interstitial site would be even lower. In fact, this must be the case since the unit cell dimensions of the stoichiometrically synthesized gallium phase are considerably larger (below).

When the arc-melted button was ground and sintered at 1100°C for 2 days and 1350°C for 3 days, the lattice expanded (a=8.6507(8), c=5.869(1) Å), which must mean ordering of elements in the structure was taking place.

Even larger unit cell dimensions were obtained when stoichiometric amounts of Zr, $ZrSn_2$, and $ZrGa_3$ powders were mixed and sintered at 1000°C for 7 days (a=8.6599(6), c=5.8794(8) Å). This sample was further examined with Rietveld powder pattern refinement. The refinement started with the ideal gallium interstitial model. The Zr and Sn atoms refined well with ideal occupancies and thermal parameters. However, these parameters for gallium in the interstitial site were coupled to each other and forced each other to wrong directions, that is, too small multiplicity and thermal parameters. Final convergence was achieved when these two parameters were refined separately, with a stoichiometric composition.

The refinement data in Table 8 were obtained after refinement of the multiplicities and thermal parameters of all the atoms while the scale factor was fixed. This treatment could be justified by the more realistic values thus obtained; otherwise, the thermal parameter of

Table 8. Rietveld refinement parameters for $Zr_5Sn_3Ga$[a]

| atom | occupancy[b] | x | $B_{iso}$ |
|---|---|---|---|
| Sn | 1.000(8) | 0.6117(5) | 1.54(9) |
| Zr1 | 0.99(2) | 1/3 | 1.2(2) |
| Zr2 | 1.00(1) | 0.2674(5) | 1.4(1) |
| Ga | 0.99(3) | 0 | 1.3(4) |

| | | |
|---|---|---|
| 2θ range | 15 - 90 (Cu Kα) | |
| step in 2θ | 0.02 | |
| Profile R | 8.11 | |
| | $R_w$ | 10.78 % |
| Bragg | R(I) | 1.43 |
| | R(F) | 0.72 % |

[a]Refined composition: $Zr_{3.00(3)}Zr_{1.98(4)}Sn_{3.00(2)}Ga_{0.99(3)}$.

[b]Refined with the scale factor fixed (see text).

gallium was too small compared with the other atoms because of probable coupling with the scale factor.

The possiblity of substoichiometric gallium interstitial phase is ruled out by a sintering reaction of the composition $Zr_5Sn_3Ga_{0.5}$. The powder pattern lines were diffuse but the positions of the two sets of $Mn_5Si_3$-type phases could be matched with those of binary (empty) and stoichiometric gallium interstitial $Zr_5Sn_3$ phases.

**Germanium** As in the gallium case, sintering reactions successfully yielded the stoichiometric single phase of the germanium compound. Either elemental germanium or $ZrGe_2$ could be used as the germanium source.

The lattice parameters from a 1100°C (15 day) reaction were a=8.6397(5), c=5.8661(6) Å. Similar but slightly larger values were obtained from a 1350°C (3 day) reaction, a=8.6432(8), c=5.8661(9) Å. The higher temperature product may contain some mixed tin interstitals. In the former case, a few very thin needle crystals grew on the surface of the pellet. They were two small to be handled, however. These needle crystals were also obtained when a composition $Zr_5Sn_3Ge_{0.5}$ was run under the same condition. The powder pattern show broad lines out of which only binary $Zr_5Sn_3$ could be identified. There were many and very small needle crystals on the pellet. One of the crystals (0.003 x 0.003 x 0.03 mm) was picked and mounted on a glass fiber with an aid of glue. This crystal was taken to the Rigaku AFC6R diffractometer, and a data collection was made. A hexagonal unit cell was obtained from randomly registered 15 reflections (a=8.640(9), c=5.882(3) Å). The cell

parameters are very close to those of the stoichiometrically loaded sintering reactions. The refinement parameters are shown in Table 9. The structure refinement started with the ideal model with a germanium interstitial. The refinement converged to R=5.5, $R_w$=5.5 % with anisotropic thermal parameters. The refined composition was $Zr_3Zr_{1.86(4)}Sn_{2.85(6)}Ge_{0.88(4)}$. The deviations were all within standard deviations even though the magnitudes of the deviations were considerably larger than in any other cases. The very weakly diffracting nature of the small crystal must be responsible for these.

**Arsenic** As a preliminary test, powdered $Zr_5Sn_3$ was reacted with excess (Zr:As=5:3) arsenic vapor in a sealed Ta tube at 900°C for 1 day and then at 1000°C for 10 days. Evidently, there was arsenic attack on the Ta tube. The powder pattern, however, showed sharp peaks for an interstitial phase plus ZrAs. The lattice parameters (a=8.6137(5), c=5.9219(9) Å) are comparable to those for the gallium and germanium compounds. When the same reaction was run stoichiometrically under the same conditions, the amount of ZrAs was reduced to 10 %, and the interstitial phase had smaller dimensions than the previous one (a=8.6082(8), c=5.915(1) Å). The first sample had a high possibility of having mixed arsenic-tin interstitials.

A sintering reaction at 1350°C for 5 days starting with premade ZrAs powder yielded almost a single phase with a few faint extra lines, but with dimensions (a=8.6103(8), c=5.920(2) Å) close to those of the second sample. Even smaller lattice parameters (a=8.6037(6), c=5.9200(9) Å) were obtained when stoichiometric amounts of $Zr_5Sn_3$ powder and arsenic

Table 9. Refinement parameters for $Zr_5Sn_3Ge$[a]

| atom | occupancy | x | thermal parameters ($\times 10^3$) | | |
|---|---|---|---|---|---|
| | | | $U_{11}$ | $U_{22}$ | $U_{33}$ |
| Sn | 0.95(2) | 0.6126(3) | 12(1) | 9(1) | 12(1) |
| Zr1 | 0.93(2) | 1/3 | 7(2) | 7(2) | 10(2) |
| Zr2 | 1 | 0.2724(4) | 21(1) | 12(2) | 24(2) |
| Ge | 0.88(4) | 0 | 4(3) | 4(3) | 9(4) |

| | |
|---|---|
| lattice parameters (Å) | |
| a | 8.6397(5) |
| c | 5.8661(6) |
| $2\theta_{max}$, ° | 55 |
| crystal size (mm) | 0.003 x 0.003 x 0.03 |
| octants | h,±k,±l |
| reflections | |
| measured | 1101 (h≥k) |
| observed | 664 |
| independent | 130 |
| $R_{ave}$, % | 10.8[b] |
| R, % | 5.5 |
| $R_w$, % | 5.5 |
| largest peak (e/Å$^3$) | 3.6 (0.44,0.02,0.24); -3.1 |
| absorption coeff. ($cm^{-1}$, Mo Kα) | 201 |
| absorption correction | DIFABS |

[a]Refined composition: $Zr_3Zr_{1.86(4)}Sn_{2.85(6)}Ge_{0.88(4)}$.

[b]Includes all the reflections.

were first reacted at 500°C in a silica tube before the powder was pelleted and sintered at 1100°C for 13 days in a tantalum tube.

The last data seem to represent the stoichiometric phase judging from the single phase nature and the well defined crystal dimensions. The second phase may be contaminated by tin mixing because the material balance forced the system to be tin-rich. The third sample, even though it is almost a single phase, has unusually different sizes for the standard deviations for the lattice parameters. Gross inhomogeneity due to dynamic arsenic (and zirconium) loss to tantalum at the high temperature could account for the large standard deviation of the c-parameter of this sample.

In order to test the possibility of substoichiometric interstitial phase, $Zr_5Sn_3$ and $Zr_5Sn_3As$ in equal weights were sintered at 1100°C for 14 days. The powder pattern consisted of diffuse lines of an interstitial phase with line positions between those of the two limiting phases. Even though the diffuse lines must imply incomplete equilibrium, it seems possible to have compositions with partially occupied interstitial positions in temperature range of 1000 to 1350°C.

**Selenium** Similar approaches to those used in arsenic case were employed in this system. Powders of $Zr_5Sn_3$ and a three-fold excess of selenium were reacted in a Ta tube at 900°C for 1 day and 1000°C for 10 days. The result was a mixture of many phases among which the $Zr_3Se_2$ and an interstitial phase (a=8.567(1), c=5.963(1) Å) could be distinguished. Selenium attack on Ta must have taken place, even though it was not clear from the powder pattern. When the amount of selenium

was held to the stoichiometric value, the powder pattern became much simpler and was composed of $Zr_5Sn_3Se$ (a=8.5595(4), c=5.9495(5) Å) plus $Zr_3Se_2$ (< 10 %) only. Another sintering reaction of Zr, $ZrSn_2$, and $ZrSe_2$ at 1000°C for 9 days yielded similar results (a=8.5572(6), c=5.9535(7) Å). The invariability of the lattice dimensions of the interstitial phase in these two reactions suggest that they are stoichiometric. However, partial interstitial phase may also exist since arsenic and sulfur showed such behavior.

Several attempts were made to grow single crystals of this phase with vapor phase transport techniques with $ZrCl_4$ as a transporting agent. However, most of these reactions crystallized the $Zr_3Se_2$ phase, not the desired one. Nevertheless, the impurity of $Zr_3Se_2$ from sintering reaction could be separated by this technique from the desired $Zr_5Sn_3Se$ when a temperature gradient was utilized in the transport reaction. The powder pattern of the microcrystalline part of the reaction products show single phase of a selenium interstitial compound with a larger lattice dimensions (a=8.5626(5), c=5.9617(7) Å) than the previous ones. It is suspected, however, that this phase may be contaminated by mixed tin because, judging from the amount of the crystal $Zr_3Se_2$, the overall composition of the interstitial sample must be very selenium deficient.

**Substoichiometric tin interstitial** The stoichiometric $Zr_5Sn_4$ phase and the single crystal structure refinement of $Zr_5Sn_{3.18}$ phase arc-melting were discussed in Part I. In this section, the single crystal refinement of another substoichiometric phase will be discussed.

The difficulty in obtaining homogeneous samples in $Zr_5Sn_3$-$Zr_5Sn_4$ system from annealing reactions around 1000°C was already described in Part I. In order to overcome the sluggish diffusion, high temperature annealing at 1800°C of an arc-melted button of nominal composition $Zr_5Sn_3$ in a capped molybdenum crucible was attempted. The resultant powder pattern showed a slightly larger unit cell dimension (a=8.4802(5), c=5.7950(7) Å) than did $Zr_5Sn_3$ at low temperature. Partial tin self-interstitials seemed evident. Nevertheless, the lines did not show tailing in the powder pattern, meaning better homogeneity than the as-cast or low temperature annealed samples. A single crystal was obtained from the crushed button, and data collection was carried out with the CAD4 diffractometer. It was hoped that the refinement would reveal stoichiometric empty $Zr_5Sn_3$ structure. However, the difference Fourier after the refinement with the ideal model of empty $Zr_5Sn_3$ showed a large residual peak at the origin, and therefore, partial tin was included in the refinement. The refinement converged with anisotropic thermal parameters of all the atoms (R=2.1, $R_w$=4.9 %). The composition was determined as $Zr_{2.97(2)}{}^{Zr_2}Sn_{3.03(1)}{}^{Sn}0.096(6)$. Overall features of the structure resemble those of the $Zr_5Sn_{3.18}$ structure (Part I). The crystallographic parameters and are listed in Table 10. The lattce parameters of this phase are between those of empty $Zr_5Sn_3$ (a=8.4560(7), c=5.779(1) Å) and $Zr_5Sn_{3.18}$ (a=8.5036(9), c=5.820(1) Å),[27] (Part I) confirming the amount of the interstitial tin in the crystal structure.

Table 10. Refinement parameters for $Zr_5Sn_{3.10}$[a]

| atom | occupancy | x | thermal parameters (x $10^3$) | | |
|---|---|---|---|---|---|
| | | | $U_{11}$ | $U_{22}$ | $U_{33}$ |
| Sn1 | 1.011(4) | 0.6087(1) | 4.0(3) | 1.9(5) | 3.5(5) |
| Zr1 | 1 | 1/3 | 2.0(4) | 2.0(4) | 8.0(7) |
| Zr2 | 0.990(6) | 0.2480(2) | 6.4(6) | 2.3(7) | 7.1(7) |
| Sn2 | 0.096(6) | 0 | 20(8) | 20(8) | 10(1) |

[a]Refined composition: $Zr_{2.97(2)}Zr_2Sn_{3.03(1)}Sn_{0.096(6)}$.

**Iron, cobalt, and nickel**

These systems were characterized by the fluctuating lattice parameters of the interstitial phases depending on synthetic conditions. This fluctuation was found to be caused by the formation of mixed interstitials of tin and the desired elements plus other phases. The results of the iron system led to the study of other compositions in Zr-Sn-Fe system and finally to the finding of two new phases.[39] These phases will be discussed in Part IV as far as their syntheses and structures. In this section, the diagnosis of the mixed interstitial problem will be discussed in detail.

Iron This system has been extensively studied in the hope of making a new one-dimensional magnetic material. Various techniques were applied for the syntheses.

A seemingly single phase was obtained from an arc-melting reaction of the stoichiometric composition. The lattice parameters were expanded considerably from those of the host (a=8.599(2), c=5.853(1) Å). However, there always was a very diffuse but evident extra line in the powder pattern that could be attributed to $ZrFe_2$. This indicated that the interstitial phase was not stoichiometric. Annealing these arc-melted buttons at 1000°C to homogenize them only made the line of the interstitial phase very diffuse. The same is true up to 1150°C.

Sintering reactions at the temperature range 1000-1150°C starting with combinations of $Zr_5Sn_3$ and Fe or Zr, $ZrSn_2$ and Fe always yielded different products from the arc-melting and annealing reactions. The powder patterns were composed of three different phases; two $Mn_5Si_3$

types and $ZrFe_2$. The lattice parameters of the $Mn_5Si_3$ type phases varied depending on the loaded composition (a=8.4219(5), c=5.7632(6) and a=8.671(1), c=5.884(1) Å from a $Zr_5Sn_3Fe$ composition; a=8.412(2), c=5.788(2) and a=8.7231(7), c=5.912(1) Å from a $Zr_5Sn_3Fe_{0.75}$ composition). These are distinctly different from the binary $Zr_5Sn_3$ and $Zr_5Sn_4$ phases and even from the as-cast iron interstitial compound. The smaller lattice parameters from each case must correspond to iron-substituted $Zr_5Sn_3$ phases on the zirconium sites. The identity of the larger phases is ambiguous; they are too large for an iron-only interstitial and too small to be binary $Zr_5Sn_4$. Moreover, the Zr-Sn system does not have a solid solution at this temperature. Mixed interstitial of iron and tin would be the most plausible answer.

The powder patterns from high temperature (above 1300°C) annealing were different from those obtained at 1000-1150°C. They usually looked like single phases except that the $ZrFe_2$ line was present with a lot lower intensity in each of the powder patterns. The lattice parameters of the as-cast samples were preserved. A similar problem to that encountered with arc-melted binary Zr-Sn samples (Part I) was assumed, and in this case, with the crystallites of $ZrFe_2$ plus the interstitial phase in the as-cast. An arc-melted button was ground and sintered at 1300°C for 3 days in an attempt to remove these crystallites. The powder pattern appeared to be that of a single phase. In order to confirm the compositions, the annealed and sintered samples from 1300°C reactions were examined with SEM/EDX. The EDX of the annealed button showed three distinct compositions; $Zr_5Sn_{3.64}Fe_{0.32}$ as a major and

$Zr_5Sn_{3.98}Fe_{0.63}$ and $ZrSn_{0.75}Fe_{1.08}$ as minor components. The analyses of the minor phases were not as accurate because the regions were too small to analyze quantitatively with EDX. Nonetheless, it was obvious that even the seemingly single phase sample according to the powder pattern had extra phases. Moreover, the compositions of the major interstitial phase was not what was expected. It was rather close to $Zr_5Sn_3(Sn_{2/3}Fe_{1/3})$. The sintered sample was no better in terms of the composition of the major phase. The compositions determined were $Zr_5Sn_{3.29}Fe_{0.49}$ from the majority of the sample and $ZrSn_{0.04}Fe_{1.65}$ from the minor islands. The composition of the interstitial phase in this sample could be approximated as $Zr_5Sn_3(Sn_{1/3}Fe_{1/2})$.

The EDX/SEM results indicate that there are mixed interstitial, and, in conjunction to the lattice parameters, that the arc-melting reaction gives approximately $Zr_5Sn_3(Sn_{1/3}Fe_{1/3})$ composition. The other phase is tin-substituted $ZrFe_2$.

When an arc-melting reaction was carried out with $Zr_5Sn_3(Sn_{1/3}Fe_{1/3})$ composition, the product button became extremely fragile, and the lattice parameters were close to the as-casts of stoichiometric reactions. Furthermore, the button did not respond to a magnetic field at room temperature. The previous samples were attracted by a magnet, a probable sign of the presence of $ZrFe_2$. Likewise, when a $Zr_5Sn_3Fe_{1/3}$ composition was arc-melted, the button reacted to a magnet, and the powder pattern was composed of $ZrFe_2$ plus broad lines of a $Mn_5Si_3$-type phase with low and high angle edges that corresponded to the line positions of $Zr_5Sn_{\sim 3.3}$ and $Zr_5Sn_3$, respectively. This is a good

indication that the iron atoms are only incorporated into the interstitial sites with a certain amount of tin.

The above results prompted a further study on the solid solution range of $Zr_5Sn_3$ host for mixed iron and tin interstitials. Compositions $Zr_5Sn_3(Sn_xFe_{1-x})$ (x=1/3, 1/2, and 2/3) were arc-melted. The as-casts showed broad lines in the powder patterns. However, it was evident that there was no $ZrFe_2$ line except the iron-richest sample. Sensitivities to a magnetic field of these samples were in accordance to the powder patterns; only the iron-richest sample responded. The powder patterns became very sharp upon annealing at 1300°C for 8 days. The lattice parameters increased with the tin content up to a=8.7095(8), c=5.904(1) Å for x = 2/3. These samples were further analyzed with EDX for the compositions. As indicated by the sharp powder patterns, these samples were homogeneous under SEM. The determined compositions were $Zr_5Sn_{3.28}Fe_{0.53}$, $Zr_5Sn_{3.30}Fe_{0.42}$, and $Zr_5Sn_{3.52}Fe_{0.33}$ (aveages for two data for each) for x=1/3, 1/2, and 2/3, respectively. The first two showed very small amounts of $ZrFe_2$. The composition of a 1300°C annealed sample for $Zr_5Sn_{3.33}Fe_{0.33}$ was determined as $Zr_5Sn_{3.19}Fe_{0.36}$.

When these 1300°C annealed samples were annealed at 1000°C for 10 days, the powder patterns became similar to the sintering reaction products at the same temperature; there were two $Mn_5Si_3$-type phases with diffuse lines. The solid solution appear to exist only at high temperature, ≥ 1300°.

An arc-melted and annealed (1300°C, 8 days) sample of

$Zr_5Sn_3(Sn_{1/3}Fe_{1/3})$ (or $Zr_{15}Sn_{10}Fe$) showed three extra reflections in the powder pattern. These and the other lines were indexed with a hexagonal unit cell with dimensions twice those of the original ones (a'=2a, c'=2c). In an effort to understand the ordering, single crystals were examined using X-ray oscillation and Weissenberg photographs, and on the Rigaku AFC6R diffractometer by tuning on the superlattice reflections. However, no confirmation of a superstructure was found by these X-ray means.

**Cobalt** An arc-melting reaction of a stoichiometric sample produced an interstitial phase (a=8.585(2), c=5.845(1) Å) plus $ZrCo_2$ as an impurity. Annealing this button at 1100°C yielded very diffuse lines in the powder pattern suggesting a behavior like with the iron interstitial.

Different sets of lattice parameters were obtained from sintering reactions. Stoichiometric amounts of Zr, $ZrSn_2$, and $Zr_2Co$ powders to produce $Zr_5Sn_3Co$ were mixed, pelleted, and sintered at 1650°C for an hour in a sealed tantalum container in an induction furnace. The pellet partly melted and reacted with tantalum tube. The unit cell dimensions (a=8.5937(6), c=5.8569(9) Å) of the interstitial phase were larger than for the as-cast sample. In addition to this, the $ZrSnCo_2$ phase was found in the powder pattern, indicating that the interstitial phase did not have stoichiometric amount of cobalt.

Another sintering reaction at 1350°C for 3 days yielded even larger dimension for the interstitial phase (a=8.6013(7), c=5.870(1) Å). Since the powder pattern of this sample appeared to be that of the pure phase,

a Rietveld analysis was carried out. The refinements of the thermal parameters and the multiplicities of the atoms in their ideal positions revealed that the multiplicity of the interstitial cobalt appeared to be 120 % while the other atoms had close to the ideal values. It is very obvious that tin atoms are mixed with cobalt in the interstitial site.

Inspired by the result of iron interstitial system as well as the antimony analogue (Part IV), a composition $Zr_5Sn_3(Sn_{1/3}Co_{1/3})$ was arc-melted. The button was extremely brittle, and the lattice parameters (a=8.5934(7), c=5.861(1) Å) were in the range of the values from other samples. These observations are very similar to those of iron interstitial system. Therefore, it was concluded that the cobalt interstitial phase had mixed tin and partial cobalt interstitials.

**Nickel** Similar to the iron and cobalt stoichiometric cases, as-cast products of a stoichiometrically loaded reaction showed an interstitial phase (a=8.5755(4), c=5.8538(6) Å) and $ZrNi_3$. Sintering reactions at 1600°C and 1300°C produced similar powder patterns except that the line positions were shifted from those of the as-cast.

When a composition $Zr_5Sn_3(Sn_{1/3}Ni_{1/3})$ was arc-melted, almost the same powder pattern of a single $Mn_5Si_3$-type phase was obtained as for the stoichiometric reactions (a=8.5812(6), c=5.8577(8) Å). Therefore, a mixed tin and nickel interstitial phase was concluded to be the phase in this system.

## Other attempted interstitial phases

**Fluorine and chlorine** Since many elements in second and third periods successfully formed interstitial phases, whether one could synthesize halogen interstitial phases was an intriguing question. There are some examples of halogen interstitial phases in $Mn_5Si_3$-type hosts of alkaline-earth metals and pnictogens. These phases could be understood as valence compounds from the structures.

Stoichiometric amounts of Zr, $ZrSn_2$ and $ZrF_4$ or $ZrCl_4$ powders were pressed into pellets, and these pellets were heated at 700°C for 5 days and then at 1000°C for 7 days. The products showed white needle crystals of zirconium halides indicating that halides did not form interstitial phases with the $Zr_5Sn_3$ host.

The powder pattern of fluorine compound showed $Zr_5Sn_3$ and $Zr_5Sn_4$ phases which agreed with the observation of $ZrF_4$. However, the chlorine compound showed an additional phase: Gem-like crystals were embedded in the pellet which, otherwise, was $Zr_5Sn_3$ as confirmed by the powder pattern. A crystal was separated from the matrix and placed in a capillary. The oscillation photographes showed well defined peaks. This crystal was eventually mounted on the SYNTEX diffractometer. The reflections from rotation photograph were indexed in an monoclinic cell ($a$=5.290, $b$=5.191, $c$=5.123 Å, $\beta$=99.27°). These are very close to the reported values of monoclinic zirconium. Monoclinic zirconium has been known since 1968;[40] however, no structural detail has been reported. Therefore, data collection was made but the refinement has been unsuccessful. The attempted models from Patterson map did not converge.

The presence of zirconium as well as $ZrCl_4$ and $Zr_5Sn_3$ upsets the material balance, and this can not be expained. At any rate, these two reactions demonstrated the inability to form halogen interstitial phases.

**Titanium to manganese** Several preliminary reactions were run by arc-melting technique to see whether these were possible interstitials phases. The results were all negative. The titanium sample, after being annealed at 1000°C for 3 days, showed only very diffuse lines in the powder pattern. Titanium substitution to the zirconium sites is assumed because they are in the same group, and there are some examples of such isomorphous substitution in the $Zr_5Sb_3$-Ti system.[41]

The vanadium compound yielded a sharp powder pattern from the as-cast sample. However, the lattice parameters (a=8.4508(5), c=5.7653(6) Å) of the apparently $Mn_5Si_3$-type phase are close to the binary $Zr_5Sn_3$ phase. Even though there was a lattice expansion, the magnitude was even smaller than the boron interstitial compound. Moreover, there were a few lines that could be identified as vanadium. These results suggest that vanadium was not incorporated to the host or in a very small amount, if any.

Chromium behaved similarly to vanadium. Arc-melting and annealing reactions at 1000°C for 3 days yielded rather small lattice parameters (a=8.4987(6), c=5.8145(8) Å). There were a few unidentified extra lines in the powder pattern. When the composition was loaded as $Zr_5Sn_3(Sn_{1/3}Cr_{1/3})$ as in the iron interstitial case, the as-cast product showed a single phase of $Zr_5Sn_{3.3}$ (a=8.5535(8), c=5.8522(9) Å) plus

elemental chromium. It is evident that chromium was not incorporated into the interstitial site.

Applying arc-melting reaction to manganese is difficult because of its low boiling point. Nonetheless, the arc-melting reaction exhibited a convincing clue of the inability of manganese to form interstitial phase. When the arc-furnace was opened to air after finishing arc-melting reaction, there were many manganese particles that reacted with the air around and on the arc-melted button. If manganese were to form a compound with the host, it would not remain as element form. The lattice parameters (a=8.5261(8), c=5.833(1) Å) are larger than those of other unsuccessful cases, but much smaller than any other interstitial phases.

**Cadmium** The possibility of cadmium interstitial phase has been briefly tested by reacting $Zr_5Sn_3$ powder with cadmium at 1000°C for 11 days. Under similar conditions, the zinc compound was synthesized successfully. However, the powder pattern only showed $Zr_5Sn_3$ phase with no change in the lattice parameters at all. The relatively large atomic size of cadmium might be the reason.

**Silver** Powder sintering reactions at 1000°C were mainly tried for this system. Elemental silver or ZrAg were used for the reagents.

The resultant powder patterns consisted of $Zr_5Sn_3$ and an interstitial phase. However, the interstitial phase therein had rather different lattice parameters (a=8.670(1), c=5.912(1); a=8.717(9), c=5.938(8) Å) from different reactions under almost identical conditions, the former starting with ZrAg and the latter with elemental

silver. The lattice parameters are between those of $Zr_5Sn_3$ and $Zr_5Sn_4$. Therefore, these phases probably contain silver interstitials in different amounts. The fluctuating lattice parameters as well as the presence of $Zr_5Sn_3$ in all the reactions indicate that this system behaves as does the one with iron interstitial, that is, with mixed interstitials with a range of proportions.

## Interstitial Compounds of $Zr_5Pb_3Z$

In general, synthesis with elemental lead is limited in the choice of temperature range. Several attempted arc-melting reactions of lead and zirconium demonstrated that almost half of the lead was lost through vaporization. Therefore, a sintering reaction technique was primarily utilized. However, in order to do sintering reactions, a binary compound of Zr and Pb richer in lead than $Zr_5Pb_3$ was needed because this, zirconium powder, and the binary compounds of zirconium and the third element were to be used. Fortunately, a new phase $Zr_5Pb_4$ was found and used for this purpose. $Zr_5Pb_4$ itself is the self-interstitial compound in this series, and its synthesis and characterization will be described in the corresponding subsection. Vapor phase transport reactions were another important route for the syntheses. Unlike the tin analogues, some of the lead systems yielded crystalline products.

Because of the profound gap between lead and the second period elements in their physical properties, these elements were not investigated. In order to synthesize these compounds, very high

host (above) and at high temperature lead loss by volatilization would occur. Therefore, control over reactions and the products is thought to be extremely difficult.

The lattice parameters and synthetic conditions of the stoichiometric compounds in this system are shown in Table 11.

**Third period elements**

The syntheses of compounds in this family were straightforward with sintering reactions. However, complications in the crystal structure of vapor phase transport product with aluminum as the interstitial rendered this element different from the others.

**Aluminum** A sintering reaction of stoichiometric amounts of $Zr_5Pb_4$, Zr, and $ZrAl_2$ powders at 1000°C for 11 days yielded a single phase product (a=8.7871(5), c=5.9460(7) Å). These lattice parameters were reproducible under the same reaction conditions. This is a deep contrast to the tin analogue where sintering reactions always yielded mixtures and gave mixed interstitials. The consistency of lattice parameters as well as the reproduceability of the synthesis indicated that the stoichiometric interstitial compound was indeed obtained.

A vapor phase transport reaction with the same reagents plus $ZrCl_4$ as a transporting agent was attempted with a temperature gradient of 1000⟶950°C for 20 days. Almost complete material transport was achieved as well as very large crystals. However, the Guinier lattice parameters of these crystals were a=8.7761(9), c=5.936(1) Å, which were

Table 11. Interstitial compounds of $Zr_5Pb_3Z$

| elements | synthetic condition[b] | crystal parameters[a] | | | |
|---|---|---|---|---|---|
| | | a(Å) | c(Å) | V(Å$^3$) | c/a |
| Al | S | 8.7871(5) | 5.9460(7) | 397.60(6) | 0.677 |
| Si | S | 8.6830(6) | 5.8968(7) | 385.03(7) | 0.679 |
| P | S | 8.6044(5) | 5.9660(8) | 382.52(7) | 0.693 |
| S | S | 8.5789(7) | 6.0027(9) | 385.60(8) | 0.698 |
| Fe | S | 8.705(1) | 5.922(1) | 388.6(1) | 0.680 |
| Co | S | 8.6832(5) | 5.8851(5) | 384.28(5) | 0.678 |
| Ni | S | 8.6261(7) | 5.8916(8) | 379.66(8) | 0.683 |
| Cu | S | 8.6847(6) | 5.9123(7) | 386.19(7) | 0.681 |
| Zn | F | 8.7341(7) | 5.929(1) | 391.70(9) | 0.679 |
| Ga | S | 8.7451(5) | 5.9230(6) | 392.29(6) | 0.677 |
| Ge | S | 8.6924(6) | 5.9128(8) | 386.90(7) | 0.680 |
| As | S | 8.6298(8) | 5.953(1) | 383.9(1) | 0.690 |
| Se | S | 8.6312(8) | 5.9796(9) | 385.78(9)[c] | 0.693 |
| Ag | S | 8.767(2) | 5.965(2) | 397.0(2) | 0.680 |
| Cd | F | 8.8240(6) | 5.9876(7) | 403.76(7) | 0.679 |
| In | S | 8.8458(7) | 5.9989(8) | 406.50(9) | 0.678 |
| Sn | S | 8.838(1) | 6.000(1) | 405.9(1) | 0.679 |
| Sb | S | 8.664(1) | 5.937(1) | 386.0(1) | 0.685 |
| Te | S | 8.6770(7) | 5.964(1) | 388.9(1) | 0.687 |
| $Zr_5Pb_3$ | S | 8.5352(6) | 5.8405(7) | 368.47(7) | 0.684 |
| $Zr_5Pb_4$ | F,S | 8.873(1) | 6.019(1) | 410.4(1) | 0.678 |
| $Zr_5Pb_{>3.5}$[d] | S | 8.7419(6) | 5.9675(6) | 394.94(6) | 0.683 |

[a]Stuffed-$Mn_5Si_3$ ($Ti_5Ga_4$-type) (space group $P6_3/mcm$).

[b]S = powder sintering; F = flux.

[c]average from more than one sample.

[d]From a mixture with $Zr_5Pb_3$ in a reaction for $Zr_5Pb_{3.5}$ (see text).

considerably smaller than for the sintered products. Similar problems to those of single crystals of tin analogue grown by arc-melting might be occuring. The problem was further confirmed by an X-ray structure analysis of one of these crystals. A crystal was mounted on the CAD4 diffractometer, and data were collected.

Indexing of 25 randomly found reflections gave a hexagonal unit cell with the lattice parameters in the expected ranges, however, with 20 % of the reflections excluded; these had simple fractional h and k indices while the l indices were integral in this unit cell. Twinning with common c-axis could explain this observation. A superstructure to account for the extra reflections seemed unlikely because the fractional indices showed no systematics. However, since no film work was done on this crystal, a superstructure still remained as a possibility.

The refinement of the data with aluminum interstitial had some problems. The refined composition was $Zr_{3.07(6)}Zr_2Pb_{3.04(2)}Al_{1.79(9)}$. Alternatively, the interstitial site is 85(2) % aluminum and 15(2) % lead assuming full occupancy. The interstitial aluminum had severely elongated thermal parameters when refined anisotropically ($U_{11}/U_{33}$=1/9). Contrarily, the other atoms in the host behaved well in the refinement with correct stoichiometries and fairly isotropic thermal parameters. The poor R indices (R=3.2, $R_w$=10.6 %) also indicated that the refinement had problems. Moreover, the smaller lattice parameters of this sample than those of sintering indicated that the interstitial site was not fully occupied, that is, the crystal had more lead and less aluminum

Table 12. Refinement parameters for $Zr_5Pb_3Al$[a]

| atom | occupancy | x | thermal parameters (x $10^3$) | | |
|---|---|---|---|---|---|
| | | | $U_{11}$ | $U_{22}$ | $U_{33}$ |
| Pb | 1.012(8) | 0.6141(3) | 8.8(7) | 7.4(9) | 7.9(9) |
| Zr1 | 1 | 1/3 | 6.3(1) | 6.3(1) | 9.9(3) |
| Zr2 | 1.02(2) | 0.2701(7) | 10.3(2) | 9.9(2) | 9.7(3) |
| Al | 1.79(7) | 0 | 0.3(2)[b] | | |

[a]Refined composition: $Zr_{3.07(6)}Zr_2Pb_{3.04(2)}Al_{1.79(7)}$ (or $Zr_{3.07(6)}Zr_2Pb_{3.04(2)}Al_{0.85(2)}Pb_{0.15(2)}$).

[b]$B_{iso}$.

interstitials than the refinement results. The refinements results are presented in Table 12.

In order to overcome this mixed and partial interstitial problem, a powder of already synthesized $Zr_5Pb_3Al$ was used in another vapor phase transport reaction. A milder condition of 950⟶850°C was tried. The reaction, however, showed a little material transport and the transported material was microcrystalline.

Further study of the transport reaction with various conditions including variations of temperature and reagent ratios, should give fruitful results and an understanding of this interstitial system.

**Silicon** Stoichiometric amounts of $Zr_5Pb_4$, Zr, and Si powders were pelleted and sintered at 1000°C for 16 days. The powder pattern showed an intersititial phase plus some dim impurity lines. The same lattice parameters were obtained in another sintering reaction at 1350°C for 5 days that started with $Zr_5Pb_4$ and $Zr_5Si_4$ (a=8.6830(6), c=5.8968(7) Å). There were no extra lines in the powder pattern, meaning that the stoichiometric compound was formed.

**Phosphorus** As in the tin analogue synthesis, phosphorus attack on the tantalum tube and the high stability of ZrP gave problems in the synthesis of this phase. The first attempted sintering reaction was loaded with stoichiometric amounts of $Zr_5Pb_4$, Zr, and ZrP powders. The reaction was first carried out at 900°C for 9 days and, then, 1350°C for 5 days. An interstitial phase was formed (a=8.6022(4), c=5.9546(7) Å) plus extra lines among which unreacted ZrP was identified. A better yield was achieved when $Zr_5Pb_3$ powder was reacted with stoichiometric

amount of phosphorus vapor at 500°C for 7 days, and the product powder was sintered at 1000°C for 11 days. Almost quantitative yield of the interstitial phase (a=8.6044(5), c=5.9660(8) Å) was obtained. The c-parameters are virtually identical but the a-parameters differ by 3.4σ. About 5 % of ZrP (intensity) was identified in the powder pattern.

Since ZrP is light in weight and small in amount relative to the other reagents, the first synthesis might have started with deficient phosphorus. The almost quantitative yield and larger lattice parameters of the second synthesis suggest that it is more nearly stoichiometric.

Sulfur The synthesis of this phase follows that of the tin analogue. Stoichiometric mixture of $Zr_5Pb_4$, Zr, and $ZrS_2$ was sintered at 900°C for 9 days followed by sintering at 1350°C for 5 days. A single intersititial phase was obtained (a=8.5829(7), c=5.9891(8) Å). Similar single phase result was obtained when powder of $Zr_5Pb_3$ was first reacted with stoichiometric amount of sulfur vapor at 500°C for 7 days and, then, the mixed powder was sintered at 1100°C for 13 days (a=8.5790(6), c=5.9933(7) Å).

A slightly different set of lattice parameters was obtained when the second type of synthesis was repeated except that a stoichiometric mixture of $Zr_5Pb_4$ and Zr was used instead of premade $Zr_5Pb_3$. However, the first step in the reaction at 700°C showed lead drops in the powdered mixture. This was probably because $Zr_5Pb_4$ started decomposing at this temperature. Material imbalance was apparent, and this was reflected by the presence of the impurity phases (<5 %) in the final product. The lattice parameters of the interstitial phase were

a=8.5789(7), c=6.0027(9) Å. The a-parameter is virtually identical to the other samples, especially the second one, while the c-parameter is much larger. The difference of the c-parameters of the last two is 8.2σ. This may reflect the effect of substoichiometric sulfur interstitials seen in the tin analogue, where greater than half-occupancy of sulfur in the interstitial site changed only the c-parameters.

Therefore, the last sample that showed the largest c-parameter might be the closest to the stoichiometric phase, and these data are listed in Table 11. Since the first sample was synthesized at higher temperature than the others, it had more chance to have mixed interstitial and, therefore, its lattice parameters should not be directly compared with the others.

**Fourth period elements**

The same synthetic approaches as in the third period elements were employed. However, even with the sintering technique, which in most of the cases was successful, the syntheses of some phases were not conclusive. Some of the compounds in this series had problems of lead drop formation in the course of the syntheses. This renders these systems rather indefinite.

**Copper** Even though this phase was reported by Rieger et al.,[28] (a=8.665, c=5.926 Å), the misindexed tin analogue meant this phase needed to be reexamined.

As in the tin analogue, sintering reactions of $Zr_5Pb_4$, Zr, and

$Zr_2Cu_3$ powders at 1000°C for 8 to 12 days showed the single interstitial phase in the powder patterns. The lattice parameters (a=8.6847(6), c=5.9123(7) Å) were preserved in other stoichiometrically loaded reactions.

In a sintering reaction for a composition $Zr_5Pb_3Cu_{1/2}$ under the above conditions, there were two $Mn_5Si_3$-type phases in the powder pattern. The line positions of the small phase of these two matched well with the binary host, while the larger one had a=8.671(1), c=5.913(1) Å. The c-parameter is the same as in stoichiometric compound while the a-parameter is smaller. The difference of lattice parameter indicates that there is a range of copper capacity.

An attempted lead-flux reaction (Zr:Cu:Pb = 5:1:20) to grow single crystal of this phase at 700° with gave considerably larger lattice parameters (a=8.7675(9), c=5.9665(9) Å). These are presumably the result of a mixed intersitial phase of copper and lead.

It appears that the copper interstitial system can have both mixed and substoichiometric interstitials which is similar to the tin analogue with copper interstitials.

**Zinc** Powdered $Zr_5Pb_3$ was reacted with a stoichiometric amount of zinc in a tantalum tube at 1000°C for 9 days. The product showed over 90% of interstitial phase plus zinc and an unidentified impurity. This powder was pressed into a pellet and sintered at 1000°C for 12 days. The resultant powder pattern showed an unchanged lattice parameters (a=8.741(1), c=5.936(2) Å) with some extra lines (unidentified).

Single crystal growth was tried with $Zr_5Pb_3$ powder and zinc (300-fold excess) as a flux medium. After reaction at 1000°C for 7 days, there were a few very small needle crystals as well as the major black powder. The powder was an interstitial phase whose lattice parameters were slightly different (a=8.7341(7), c=5.929(1) Å) from above reaction. A single crystal was selected and data collection was carried out with the CAD4 diffractometer. The systematic extinction conditions confirmed the expected space group.

Refinement with an ideal zinc interstitial model showed that the multiplicity of interstitial zinc required more electrons than full zinc occupancy could provide. Lead was included as a mixed interstitial and its multiplicity was refined while the sum of this and zinc was held at unity. Final convergence was achieved with $Zr_5Pb_3(Zn_{0.95(2)}Pb_{0.05(2)})$, or $Zr_5Pb_3Zn_{1.09(6)}$ (Table 13; R=2.8, $R_w$=3.2 %). The occupancies of the atoms in the host were not refined. Within 2σ the refinement was stoichiometric.

Another single crystal growth was tried with the vapor phase transport technique. Powdered $Zr_5Pb_4$ and Zr were loaded in a 7 cm-long tantalum tube with $ZnCl_2$. Since $ZnCl_2$ would be reduced by Zr to form Zn and $ZrCl_4$, their amounts were calculated accordingly. A temperature gradient of 1000⟶950°C was applied for 20 days. The material was almost completely tranported, and there were many $ZrCl_4$ crystals, confirming above presumption. Needle crystals were obtained almost quantitatively. The powder pattern of the powdered needles showed an interstitial phase whose lattice parameters (a=8.7346(7), c=5.9327(9) Å)

Table 13. Data collection and refinements parameters for $Zr_5Pb_3Zn$[a] from flux reaction

| atom | occupancy | x | thermal parameters (x $10^3$) | | |
|---|---|---|---|---|---|
| | | | $U_{11}$ | $U_{22}$ | $U_{33}$ |
| Pb1 | 1 | 0.6157(1) | 5.7(4) | 3.9(5) | 5.4(5) |
| Zr1 | 1 | 1/3 | 5.2(8) | 5.2(8) | 8(2) |
| Zr2 | 1 | 0.2681(3) | 7.2(9) | 6(1) | 8(1) |
| Zn | 0.95(2) | 0 | 3(2) | 3(2) | 1(3) |
| Pb2 | 0.05(2) | | | | |

| | |
|---|---|
| lattice parameters (Å) | |
| a | 8.7341(7) |
| c | 5.929(1) |
| crystal size (mm) | 0.005 x 0.005 x 0.01 |
| $2\theta_{max}$, ° | 45 |
| octants | h,k,±l |
| reflections | |
| measured | 717 |
| observed | 458 |
| independent | 135 |
| $R_{ave}$, % | 3.7 |
| R, % | 2.8 |
| $R_w$, % | 3.2 |
| largest peak (e/Å$^3$) | 2.6 (0, 0.39, 0.64) |
| absorption coeff. ($cm^{-1}$,Mo Kα) | 745 |

[a]The occupancy of the interstitial atoms only was refined assuming full occupancy on this site. Refined composition: $Zr_5Pb_3Zn_{0.95(2)}Pb_{0.05(2)}$.

were closer to those of the first reaction. A crystal was mounted on a capillary, and data collection was made with the Rigaku AFC6R diffractometer.

The crystal had a similar problem to the one with aluminum interstitials. Among the 15 reflections found from a random search, 2 of them could not be indexed with a hexagonal unit cell; their h and k indices were fractional and the l's were integral. A satellite crystal sharing the same c-axis with the main crystal appeared to be responsible. Another support for this was obtained by a zero-layer Weissenberg photograph along the c-axis. Every spot in the photograph was split into two with a 3° separation.

The refinement with an ideal model of zinc interstitial showed a non-positive definite isotropic thermal parameter of the interstitial zinc. An interstitial mixed with about 10 % lead was calculated from the multiplicity refinement. Further refinement with anisotropic thermal parameters of all the atoms as well as the proportion of lead and zinc in the interstitial site resulted in a converged solution (R=8.9, $R_w$=11.2 %). DIFABS was applied and the refinement went to R=6.1, $R_w$=6.6 %. However, the R-indices were still too high and the statistics of the $F_o$ vs. $F_c$ showed that a series of reflections 001 (l=2n) had the worst fit. This might be due to either the satellite crystal or a poor absorption correction of the needle crystal. These reflections were taken out one by one and the R-indices improved accordingly. Removal of 004 resulted in R=4.1, $R_w$=4.5 %, and the R-indices improved progressively with additional removal of 002 (R=3.0,

$R_w$=2.8 %), 006 (R=2.9, $R_w$=2.7 %), and 112 (R=2.7, $R_w$=2.6 %). The removal of 112 reflection was justified by the reduction of residual electron density from 4.2 to 2.8 $e^-/Å^3$ at 0,0,1/4 position. The removal of reflections did not affect the refinement parameters significantly. The refined composition $Zr_3Zr_{2.04(2)}Pb_{3.00(3)}(Zn_{0.880(9)}Pb_{0.120(9)})$ (Table 14) had more interstitial lead than the flux grown single crystal.

The variations of the lattice parameter must reflect the types and the amount of interstitial elements. Therefore, with more lead, the larger lattice parameters were observed. The lattice parameters of the last sample lie between those of the first two, meaning that the first sample has more mixed lead interstitial than the last sample. The unidentified extra lines in the powder pattern of the first sample might be a zinc-rich zirconium phase.

**Gallium** The single phase product was easily synthesized through a sintering reaction of $Zr_5Pb_4$, Zr, and $ZrGa_3$ in stoichiometric ratios at 1000°C for 7 days. The single phase nature of the product indicates that this is a stoichiometric compound. The lattice parameters (a=8.7451(5), c=5.9230(6) Å) are close to those of the zinc compound.

The half-stoichiometric compound was investigated with another sintering reaction under identical condition. The powder pattern showed very clearly two phases; $Zr_5Pb_3$ and $Zr_5Pb_3Ga$.

**Germanium** Attempted syntheses of this phase were always accompanied by free lead in the product. These reactions were carried out by sintering of $Zr_5Pb_4$, Zr, and $ZrGe_2$ at 1000°C for 7 to 11 days.

Table 14. Data collection and refinement parameters for $Zr_5Pb_3Zn$[a] from a vapor phase transport reaction with $ZrCl_4$

| atom | occupancy | x | thermal parameters (x $10^3$) | | |
|---|---|---|---|---|---|
| | | | $U_{11}$ | $U_{22}$ | $U_{33}$ |
| Pb1 | 1.00(1) | 0.61582(6) | 7.8(4) | 6.4(4) | 5.6(5) |
| Zr1 | 1.02(1) | 1/3 | 8.2(8) | 8.2(8) | 3(1) |
| Zr2 | 1 | 0.2686(2) | 8.5(7) | 8.7(8) | 7(1) |
| Zn | 0.880(9) | 0 | 10(1) | 10(1) | 7(1) |
| Pb2 | 0.120(9) | | | | |

| | |
|---|---|
| lattice parameters (Å) | |
| a | 8.7346(7) |
| c | 5.9327(9) |
| crystal size (mm) | 0.1 x 0.1 x 0.4 |
| $2\theta_{max}$, ° | 55 |
| octants | ±h,k,±l |
| reflections | |
| measured | 1809 |
| observed | 1429 |
| independent | 172[b] |
| $R_{ave}$, % | 14.1[c] |
| R, % | 2.6 |
| $R_w$, % | 2.6 |
| largest peak (e/Å$^3$) | 2.8 (0, 0, 0.25) |
| second. ext. coeff (x $10^{-7}$) | 20(2) |

[a]Refined composition: $Zr_3Zr_{2.04(2)}Pb_{3.00(3)}(Zn_{0.880(9)}Pb_{0.120(9)})$.

[b]Without the rejected four reflections (see text).

[c]For all data.

There were $Zr_5Ge_3$ and a seemingly $Zr_5Pb_3$-based interstitial phase (a=8.723(1), c=5.928(1) Å). Probably, the decomposition of $Zr_5Pb_4$ occurs before germanium is accommodated in the interstitial site. Alternatively, germanium substitution for lead in the host could explain this observation. Since $Zr_5Ge_3$ phase was obtained in the product, the latter appears to be the case.

In contrast to the low temperature reactions, a 1350°C sintering reaction yielded a single phase interstitial product but with a smaller unit cell dimension (a=8.6924(6), c=5.9128(8) Å). However, these values are much smaller than the gallium ones and cannot be taken for the stoichiometric phase.

**Arsenic** Drops of lead were found in most of the attempted reactions in this system. The prevailing stability of ZrAs and the decomposition of $Zr_5Pb_4$ appear to be the explanation. Many reactions with various techniques were attempted, including sintering of $Zr_5Pb_4$, Zr, ZrAs (or As) at 1000°C to 1350° and reaction of $Zr_5Pb_3$ with As vapor at 500°C followed by 1000°C sintering. Most of the reactions had the lead drop problem.

An incidental sintering reaction of arsenic with $Zr_5Pb_3$ at 1000°C for 7 days yielded a relatively clean powder pattern (a=8.6298(8), c=5.953(1) Å) with no lead drop but still with ZrAs (< 10 %) and a few extra lines.

The synthesis is indefinite. The lattice parameters are subject to confirmation even though they are about what would be expected.

**Selenium** The general scheme of the synthesis followed that of tin analogues. The interstitial compounds obtained were reproducible. The powder patterns were clean except a few lines of $Zr_3Se_2$ with very weak intensities (<5 %). A 1350°C sintering of mixture of $Zr_5Pb_4$, Zr, Se prereacted at 700°C yielded a=8.632(1), c=5.979(1) Å. A lower temperature sintering of $Zr_5Pb_4$, Zr, $ZrSe_2$ at 1000° for 9 days gave a=8.6303(6), c=5.9802(7) Å. The lattice parameters are so close to each other that they can be considered as those of the stoichiometric phases.

## Fifth period elements

**Silver** Unlike the tin analogue, the synthesis of this phase was straightforward via sintering reaction of stoichiometric mixture of Zr, $Zr_5Pb_4$, and ZrAg at 1000°C for 13 days. The single phase in the powder pattern was indexed to give a=8.767(2), c=5.965(2) Å.

The powder of this product was used for a vapor phase transport reaction with $CdI_2$ under a temperature gradient of 850°⟶800°C. Neither material transport nor crystallization occurred. The lattice parameters were larger than from the above sintered phase. Mixed interstitials of lead, cadmium, and silver are assumed for this phase.

**Cadmium** The synthetic techniques possible for this phase are limited because of the volatility of cadmium and the unavailability of a Zr-Cd binary phase. Direct reaction of $Zr_5Pb_3$ with cadmium appeared to be the only feasible route. However, the conditions of such reaction turned out to be critical for the syntheses.

When stoichiometric amount of $Zr_5Pb_3$ powder and cadmium were reacted at 1000°C for 11 days, there were two distinct $Mn_5Si_3$-type phases. The smaller one had lattice dimensions very close to those of the binary $Zr_5Pb_3$, and the larger one had a=8.790(2), c=5.966(2) Å, somewhat close to what was expected. There were also cadmium drops found in the products suggesting an incomplete reaction. The reaction temperature of 1000°C might have been too high to use for elemental cadmium. Therefore, a temperature below the boiling point of cadmiun (765°) was tried. A powder of $Zr_5Pb_3$ reacted with excess cadmium (Zr:Cd = 1:1) at 700°C for 7 days followed by quenching yielded a very peculiar result. There were many metallic needle crystals grown on the surface of what appeared to be unreacted cadmium. The reaction was quantitative as no other zirconium or lead phases were found, and the crystals were easily separated from the cadmium mechanically. The powder pattern of the crystal showed a single interstitial phase (a=8.8240(6), c=5.9876(7) Å). Some of the crystals were tested with ocsillation photographs and unfortunately, they were all multiple.

This observation of quantitative crystal growth, though not of good quality, is highly reproducible under the same reaction conditions. However, some variations of the conditions to improve the crystal quality were unsuccessful and even worse. Slow cooling (-4°/hr to 300°C) after 7 days of reaction at 700°C as above produced the same result as did quenching except that the crystal size was much reduced.

More interestingly, when the same quenched reaction was started with a stoichiometric mixture of $Zr_5Pb_4$ and Zr powders, there was no crystal

grown at all. The powder pattern, however, showed only the same interstitial phase as above.

Vapor phase transport reaction of the crystalline product with $ZrCl_4$ at 900°C to a cooler temperature of ~750°C gave a mixture of $Zr_5Pb_4$ powder and cadmium. It is evident that the cadmium interstitial phase is only stable at lower temperatures. The dependence of crystallization on reagent type cannot be explained with these results only. Further study is necessary.

Indium A quantitative yield of this phase was obtained from a powder sintering reaction of stoichiometric $Zr_5Pb_4$, Zr, and $ZrIn_2$ powders at 1000°C for 11 days. The single phase product had lattice dimensions (a=8.8458(7), c=5.9989(8) Å) that would be expected for the atomic size of indium.

Tin A sintering reaction of $Zr_5Pb_4$, Zr, and $ZrSn_2$ in stoichiometric ratios at 1000°C for 11 days yielded almost a single phase in the powder pattern (a=8.838(1), c=6.000(1) Å). However, the lines were rather diffuse implying more or less incomplete reaction or a distribution of tin substitution products.

Additional sintering of this sample at 1000°C for 7 days did not improve the line quality in the powder pattern; however, the line positions for the interstitial phase were virtually unchanged.

Several more reactions in the temperature range of 1000-1350°C showed different results. There were what was presumed to be $Zr_5Pb_3Sn$, $Zr_5Sn_3$, and lead drops. The line positions of the tin interstitial phase corresponded well to those of above sample (broad lines). The

invariant lattice parameters of the interstitial phase indicate that this is the stoichiometric phase. The presence of lead drops in many of the reactions indicates that the synthesis is difficult.

**Antimony** Stoichiometric mixture of $Zr_5Pb_4$, Zr, and element antimony was sintered at 1350°C for 3 days. There was evidence of antimony attack on the tantalum tube. The powder pattern also showed $Ta_5Sb_4$ phase in addition to an interstitial phase.

Since antimony loss was apparent, this phase was suspected to be substoichiometric. Therefore, $ZrSb_2$ instead of element Sb was used thereafter. Sintering reactions at 1000°C for 7 days to 14 days yielded somewhat diffuse powder patterns. Nevertheless, the interstitial phases were identical to one another, and the antimony attack on tantalum was not apparent, if any. The same result, but with a much sharper powder pattern, was obtained from a 1350°C (5 days) sintering reaction, a=8.664(1), c=5.931(1) Å. Even though the product was a single phase without any apparent antimony or lead loss, the lattice parameters are much smaller than those of tin phase, implying that this was possibly a substoichiometric phase.

**Tellurium** Almost quantitative yields of this phase product were reproducibly obtained from various reactions. Sintering reactions of $Zr_5Pb_4$, Zr, and $ZrTe_3$ at 1000°C for 16 days, direct reaction of $Zr_5Pb_3$ and excess tellurium at 1000°C for 17 days in tantalum tube, and reaction of $Zr_5Pb_3$ and stoichiometric tellurium at 500°C followed by sintering at 1100°C for 8 days were tried. The lattice parameters were all identical. However, there always was an impurity phase of $Zr_3Te_2$

(< 10 %).

**Lead**

The self-interstitial phase was first encounted when a fluxed reaction of zirconium in lead (Zr:Pb=1:10) was performed at 800°C for 7 days. There was black powder left in the alumina crucible. The powder pattern was composed of two $Mn_5Si_3$-type phases, one of which had the lattice parameters of the reported $Zr_5Pb_3$ and the other had larger dimensions (a=8.873(1), c=6.019(1) Å). A self-interstitial was assumed for this new phase.

Since the assumed interstitial compound was accompanied by the lead-poorer $Zr_5Pb_3$ phase in the same product, the reaction condition of 800°C was thought to be too vigorous. The milder condition of 700°C was applied in a repeat reaction. After 7 days of flux reaction, the product was mainly composed of the desired phase plus about 5% (intensity) of $Zr_5Pb_3$.

In order to confirm the supposed stoichiometry $Zr_5Pb_4$, the product powder was reacted with stoichiometric Zr to make $Zr_5Pb_3$ through a sintering reaction at 1000°C for 7 days. The homogeneous-looking product pellet showed a single phase $Zr_5Pb_3$ (a=8.5352(6), c=5.8405(7) Å), confirming the composition of the new phase.

A sintering reaction of the composition $Zr_5Pb_{3.5}$ at 1000°C yielded two $Mn_5Si_3$-type phases; one was $Zr_5Pb_3$ and the other had a=8.7419(6), c=5.9675(6) Å. These values are considerably smaller that those of stoichiometric $Zr_5Pb_4$ meaning that this is a substoichiometric self-

interstitial phase. The interstitial lead content in this sample is more than half. Obviously, there is a high temperature solid solution between $Zr_5Pb_3$ and $Zr_5Pb_4$ as in zirconium-tin system (Part I). The lead-rich side has such a phase breadth below 1000°C whereas the zirconium-rich side still remains as line phase at this temperature.

The $Zr_5Pb_4$ phase could be easily synthesized by reaction of zirconium powder with a stoichiometric amount of lead in a tantalum tube at 800° to 1000°C.

The self-interstitial nature of this phase was further evidenced by X-ray crystal structure refinements of two single crystals grown from vapor phase transport reactions. The first attempt was made with $CdI_2$ as the transporting agent. Previously synthesized $Zr_5Pb_4$ powder was loaded in a tantalum tube with the transporting agent. A temperature gradient of 950⟶900°C was employed for 23 days. A black powder was found in the hot zone while the large crystals (3.0 x 0.5 x 0.5 mm) were deposited on the cold end. The powder pattern of the residue powder showed a mixture of two $Mn_5Si_3$-type phases, the larger one being smaller that the $Zr_5Pb_4$ in dimensions. Most obviously, this reaction had the risk of cadmium contamination, especially on the interstitial site. This problem was reflected by the small lattice parameters (a=8.828(3), c=5.991(2) Å) as well as the lead-deficient result of the composition refinement, $Zr_{2.98(1)}Zr_2Pb_{2.988(6)}Pb_{0.868(3)}$ (Table 15). A crystal from this reaction was analyzed by EDX to see if there was cadmium, only to find just zirconium and lead.

Table 15. Data collection and refinement parameters for $Zr_5Pb_{3.9}$[a] from vapor phasr transport reaction with $CdI_2$

| atom | occupancy | x | thermal parameters (x $10^3$) | | |
|---|---|---|---|---|---|
| | | | $U_{11}$ | $U_{22}$ | $U_{33}$ |
| Pb1 | 0.996(2) | 0.61551(6) | 4.3(2) | 2.6(2) | 3.9(2) |
| Zr1 | 1 | 1/3 | 3.2(4) | 3.2(4) | 3.3(7) |
| Zr2 | 0.993(4) | 0.2799(2) | 6.0(4) | 5.7(6) | 8.6(6) |
| Pb2 | 0.868(3) | 0 | 3.2(2) | 3.2(2) | 3.0(4) |

| | |
|---|---|
| lattice parameters (Å) | |
| a | 8.828(3)[b] |
| c | 5.991(2) |
| crystal size | 0.15 x 0.15 x 0.5 |
| $2\theta_{max}$, ° | 55 |
| octants | h,k,±l |
| reflections | |
| measured | 739 |
| observed | 580 |
| independent | 175 |
| R, % | 1.6 |
| $R_w$, % | 2.4 |
| largest peak (e/Å$^3$) | 1.9 (0.08, 0.78, 0.25) |
| second. ext. coeff. (x $10^{-7}$) | 4.05(7) |
| absorption coeff. ($cm^{-1}$,Mo Kα) | 896 |

[a]Refined composition: $Zr_{2.98(1)}Zr_2Pb_{2.988(6)}Pb_{0.868(3)}$.

[b]Lattice parameters from single crystal diffractometer.

A second reaction was performed with $ZrCl_4$ as transporting reagent instead of $CdI_2$. A temperature gradient of 1000⟶950°C was found to be the best condition for crystal growth. However, no material transport occurred. Several crystals were grown in the hot zone, and one of them was used for data collection with the CAD4 diffractometer. The crystallographic and refined parameters are listed in Table 16. Because of the large absorption coefficient of this crystal, DIFABS was applied for the absorption correction. The refined composition was $Zr_3Zr_{2.06(2)}Pb_{3.02(1)}Pb_{0.940(5)}$, slightly lead poor from stoichiometric $Zr_5Pb_4$. The deficient site is the interstitial site; the others are effectively stoichiometric.

**3d transition metal elements**

**Chromium** A sintering reaction of $Zr_5Pb_4$, Zr, and $ZrCr_2$ powders at 1350°C for 3 days yielded a seemingly single phase product. However, the lattice dimension was even smaller than that of the binary host, meaning probable chromium substitution on the zirconium site, not an interstitial compound. An EDX analysis made on this pellet showed no signal for chromium or only a very small peak for it with imagination. It is not clear where the chromium element went with these experiments. A possible explanation is that chromium did not form interstitial compound and having vapor pressure of $10^{-2}$ torr at the reaction temperature, evaporated and was taken up by the tantalum container. According to the phase diagram, the solubility of chromium in tantalum at 1300°C is about 10 %.

Table 16. Data collection and refinement parameters for $Zr_5Pb_4$[a]

| atom | occupancy | x | thermal parameters (x $10^3$) | | |
|---|---|---|---|---|---|
| | | | $U_{11}$ | $U_{22}$ | $U_{33}$ |
| Pb1 | 1.005(3) | 0.6154(1) | 4.6(3) | 4.0(4) | 4.9(3) |
| Zr1 | 1.031(9) | 1/3 | 4.9(7) | 4.9(7) | 6(1) |
| Zr2 | 1 | 0.2810(3) | 5.6(8) | 7(1) | 7.7(9) |
| Pb2 | 0.940(5) | 0 | 3.3(4) | 3.3(4) | 3.7(6) |

| | |
|---|---|
| lattice parameters (Å) | |
| a | 8.851(1)[b] |
| c | 6.009(1) |
| crystal size (mm) | 0.2 x 0.1 x 0.5 |
| $2\theta_{max}$, ° | 65 |
| octants | h,±k,±l |
| reflections | |
| measured | 934 |
| observed | 731 |
| independent | 278 |
| $R_{ave}$, % | 2.5 |
| R, % | 3.7 |
| $R_w$, % | 4.1 |
| largest peak (e/Å$^3$) | 2.4 (0.05,0.11,0.25) |
| second. ext. coeff. (x $10^{-7}$) | 2.92(5) |
| absorption coeff. ($cm^{-1}$,Mo Kα) | 888.6 |

[a]Refined composition: $Zr_3Zr_{2.06(2)}Pb_{3.015(9)}Pb_{0.940(5)}$.

[b]Lattice parameters from the diffractometer; the corresponding values for the stoichiometric compound are a=8.873(1), c=6.019(1) Å.

The inability for chromium to form interstitial compound is evident through comparison with the other successful element examples of cobalt and nickel under the identical synthetic conditions. The disappearance of chromium must be a result of unbound chromium in the reaction.

**Manganese** The first attempt for this phase was made with a 1000°C sintering reaction of $Zr_5Pb_4$, Zr, and $ZrMn_2$ powders. After 19 days of the reaction, the resultant powder pattern showed two distinct $Mn_5Si_3$-type phases. The larger one (a=8.790(2), c=5.981(2) Å) was too large to be considered as the stoichiometric interstitial phase. The smaller one was even smaller than the host, meaning probable manganese substitution for zirconium, as in chromium case. The large phase could be understood as a partial self-interstitial phase of lead, possibly mixed with manganese.

Raising the reaction temperature did not help the synthesis. Instead, single phase $Zr_5Pb_3$ was found from a 1350°C sintering reaction as judged by the powder pattern. Manganese vaporization seemded to have occurred, and this must be because of the non-existence of the desired phase.

**Iron** Several attempts were carried out to synthesize this phase. A sintering of $Zr_5Pb_4$, Zr, and $ZrFe_2$ at 1000°C yielded a very similar result to that in manganese system; two $Mn_5Si_3$-type phases with one close to the larger phase in manganese case (a=8.789(2), c=5.971(2) Å) and the other smaller than binary $Zr_5Pb_3$ in unit cell dimensions. The same interpretation as in manganese system could be applied.

The lattice parameters of the products for other 1000°C sintering reactions fluctuated. This is very similar to the $Zr_5Sn_3$-Fe system and can be attributed to similar mixed interstitial compound formation.

One such example was erroneously considered to be stoichiometric phase, and a magnetic study was carried out with a SQUID magnetometer. This gave a very weak ferromagnetic signal whose overall behavior was very similar to that of amorphous $ZrFe_2$, an indication of nonstoichiometric and mixed lead and iron interstitial phase formation.

However, unlike the manganese case, raising the sintering temperature to 1350°C did produce a single phase whose lattice parameters fell in the expected range (a=8.705(1), c=5.922(1) Å). It is not certain, however, whether this phase is the stoichiometric iron interstitial phase or a lead and iron mixed phase. However, the lattice parameters are close to those of cobalt and nickel interstitial phases, and therefore, are taken as those for the stoichiometric phase.

There appears to be a borderline between manganese and iron in the interstitial capability of $Zr_5Pb_3$ host.

**Cobalt and Nickel** These phases were briefly investigated by sintering reactions at 1350°C. $ZrCo_2$ and ZrNi were synthesized by arc-melting reactions, and their powders were used as reagents. The reaction products appeared homogeneous and their powder patterns consisted of single phases (a=8.6832(5), c=5.8851(5) Å for the cobalt and a=8.6261(7), c=5.8916(8) Å for the nickel phases). The lattice parameters are close to each other and to those of the high temperature iron phase. The single phase nature and the close lattice parameters

within these phases support the idea that these are stoichiometric phases.

# DISCUSSION

For most of the systems, the interstitial compounds formed have been examined thoroughly to confirm the stoichiometries. Besides the single crystal and powder structure refinements, syntheses with various conditions and compositions have given indications.

The unit cell volumes of the interstitial compounds are plotted as a function of atomic volume of the interstitial elements (Figure 2). The atomic volumes were calculated for spheres of atoms with Pauling's single bond metallic radii.[42] Since the metallic radii for the chalcogens, phosphorus, and the second period elements are not available, the covalent radii for these elements were used. The plots, therefore, have inherent uncertainties in the atomic volumes used. Such uncertainties are even more severe because the radii do not correspond to the same environments. Moreover, since the bond formation between the interstitial elements and the surrounding zirconium is accompanied by the changes of the coordination number of zirconium and should affect the zirconium-tin (lead) bonds, the unit cell volume is not determined by the interstitial atom size. However, the plots, by averaging out the scattering effects, still provide some insights.

The plots are roughly linear. The slopes of the lines for $Zr_5Sn_3Z$ and $Zr_5Pb_3Z$ have to be close to each other if the unit cell volume increase is strictly proportional to the size of interstitial element. Alternatively, the slope of the $Zr_5Sn_3Z$ system may be steeper since the unit cell volume change is buffered by the void volume of the empty

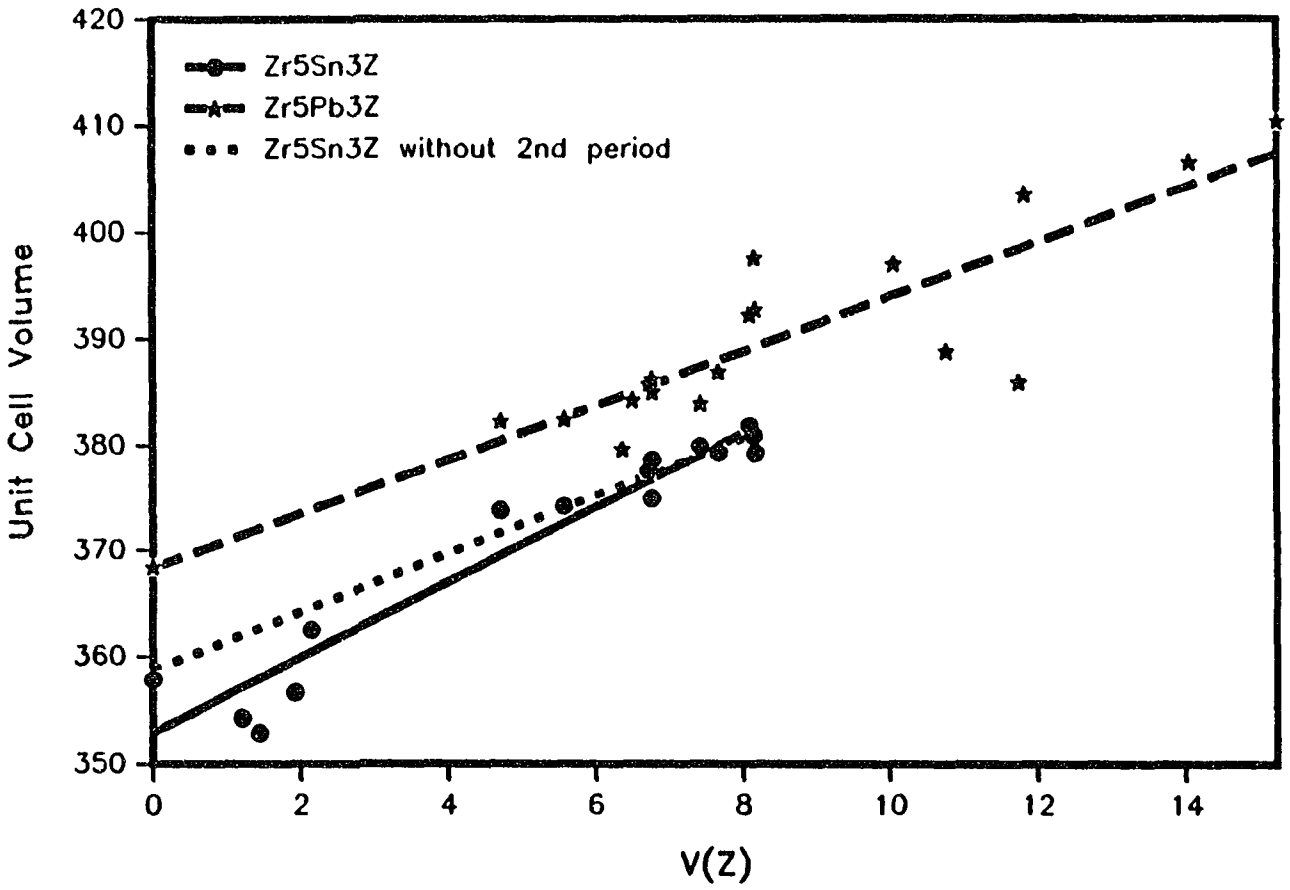


Figure 2. Unit cell volume vs. interstitial atom size plots of $Zr_5Sn_3Z$ and $Zr_5Pb_3Z$. The zero atom sizes correspond to the hosts. The solid line for $Zr_5Sn_3Z$ is for all data, and the dotted line is without the data for the second period interstitials.

interstitial site of the host, and this void volume may be larger in the larger $Zr_5Pb_3$ host.

The plots follow the second possibility, that is, the $Zr_5Sn_3Z$ line has the greater slope. However, the crystal structure refinements (below) indicate that the second period interstitials have different effects than the others, and taking these data out of the $Zr_5Sn_3Z$ plot produces the same slopes for both systems. The two parallel lines thus obtained can be understood as the unit cell volume increase without or with a very small buffer effect.

Other insights can be obtained from the plots of unit cell volume vs. group number of the interstitial element for the $Zr_5Sn_3$ (Figure 3) and $Zr_5Pb_3$ (Figure 4) systems. These unit cell volumes are decreased as the group number increases. The unit cell volume trends in the fourth period in both systems and in the fifth period in the lead system follow that of metallic radii of elements, that is, the unit cell volumes are the largest at the aluminum group interstitials.[42] The covalent (tetravalent) radii monotonously decrease from copper through selenium and silver through tellurium.[43] The minimum values around the pnictides in the lead host resemble those of in $Zr_5Sb_3Z$ interstitial systems.[33] This behavior was attributed to the repulsions between contiguous chalcogenide atoms in the antimony hosts, and such repulsion effect was also detected in the lattice parameter vs. sulfur content plot in $Zr_5Sn_3S_x$ system. Such effects are not apparent in the plot of the unit cell volume for the $Zr_5Sn_3Z$ system, but the plots of lattice

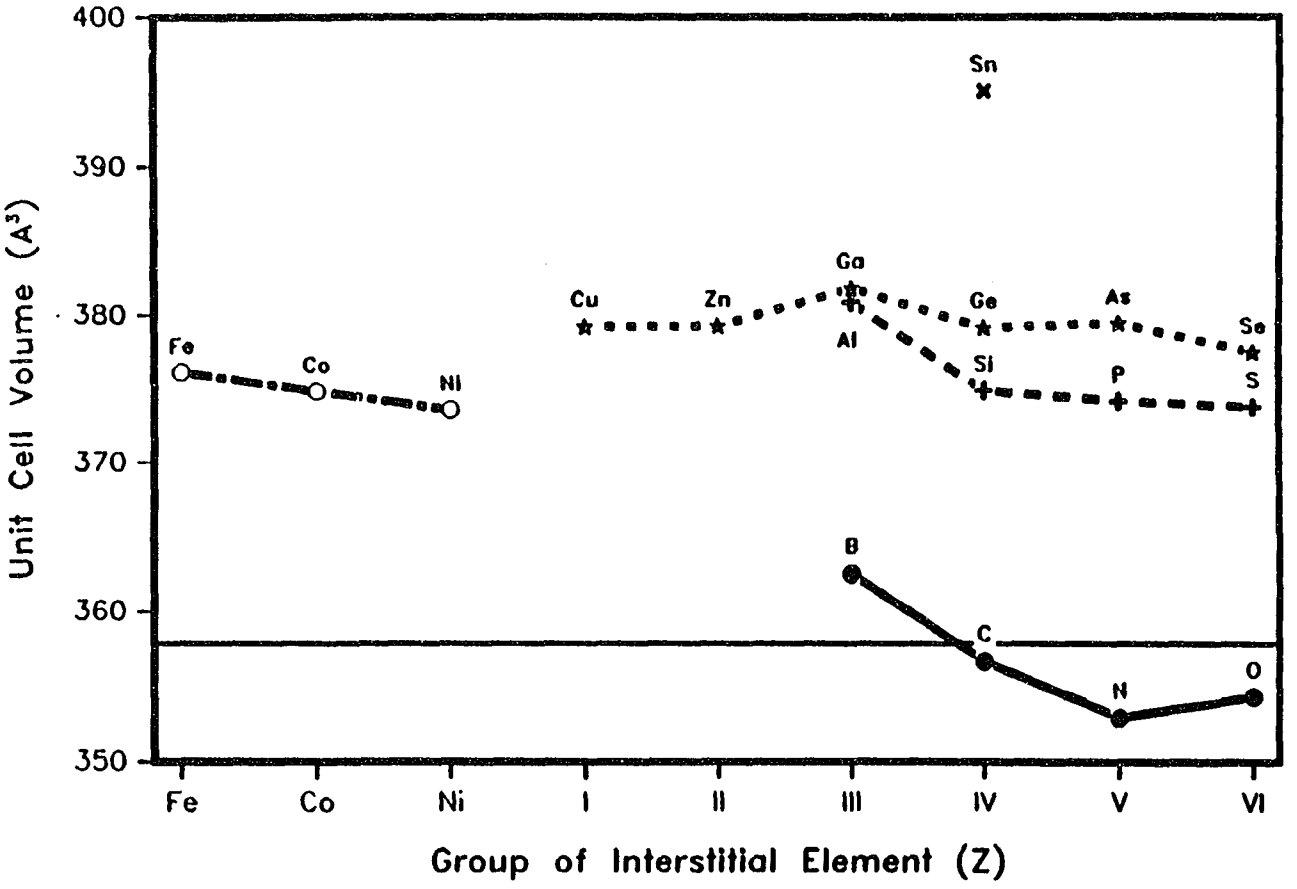


Figure 3. Unit cell volume vs. group number of the interstitial element in $Zr_5Sn_3Z$ systems. The horizontal line is for the empty host $Zr_5Sn_3$.

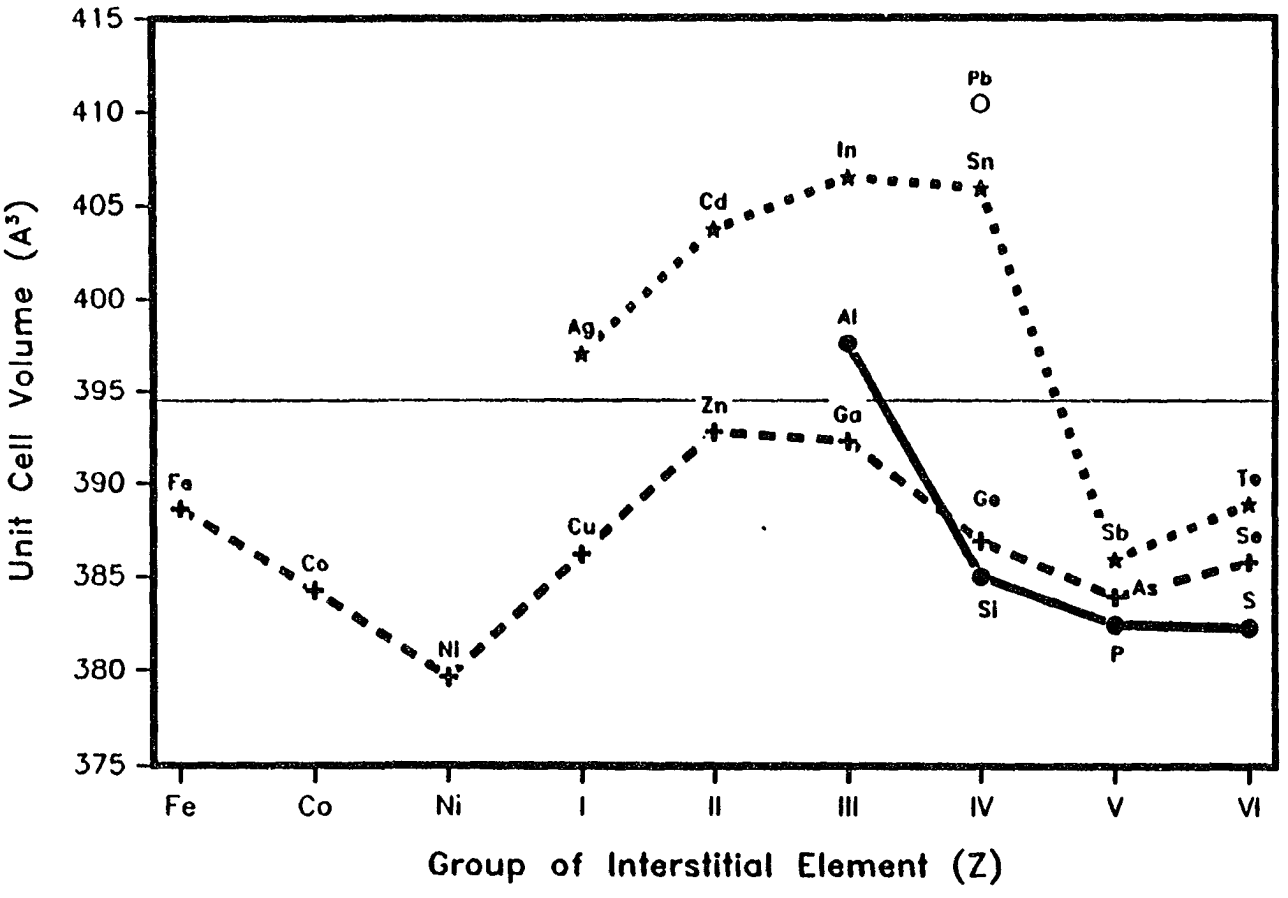


Figure 4. Unit cell volume vs. group number of the interstitial element in $Zr_5Pb_3Z$ systems. The horizontal line is for the partial self-interstitial $Zr_5Pb_{>3.5}$ (see text). The unit cell volume for the empty $Zr_5Pb_3$ is 368.47(7) $Å^3$.

parameter and c/a ratio vs. group number (Figures 5 and 7, respectively) clearly show such evidences (below).

The $Zr_5Sn_3Z$ system shows smooth changes of the unit cell volume with group whereas the $Zr_5Pb_3Z$ system has some abrupt changes at aluminum-phosphorus and tin-antimony. As mentioned earlier (Results), these systems had problems in syntheses, and the lattice parameters were concluded not to represent the stoichiometric phases.

The a- and c-parameter plots against the same variable as above show the similar problems of these compounds (Figures 5 and 6). The compounds that are already distinguished in the unit cell volume vs. group number plot have abrupt changes in these plots. In addition to these, the nickel interstitial in $Zr_5Pb_3$ also appears to need consideration.

The c/a ratios of the hexagonal unit cells were also plotted (Figures 7 and 8). The increases of the c/a ratios in the pnictides and chalcogenides are probably due to the repulsions between contiguous interstitial atoms that have anionic character. The separation between interstitial sulfur atoms, 2.98 and 3.00 Å in $Zr_5Sn_3S$ and $Zr_5Pb_3S$, respectively, are much shorter than those in $Zr_{21}S_8$ (the shortest is 3.41 Å).[44] The decrease of c/a and the c-parameter from sulfur to selenium (and tellurium in the lead host) can be explained by a decrease of anionic characters of the chalcogen atoms. However, these did not seem to give any further information as far as detecting troublesome data. Even the suspicious data for aluminum, nickel, antimony, and tellurium interstitials of $Zr_5Pb_3Z$ cannot be distinguished in this plot.

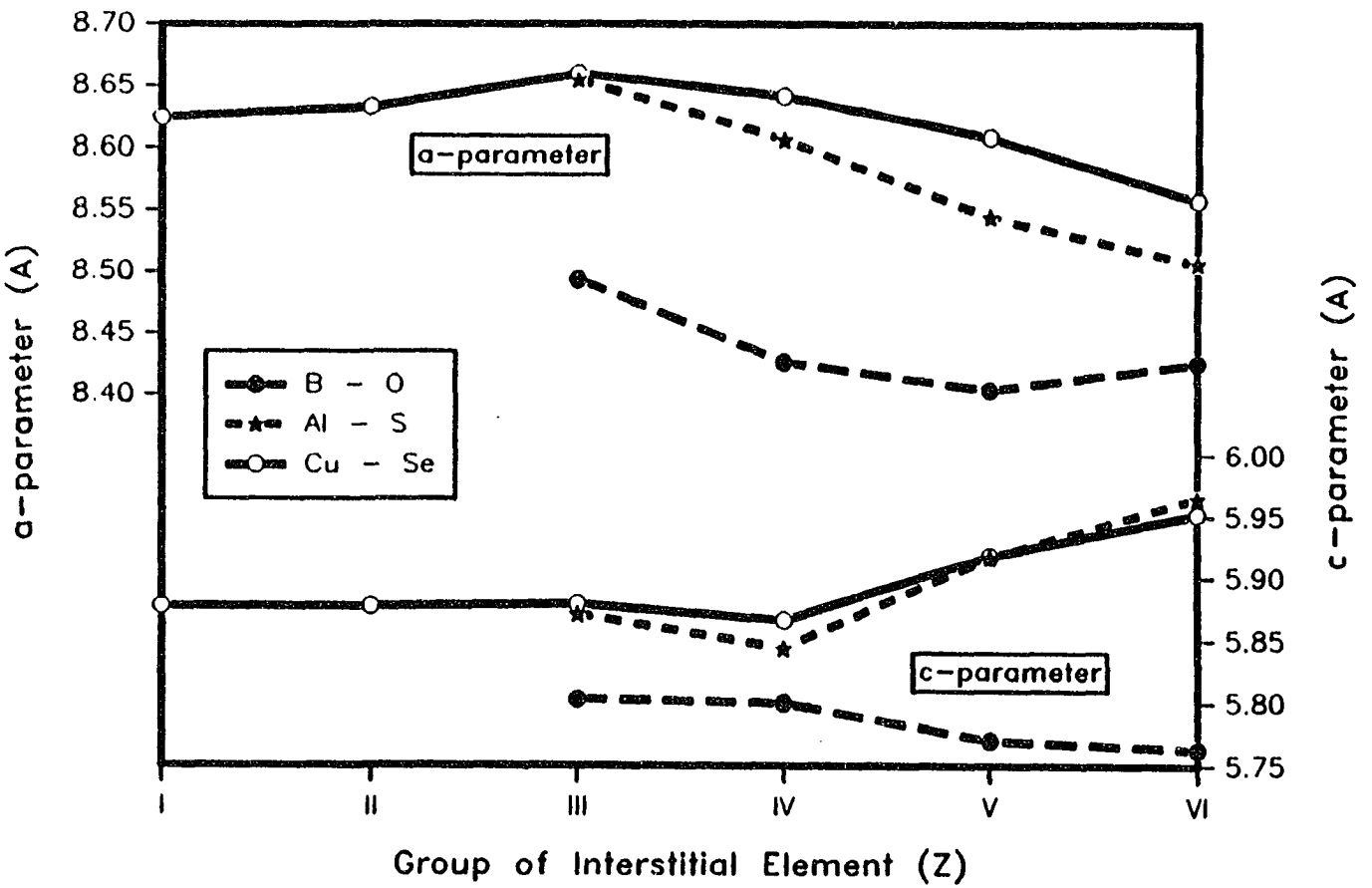


Figure 5. Lattice parameter vs. group number of the interstitial element of $Zr_5Sn_3Z$. Upper three lines are for the a-parameters (left axis), and the lower three are for the c-parameters (right axis). The empty $Zr_5Sn_3$ has a = 8.4560(7), c = 5.779(1) Å and the stuffed $Zr_5Sn_4$ has a = 8.7656(7), c = 5.937(1) Å.

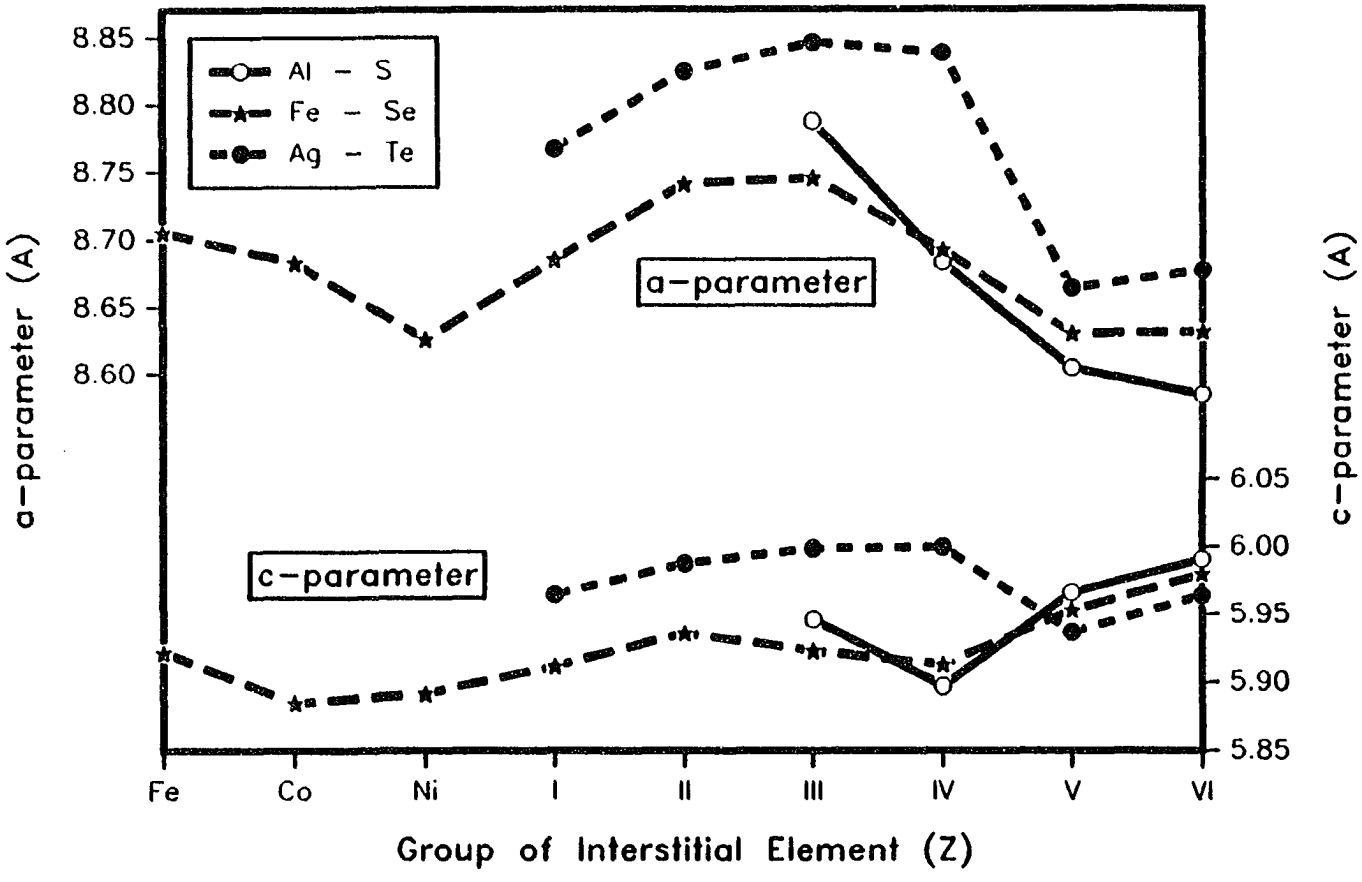


Figure 6. Lattice parameter vs. group number of the interstitial element of $Zr_5Pb_3Z$. Upper three lines are for the a-parameters (left axis), and the lower three are for the c-parameters (right axis). The empty $Zr_5Pb_3$ has a = 8.5352(6), c = 5.8405(7) Å and the stuffed $Zr_5Pb_{3+x}$ has a = 8.7419(6), c = 5.9675(6) and a = 8.873(1), c = 6.019(1) Å for x = ~>0.5 and 1.0, respectively.

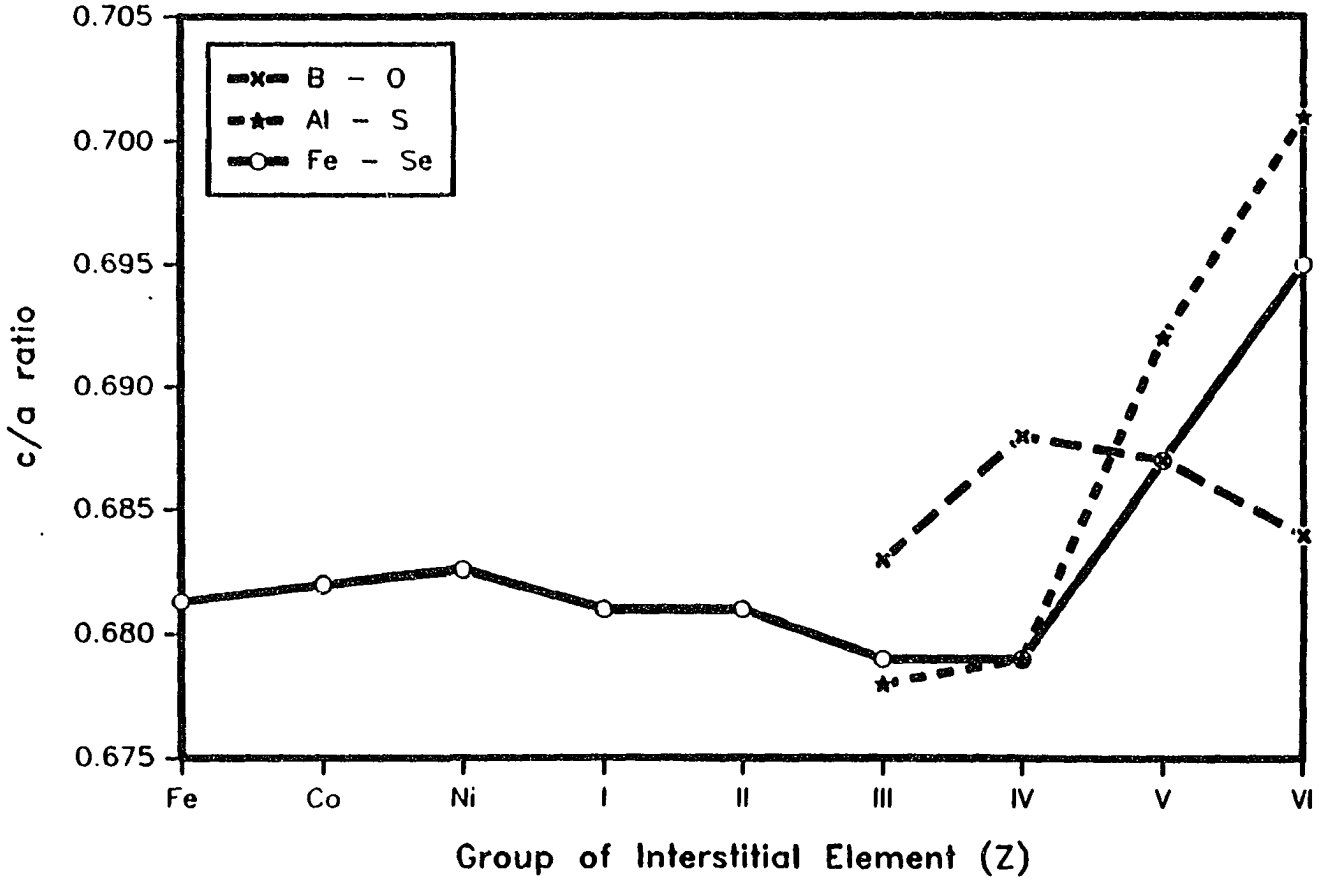


Figure 7. c/a ratios of the hexagonal unit cells of $Zr_5Sn_3Z$.

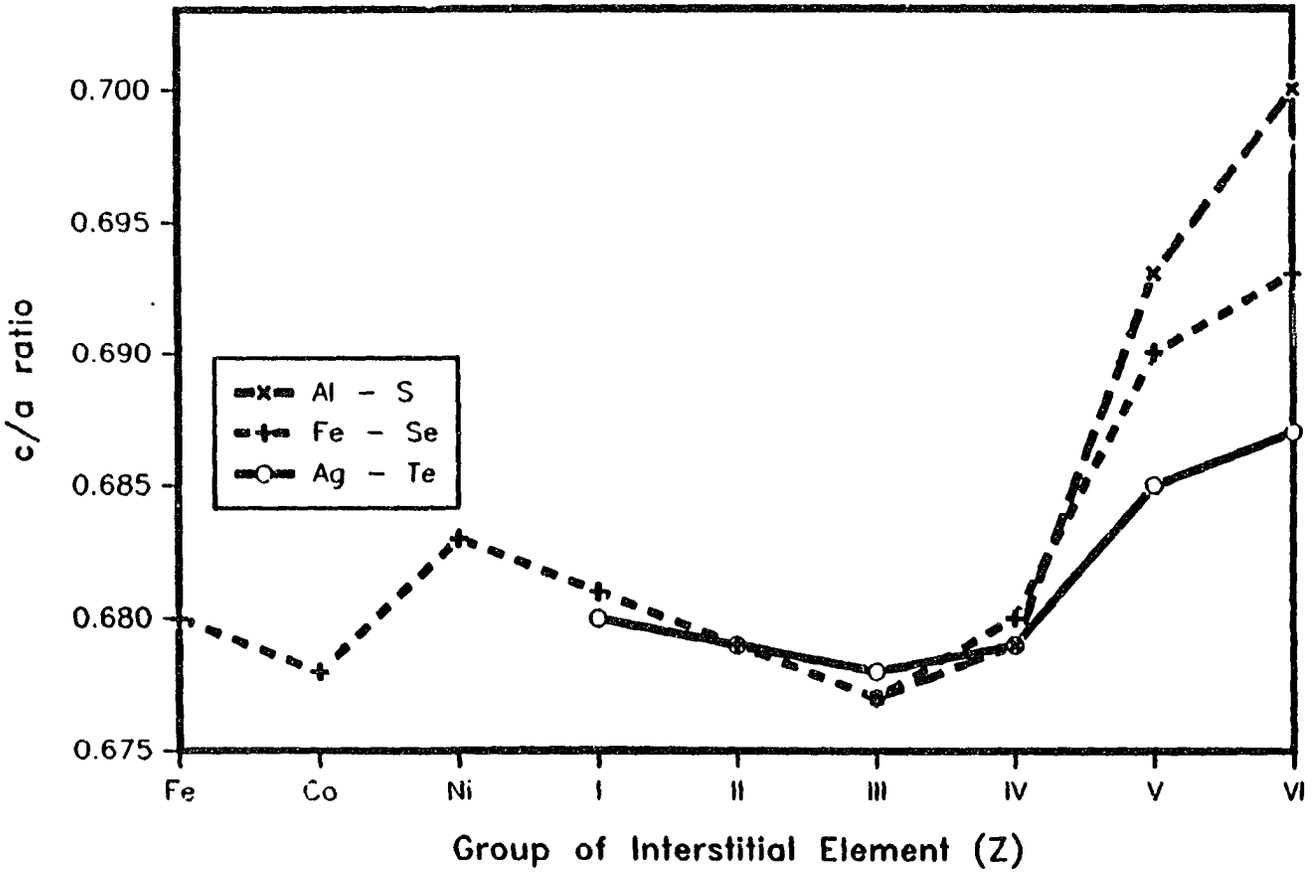


Figure 8. c/a ratios of the hexagonal unit cells of $Zr_5Pb_3Z$.

Another interesting comparison was obtained in the comparison of the unit cell volume increment of an interstitial element in the two host structures (Figure 9). Both systems show very close increments for silicon, copper, gallium, and tin interstitials. Except for the aluminum and zinc interstitials, the $Zr_5Pb_3Z$ system show smaller volume increments than the $Zr_5Sn_3Z$. This could be explained by a larger buffer effect of the $Zr_5Pb_3$ host. The arsenic and germanium phases show the largest differences of the volume increments between the different hosts. The problems in the syntheses of $Zr_5Pb_3Ge$ and the arsenic interstitial phases of both hosts were already discussed in the RESULTS section. The lattice parameters of the first were obtained from a 1350°C reaction in which large amount of lead mixing as well as partial occupancy might have taken place.

The above plots indicate that the aluminum, nickel, germanium, antimony, and tellurium interstitials in the $Zr_5Pb_3$ host and $Zr_5Sn_3As$ are to be taken with reservations.

In general, the element series of aluminum to sulfur and copper to selenium in both tin and lead systems can form stoichiometric interstitial phases in the temperature range of 1000°C-1500°C. The lead host also forms stoichiometric compounds with silver, cadmium, and most of the fifth period main group elements. The attempted syntheses of interstitial phases of boron to oxygen in $Zr_5Sn_3$ were always accompanied by impurity phases. However, the consistencies of the cell dimensions imply that stoichiometric phases were formed in addition to the

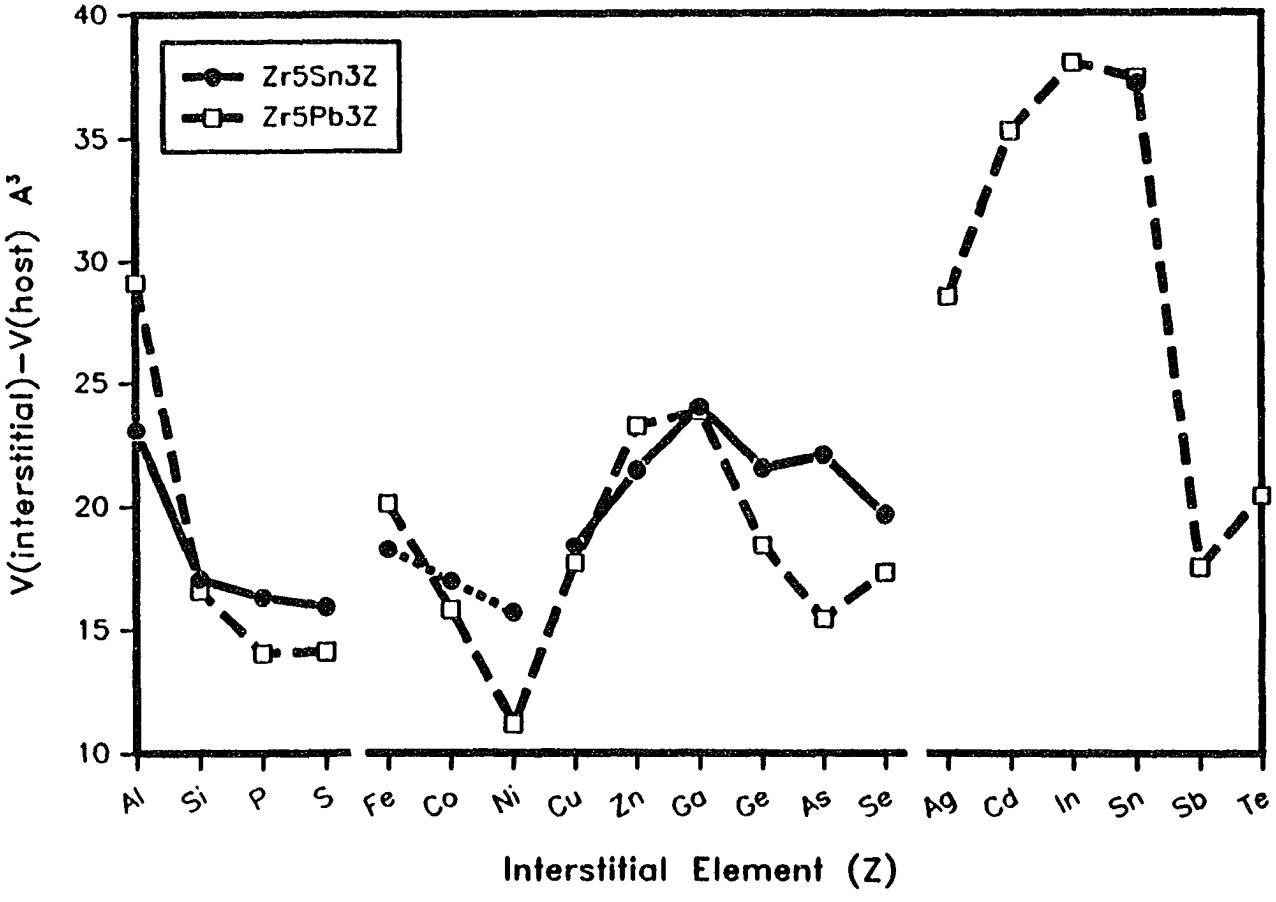


Figure 9. The unit cell volume increments (V(interstitial)-V(host)) of $Zr_5Sn_3Z$ and $Zr_5Pb_3Z$. Only the elements that formed interstitial phases in both hosts are shown for clarity except those Ag through Te in $Zr_5Pb_3Z$ to show the relative value in $Zr_5Sn_4$ with respect to these. The data for Fe, Co, Ni in $Zr_5Sn_3(Sn_{1/3}Z_{1/3})$ (dotted line) are also included for comparison.

undisputable evidences of single crystal structure refinements for the carbon and oxygen phases.

However, for some of the elements, the stoichiometric compositions are only the extremes of a range of interstitial capability. Oxygen and sulfur compounds of $Zr_5Sn_3$ system showed that substoichiometric compositions were synthesized as single phases at 1000°C-1100°C. A similar behavior is inferred for the other chalcogenide systems. Phosphorus and arsenic systems also appear to have such a behavior judging from the fluctuations of the lattice parameters even though these were not pursued in this study. Copper might be an another example; however, since it is next to nickel, which showed mixed interstitials, tin mixing in the interstitial site is also possible.

Other elements showed clear evidences that they prefer to form either a stoichiometric or no interstitial phases in the temperature range investigated. However, since interstitial capability will depend on temperature, the above statement must not be applied to other temperature regions, especially above 1350°C. Above 1350°C, self-interstitials are formed in the binaries, and thses may interfere in the ternary systems.

The distinctions between the interstitial capacities of the two hosts for the fifth period elements (silver to tellurium), except for tin, appear to be due to electronic reasons as well as the size differences of the hosts. Probably the $Zr_5Pb_3$ host is more flexible that the other, and this may contribute to the larger interstitial capability of this. However, the tin interstitials in both hosts cannot

be accounted for by this "space filling" discussion. The competition for the electrons of the antiprismatic zirconium between the interstitial atom and the tin or lead in the host might be the controlling factor. This also seem to explain, though very qualitatively, why those elements to the left of iron in the periodic table cannot be incorporated interstitially.

The single crystal structure refinements, although some of them are inconclusive, provide some insights into the nature of bonding of the interstitial compounds (Table 17). The refinement results of $Zr_5Sn_{3.10}$ and $Zr_5Sn_{3.18}$ single crystals provide good references. If the atomic distances in the partially tin occupied phases are assumed to be changing proportionally, the atomic distances in the empty host can be extrapolated from these two results. These also could be taken as references in discussing the atomic distance trends in interstitial compounds.

The most obvious changes of atomic distances with carbon or oxygen interstitials are the emerging zirconium to interstitial bonds and a shortening of the Zr2-Zr2 bonds by ~0.1 Å within the confacial chain. The latter must be a simple consequence of the strong zirconium-interstitial interactions which pull the zirconium atoms towards the interstitial atoms. The next most obvious changes are the increases in the distance between Zr2-Sn and Zr1-Zr1 (in the linear chain) both by ~0.05 Å, while the Zr1-Sn distances are unchanged or slightly shortened. Over all, the net effect is pulling in the zirconiums around the

Table 17. Important atomic distances of $Zr_5Sn_3Z$

| bond type | Z | | | | | | | | |
|---|---|---|---|---|---|---|---|---|---|
| | empty[a] | $Sn_{0.10}$ | $Sn_{0.18}$ | C | O | $Al_{1.12}$ | $Ga_{0.84}$ | $Ga^b$ | Ge |
| Zr2 - Z | 2.536 | 2.551(1) | 2.592(1) | 2.459(1) | 2.4562(8) | 2.712(2) | 2.694(1) | 2.744 | 2.775(3) |
| Zr2 - Sn | | | | | | | | | |
| interchain | 3.068 | 3.058(2) | 3.035(1) | 3.102(2) | 3.093(1) | 2.984(2) | 2.991(1) | 2.983 | 2.939(5) |
| out-of-plane | 3.1423 | 3.1413(6) | 3.139(1) | 3.1973(8) | 3.1875(6) | 3.1053(7) | 3.1151(5) | 3.122 | 3.104(2) |
| in plane | 2.9030 | 2.9076(7) | 2.918(0) | 2.9142(9) | 2.9190(5) | 2.9495(8) | 2.9533(6) | 2.982 | 2.977(4) |
| Zr1 - Sn | 2.9844 | 2.9895(3) | 3.001(0) | 2.9641(3) | 2.9582(2) | 3.0396(3) | 3.0344(2) | 3.058 | 3.054(3) |
| Zr2 - Zr2 | | | | | | | | | |
| out-of-plane | 3.5646 | 3.5801 | 3.615(1) | 3.443(2) | 3.445(2) | 3.7107(8) | 3.6970(5) | 3.744 | 3.767(3) |
| in plane | 3.6143 | 3.6456 | 3.716(1) | 3.5118(7) | 3.5017(6) | 3.958 | 3.9212 | 4.013 | 4.076 |
| Zr1 - Zr2 | 3.566 | 3.5600 | 3.547(1) | 3.605(1) | 3.6004(6) | 3.515(1) | 3.5254(7) | 3.533 | 3.500(4) |

[a]Extrapolated from those of $Zr_5Sn_3Sn_{0.10}$ and $Zr_5Sn_3Sn_{0.18}$.

[b]Calculated from the coordinates of the Rietveld refinement.

interstitial atom closer making them more isolated, while the rest of the structure remains virtually unchanged.

The atomic distances with gallium (Rietveld) and germanium interstitials show different trends of atomic distances. These two cases have virtually the same atomic distances, probably because they are neighbors to each other and have close atomic sizes. On the other hand, this similarity indicates that the refinement result for the germanium compound also is worthy of consideration in discussing bond distances even though the refinement had problems of unusually large standard deviations. Almost opposite trends to those with the second period examples are observed in these systems. The Zr2-Sn distances are shortened except that between edge-bridging tin and zirconium at the same z-level which already has the shortest bond distance among these in the host. The interchain Zr2-Sn bond appears to be the most affected. It becomes comparable to or even shorter than the in-plane Zr2-Sn distance. The separation between two different types of zirconiums becomes less by 0.03 to 0.06 Å. The increased Zr2-Zr2 distances within an octahedron are mere consequences of the expansion of the interstitial site. The Zr1-Sn separation become larger due to the interstitial event. The net effect in these cases is expansion of the zirconium octahedra, pushing the tin atoms surrounding it towards the zirconiums of the neighboring octahedral chains at the expense of the other type of zirconium-tin bonds. The shortened distance between different zirconiums is suspected to not have any significant bonding effect. They probably change as a result of matrix effect.

The mixed tin-aluminum as well as the partially occupied gallium phases show some distinctions relative to the fully occupied examples in their atomic distance trends. The Zr2-Zr2 distances in the octahedral chain as well as the zirconium-interstitial distances are reflections of the occupancies, and the interstitial sizes are considerably smaller than the stoichiometric gallium and germanium phases. This is not very clear in 84 % gallium compound. However, for the aluminum case, if one assumes full occupation by aluminum, the in-plane Zr2-Zr2 distances, for example, should be larger than those in the stoichiometric gallium or germanium cases because aluminum is larger than both of these, opposite to the observation. This is a clear indication of vacant interstitial site which, in turn, means more tin than the constrained refinements yielded, in support of the lattice parameter discussion in the RESULTS section. Therefore, single crystals generated by arc-melting can be concluded to be defective in many qualifications.

The single crystal refinements of some interstitial phases of $Zr_5Pb_3$ host also provide some understanding even though these are less systematic than the $Zr_5Sn_3$ host systems (Table 18). The slightly different amounts of mixed lead-zinc interstitial do not seem to affect the bond distance significantly. However, such a difference of interstitial occupancy is much more pronounced in the lead self-interstitial case. In general, larger atomic sizes and higher occupancies give large atomic distances for most of the bond types.

Comparisons between different interstitials are rather complicated. Since the $Zr_5Pb_3Zn$ and $Zr_5Pb_4$ are almost stoichiometric, these will be

Table 18. Important atomic distances of $Zr_5Pb_3Z$

| Bond type | Z | | | | |
|---|---|---|---|---|---|
| | $Al_{1.79}$ | $Zn_{1.09}$ | $Zn_{1.21}$ | $Pb_{0.87}$ | $Pb_{0.94}$ |
| Zr2 - Z | 2.789(5) | 2.771(6) | 2.776(6) | 2.889(1) | 2.912(2) |
| Zr2 - Pb | | | | | |
| interchain | 3.010(7) | 3.036(7) | 3.033(7) | 2.962(2) | 2.967(3) |
| out-of-plane | 3.130(2) | 3.133(2) | 3.133(2) | 3.135(4) | 3.1469(8) |
| in-plane | 3.001(2) | 2.982(2) | 2.982(2) | 3.0391(5) | 3.0586(9) |
| Zr1 - Pb | 3.0936(7) | 3.0944(8) | 3.0953(8) | 3.1266(2) | 3.1420(3) |
| Zr2 - Zr2 | | | | | |
| out-of-plane | 3.789(3) | 3.778(4) | 3.782(4) | 3.8830(6) | 3.908(1) |
| in-plane | 4.094(8) | 4.06(1) | 4.06(1) | 4.279(2) | 4.308(2) |
| Zr1 - Zr2 | 3.553(4) | 3.558(4) | 3.556(4) | 3.5370(8) | 3.550(1) |

compared in detail. The most obvious differences between these are in the confacial zirconium chain. The zirconium (Zr2)-interstitial, and Zr2-Zr2 bond distances both are much larger for the lead interstitial. These are, of course, natural consequences of the larger atomic size of lead. The three types of Zr2-Pb1 distances change differently on moving from zinc to lead interstitials. The out-of-plane Zr2-Pb distance increases by ~0.01 Å (almost negligible). The in-plane edge-bridging one is increased by ~0.08 Å. However, the interchain Zr2-Pb distances shorten by ~0.07 Å, meaning more lateral interactions in the lead interstitial. The chain zirconium (Zr1) to lead distance is increased by ~0.05 Å. Therefore, the lead interstitial compound has more interactions between the octahedral chains via linking lead and more isolated linear zirconium chains than the zinc phase. This might be a result of the expansion of the octahedral zirconium unit as in the gallium and germanium interstitials of $Zr_5Sn_3$.

The comparison between the aluminum interstitials of the two hosts is not very revealing, mainly because of the uncertainty in the compositions. In most of the bond types, the lead compound has larger distances by 0.03-0.15 Å, and this is considered to be because of the matrix effect.

The atomic distances between Zr2 and interstitial elements within $(Zr2)_6Z$ antiprisms are worthy of note. They are usually much shorter than those in binary Zr-Z compounds, typical for cluster compounds.[33,45] The Zr-Zn distance in $Zr_5Pb_3Zn$ (2.771 Å) compares well with that of $Zr_5Sb_3Zn$ (2.747 Å)[33] which, in turn, is much less than those of ZrZn

(2.89 Å)[46] and $ZrZn_2$ (2.97 Å).[47] The Zr-Ga distance in $Zr_5Sn_3Ga$ (2.744 Å) also is much shorter than those in $ZrGa_3$ (2.808-2.950 Å).[23] Atomic distances for Zr-Ge and Zr-Pb are not available in the literature. However, the latter can be obtained from the crystal structure of $Zr_5Pb_4$ itself. The Zr-Pb distances within the $(Zr2)_6Pb$ antiprism is 2.912 Å, shorter that the other types of Zr-Pb, 2.967-3.147 Å.

However, the distances of Zr2-C (2.459 Å) and Zr2-O (2.4562 Å) in the crystal structures show different trends. They are larger than those in ZrC (2.348 Å)[48] and $ZrO_{0.7}$ (2.292 Å),[49] respectively. The larger distance in these interstitial phases are likely because, in part, of the higher coordination numbers of Zriconium atoms in these structures.

Comparison with the single crystal structure results in $Zr_5Sb_3Z$ system exhibits a contrast. The host structures in all $Zr_5Sn_3Z$ were refined stoichiometrically whereas the aluminum and silicon phases in $Zr_5Sb_3Z$ had these elements in the antimony site.[38]

The results of some vapor phase transport reactions deserve consideration as far as the mechanisms of these reactions and for future applications. This technique only succeeded in the lead system which implies that lead is transported as the element. The fact that $ZrCl_4$ has grown single crystals while $ZrI_4$ did not is very challenging. Considering the stabilities of these halides, $ZrI_4$ should be the better choice for transporting agent. Interstitial phases of Al, Si, P, S, Cu, Zn, Ge, As, Se, Ag, Cd, Te, Pb were tried with $ZrCl_4$, and only the Al,

Zn, and Pb systems grew single crystals. The Al and Zn systems even showed material transport. Vapor phase transport reactions require very subtle controls of the reversible equilibria, and the relative stabilities of the possible components in the gaseous state may be the controlling factor in these vapor phase transport reactions.

## REFERENCES


1. Hägg, G. Z. Phys. Chem. 1930, B6, 221.
2. Hägg, G. Z. Phys. Chem. 1931, B12, 33.
3. Rundle, R. E. Acta Crystallogr. 1948, 1, 180.
4. Goldschmidt, H. J. "Interstitial Alloys"; Plenum Press: New York, 1967.
5. Johansen, H. A. In "Survey of Progress in Chemistry"; Academic Press: New York, 1977; Vol. 8, p. 57.
6. Hume-Rothery, W. Phil. Mag. 1953, 44, 1154.
7. Klein, B. M.; Papaconstantopoulos, D. A.; Boyer, L. L. Phys. Rev. B 1980, 22, 1946.
8. Wijeyesekera, S.; Hoffmann, R. Organometallics 1984, 3, 7.
9. Kieffer, R.; Benesovsky, R.; Lux, B. Planseeberichte Pulvermetallurgie. 1956, 4, 30.
10. Parthé, E.; Rieger, W. J. Dental Res. 1968, 47, 829.
11. Aronsson, B. Acta Chem. Scand. 1960, 14, 1414.
12. Kwon, Y.-U.; Rzeznik, M. A.; Guloy, A.; Corbett, J. D. Chem. Mater. 1990, 2, 546.
13. Parthé, E.; Norton, J. T. Acta Crystallogr. 1958, 11, 14.
14. Nowotny, H.; Lux, B.; Kudielka, H. Monatsh. Chem. 1956, 87, 447.
15. Parthé, E. Powder Met. Bull. 1957, 8, 23.
16. Brewer, L.; Krikorian, O. J. Electrochem. Soc. 1956, 103, 38.
17. Schachner, H.; Cerwenka, E.; Nowotny, H. Monatsh. Chem. 1953, 84, 677.

18. Kim, S.-J.; Kematick, R. J.; Yi, S. S.; Franzen, H. F. J. Less-Commom Met. 1988, 137, 55.

19. Schachner, J. C.; Nowotny, H. Z. Metallkd. 1980, 71, 341.

20. Parthé.; Jeitschko, W.; Sadagopan, V. Acta Crystallogr. 1965, 19, 1031.

21. Brown, P. W.; Worzala, F. J. J. Less-Common Met. 1975, 41, 77.

22. Jeitschko, W.; Nowotny, H.; Benesovsky, F. Monatsh. Chem. 1963, 94, 844.

23. Pötzschke, M.; Schubert, K. Z. Metallkd. 1962, 52, 474.

24. Schubert, K.; Meissner, H. G.; Pötzschke, M.; Rossteutscher, W.; Stolz, E. Naturwissenschaften 1962, 49, 57.

25. Nandedlkar, R. V.; Delavignette, P. Phys. Status Solidi 1982, A73, K157.

26. Rossteutscher, W.; Schubert, K. Z. Metallkd. 1965, 56, 813.

27. Kwon, Y.-U.; Corbett, J. D. Chem. Mater. 1990, 2, 27.

28. Rieger, W.; Nowotny, H.; Benesovsky, F. Monatsh. Chem. 1965, 96, 232.

29. Rieger, W.; Parthé, E. Monatsh. Chem. 1968, 99, 291.

30. Hohnke, D.; Parthé, E. J. Less-Common Met. 1969, 17, 291.

31. Rieger, W.; Parthé, E. Acta Crystallogr. 1968, B24, 456.

32. Garcia, E.; Corbett, J. D. Inorg. Chem. 1988, 27, 2907.

33. Garcia, E.; Corbett, J. D. Inorg. Chem. 1990, 29, 3274.

34. Jeitschko, W.; Nowotny, H.; Benesovsky, F. J. Less-Commom Met. 1964, 7, 133.

35. Schob, O.; Nowotny, H.; Benesovsky, F. Planseeber. Pulvermet. 1962, 10, 65.

36. Boller, H.; Parthé, E. Acta Crystallogr. 1963, 16, 830.

37. Kocherzhinskii, Y. A.; Kulik, O. G.; Shishkin, E. A. Metallofizika 1976, 64, 48.

38. Garcia, E., Ph.D. Dissertation, Iowa State University, Ames, 1987.

39. Kwon, Y.-U.; Sevov, S.; Corbett, J. D. Chem. Mater. 1990, 2, 550.

40. Boisot, M. P. J. Nucl. Mater. 1968, 25, 350.

41. Sevov, S.; Corbett, J. D., Department of Chemistry, Iowa State University, Ames, IA, unpublished research, 1990.

42. Pauling, L. "The Nature of the Chemical Bond"; 3rd ed.; Cornell University Press: Ithaca, New York, 1960; p. 403.

43. Pauling, L. "The Nature of the Chemical Bond"; 3rd ed.; Cornell University Press: Ithaca, New York, 1960; pp. 246-247.

44. Franzen, H. F.; Beineke, T. A.; Conard, B. R. Acta Crystallogr. 1968, B24, 412.

45. Rogel, F.; Zhang, J.; Payne, M. W.; Corbett, J. D. Adv. Chem. Ser. 1990, 226, 369.

46. Hansen, M. "Constitution of Binary Alloys"; McGraw-Hill: New York, 1958

47. Dwight, A. B. Trans. Am. Soc. Met. 1961, 53, 479.

48. Stuart, H.; Ridley, N. J. Iron Steel Inst. 1970, 208, 1087.

49. Zainulin, Y. G.; Alyamovskii, S. I.; Shveikin, G. P.; Gel'd, P. V. Inorg. Mater. 1970, 6, 1192.

# PART IV. SUBSTITUTED $W_5Si_3$- AND $Zr_6Al_2Co$-TYPE PHASES FORMED IN THE ZIRCONIUM-ANTIMONY AND ZIRCONIUM-TIN SYSTEMS WITH IRON GROUP METALS

# SUBSTITUTED $W_5Si_3$- AND $Zr_6Al_2Co$-TYPE PHASES FORMED IN THE ZIRCONIUM-ANTIMONY AND ZIRCONIUM-TIN SYSTEMS WITH IRON GROUP METALS[1]

Young-Uk Kwon, Slavi C. Sevov, and John D. Corbett

From the Department of Chemistry,

Iowa State University, Ames, IA 50011

Published in Chemistry of Materials 1990, 2, 551.

## ABSTRACT

Arc-melting and annealing reactions near the composition $Zr_5Sb_3Fe$ yield $ZrFe_2$ plus an $Mn_5Si_3$-type phase with a composition near $Zr_5Sb_{3.3}Fe_{0.3}$. A lower antimony content and a variety of iron group metals produce tetragonal $W_5Si_3$-type phases with a narrow compositional range $\sim Zr_5Sb_{2.5}T_{0.5}$, T = Fe, Co, Ni, Ru, Rh. A single crystal study of the $W_5Si_3$-type $Zr_5Sb_{2.55(1)}Fe_{0.45(1)}$ established a mixed Sb-Fe population on the Sb1 site centering the Zr2 antiprisms (I4/mcm, Z=4, a=11.066(1), c=5.535(1) Å, $R/R_w$ = 1.9/2.8 %). The analogous Zr-Sn-Fe system contains a $W_5Si_3$-like phase $Zr_5Sn_{2+x}Fe_{1-x}$, $0 \leq x \leq 0.28$, but in this case with a lower symmetry tetragonal cell that has distinctly different mixed Fe-Sn populations centering adjacent Zr2 antiprisms (91(2) and 52(2) % Fe for x = 0.28) (I422, Z=4, a=11.1763(7), c=5.4794(6) Å, $R/R_w$ = 1.7/2.2 %). The lower symmetry cannot be deduced from powder pattern data. The hexagonal line phase $Zr_6Sn_2Fe$, previously known as the θ-phase, is obtained when still more zirconium is present ($Zr_6Al_2Co$-structure, $P\bar{6}2m$, Z=1, a=7.9675(6), c=3.4863(5) Å, $R/R_w$ = 2.6/2.9 %). Antimony systems provide analogous substitutional products $\sim Zr_5Sb_{2.3}T_{0.7}$, T = Fe, Co, Ni. Some regularities associated with the three structure types are discussed.

# INTRODUCTION

Our intensive studies of $Zr_5Sb_3$-$Zr_5Sb_3Z$ and $Zr_5Sn_3$-$Zr_5Sn_3Z$ systems have shown that phases with the parent $Mn_5Si_3$-type structure exist for a wide range of Z as an interstitial component.[2-4] However, attempts to introduce iron in this position in either system have been troublesome. These have always led to $ZrFe_2$ precipitation and to a phase with the $Mn_5Si_3$ structure but with evidently mixed Sb-Fe or Sn-Fe interstitials judging from SEM analyses.[2,4,5] Attempts to avoid the mixed products by decreasing the amount of antimony or tin produced new tetragonal phases. We herein report the identification of these as $W_5Si_3$-type structures or a lower symmetry version of the same in which iron has been systematically substituted for some of the Sb or Sn atoms. The stabilization of these phases by iron has also been explored for the neighboring transition metals (T) Co and, in part, Ni, Ru and Rh. We also attempted to repress the formation of mixed products by the addition of more zirconium. This led instead to the formation of hexagonal phases, $Zr_6Sn_2Fe$ for example, with the $Zr_6Al_2Co$ structure.

# EXPERIMENTAL

## Materials

The zirconium metal was a reactor-grade crystal bar sample with principal impurities, in ppm atomic, of Fe 680, Ni 350, Hf 100, O 220 and C 190. This was cold-rolled to sheet, cut into strips and cleaned with a solution of conc. $HNO_3$ and HF in $H_2O$ (55:25:20 v/v). The reagent-grade antimony (Allied Chemical and Dye Co.) showed no impurities in its EDX spectra, and the tin granules (Baker's Analyzed: 99.99%) produced no impurity phases on fusion. Iron sheet (Plastic Metal: 99.5%), cobalt foil (Aesar: 99.9+%), nickel sheet (Matheson Coleman & Bell), rhodium powder (Aesar: 99.9%), and ruthenium powder (Englhard: 99.9%) were used as received.

## Syntheses

All the samples were first prepared by arc-melting reactions, as before.[2,6] For rhodium and ruthenium compounds, the metal powders were first pelletized with zirconium and arc-melted to give the compositions of $Zr_5Rh_2$ and $Zr_5Ru_2$, and these were used as reagents for further reactions. Stoichiometric proportions of the elements or binary compounds were arc-melted in a Centorr 5SA single arc-furnace under an argon atmosphere. In each case, zirconium was first melted as a getter. Product buttons were turned over and remelted at least three times to ensure homogeneity. The compositions of samples so prepared were

corrected assuming that the small weight losses during melting arose solely from tin or antimony volatilization.

Since arc-melting alone may produce heterogeneous or somewhat disordered products, the buttons were next annealed in sealed Ta containers containing 0.08 mm Mo sheet as liners. The latter were found to be indispensable because sample contact with tantalum alone may lead to a significant loss of zirconium above ~1000°C.[4,5] This observation was well exemplified by an annealing reaction of a composition $Zr_5Sn_2Fe$ which converted into $Zr_5Sn_3$ and $ZrFe_2$ when contained in tantalum alone (1000°C, 9 d), while equilibration of the sample in contact with only Mo at 1350°C produced the desired phase. The tantalum containers were in turn always enclosed in evacuated and sealed silica jackets for annealing reactions at 1100°C or below. At higher temperatures, these were equilibrated under dynamic vacuum ($p \sim 10^{-6}$ torr) in a high temperature carbon furnace described elsewhere.[7] Container or other impurity elements were not detectable by SEM-EDX means in any of the products.

## SEM Studies

Photomicrographs and elemental analyses of the samples were obtained using a JEOL JSM-840 scanning electron microscope and a KEVEX EDX system. Samples were dry-polished with a sequence of very fine sandpapers and then ash. Quoted formulas are probably uncertain in the atom coefficients by about ±0.05.

## Powder X-Ray Diffraction

Powder patterns were obtained on samples mounted between pieces of cellophane tape. An Enraf-Nonius Guinier camera, Cu $K\alpha_1$ radiation ($\lambda$=1.54056 Å), and NBS (NIST) silicon as an internal standard were employed for this purpose. The known $2\theta$ values of the standard lines were fitted to a quadratic in their positions on the film, and the lattice constants of the sample then calculated by a least-squares fit to indexed reflections and their $2\theta$ values.

The powder pattern of the so-called $\theta$-phase ($Zr_6Sn_2Fe$) was indexed as hexagonal by trial-and-error means.[8] The volume of the unit cell and the approximate composition allowed an estimation of nine atoms per unit cell. Only one known structure type, $Zr_6Al_2Co$,[9] was found to match this formulation and symmetry,[10] and the powder pattern calculated using the positional parameters of the parent structure and the refined lattice parameters matched the observed one reasonably well. The single crystal structural analysis (below) subsequently confirmed the assignment.

## Single Crystal Analyses

Three crystal structures were refined with the aid of the TEXSAN package[11] and diffraction data from single crystals that were collected on a Rigaku AFC6R single crystal diffractometer with monochromated Mo $K\alpha$ radiation. Reflections in two octants were measured with $2\theta$-$\omega$ scans in all cases. Some details of the data collection and refinement are listed in Table 1. Unique aspects of the crystallography follow:

Table 1. Selected data collection and refinement parameters

| compound | $Zr_5Sb_{2.55}Fe_{0.45}$ | $Zr_5Sn_{2.3}Fe_{0.7}$ | $Zr_6Sn_2Fe$ |
|---|---|---|---|
| group, Z | I4/mcm, 4 | I422, 4 | $P\bar{6}2m$, 1 |
| cell dimensions:[a] | | | |
| a, Å | 11.066(1) | 11.1763(7) | 7.9675(6) |
| c, Å | 5.535(1) | 5.4794(6) | 3.4863(5) |
| V, Å | 667.8(2) | 684.4(1) | 191.66(4) |
| 2θ(max), ° | 75 | 55 | 60 |
| independent refl | 376 | 350 | 196 |
| μ(Mo Kα), $cm^{-1}$ | 180.3 | 164.4 | 159.6 |
| transm. factor range | 0.77-1.00 | 0.75-1.00 | 0.71-1.00 |
| R,[b] % | 1.9 | 1.7 | 2.6 |
| $R_w$,[b] % | 2.8 | 2.2 | 2.9 |

[a]Cell data from Guinier powder diffraction, λ=1.54056 Å.

[b]$R=\Sigma||Fo|-|Fc||/\Sigma|Fo|$; $R_w=[\Sigma\omega(|Fo|-(Fc|)^2/\Sigma\omega(Fo)^2]^{1/2}$; $\omega=[\sigma(Fo)]^{-2}$.

**$Zr_5Sb_{2.5}Fe_{0.5}$**

Single crystals resembling cut gems were picked from an as-cast sample of nominal composition $Zr_5Sb_{2.55}Fe_{0.67}$ that exhibited only trace amounts of other phases (see Results); the crystals were loaded in air into thin-walled glass capillaries and sealed off. The candidate crystals were checked with oscillation photographs, and one of them (no clear morphology, 0.5 x 0.5 x 0.4 mm) was selected for data collection. The 25 reflections found from a random search were indexed with a body-centered tetragonal cell. The body centering was also indicated by its previously indexed powder pattern and, therefore, this condition was imposed for data collection. After correction for absorption with the aid of a ψ-scan, the diffraction data showed additional systematic absences of 0kl(k,l=2n) with two very weak violations. Among the three possible space groups, I4cm, $I\bar{4}2m$ and I4/mcm, the last, centrosymmetric one was chosen for the first trial, and this turned out to be correct.

The application of direct methods (SHELXS-86[12]) gave two positions, and these were assigned as Sb2 and Zr1 for the starting model. One cycle of least-squares refinement and a difference Fourier synthesis revealed two more atoms, Zr2 and Fe. Refinement with isotropic thermal parameters proceeded smoothly (R=9 %), but this resulted in an unreasonably small thermal parameter for Fe. The next step was to include antimony (Sb1) in the iron position with the condition that the Sb1 and Fe occupancies sum to unity. The final refinement converged at R=1.9 %, $R_w$=2.8 % with the refined formula $Zr_5Sb_{2.55(1)}Fe_{0.45(1)}$, in excellent accord with the EDX result as well as close to the loaded

composition. The multiplicities of Zr2 and Sb2 did not deviate from unity by more than 0.5 % with Zr1 fixed, and therefore these were not varied in the final refinement. The largest residual peaks in the final difference Fourier, 2.3 and -2.0 e/Å$^3$, were <1 Å from Zr2. The result was later recognized as a substituted $W_5Si_3$-type structure.

**$Zr_5Sn_{2.3}Fe_{0.7}$**

Some single crystals were picked from a crushed button of the composition $Zr_5Sn_2Fe$ that had been annealed at 1350°C (see Results). The powder pattern could be entirely accounted for by a tetragonal $W_5Si_3$-type phase plus a small amount of $ZrFe_2$. The crystals were checked with oscillation photographs, and only two of them showed relatively few extra reflections in addition to those expected for the tetragonal phase. A reasonable set of cell parameters from lists of randomly registered reflections on the diffractometer was obtained only from the stronger reflections. This suggested that there might be severe interference from the satellite crystals, so an initial orientation matrix was determined using only reflections fitting a tetragonal cell, which also indicated that the cell was body-centered. No reflection conditions were imposed during the data collection. Three psi-scans were employed for absorption correction.

The data set confirmed the centering, and it also contained weak but statistically significant reflections in 30 out of 80 instances where systematic absences normally occur for a $W_5Si_3$-type structure (I4/mcm), namely, for h0l (or 0kl) with h(k) and l=2n + 1. Since over 90 % of the

other measured reflections were observed, the result was taken to mean that there must be a real reduction in symmetry in the structure. The only subgroup in the same Laue class with the observed absence conditions, I422 (no. 97), was subsequently found to be correct. Satisfactory solutions could not be found in other plausible space groups that lacked the subgroup relationship.

The initial model was again found with SHELXS-86. The refinement went well to R=2.2 %, $R_w$=5.2 % with anisotropic thermal parameters and a secondary extinction correction. A partial substitution of Fe by Sn in the two independent antiprism centers present with this space group was suggested by their large effective scattering. The amounts of tin substitution was roughly estimated from the iron multiplicities and so refined, after which the thermal parameters behaved normally and both could be refined simultaneously. However, $R_w$ (3.6 %) and goodness of fit (1.89) were still somewhat high, and there were 11 reflections for which $\Delta F/\sigma F > 5.0$. The worst was for (110), for which $\Delta F/\sigma F$=22.4. This was taken to arise from an accidental interference from a satellite crystal so the reflection was discarded. This changed the refined structure very slightly, but the statistics improved significantly: R=1.7 %, $R_w$=2.2 %, GOF=1.16, and only one reflection now had $\Delta F/\sigma F > 5$. The composition refined to $Zr_5Sn_{2.28(2)}Fe_{0.72(2)}$ when only Zr1 was held fixed; this compares reasonably well with the average EDX result for crystals in the initial button, $Zr_5Sn_{2.17}Fe_{0.77}$.

The correct enantiomer was confirmed by comparison of Fo and Fc values for 23 reflections for which the choice had the largest effect on Fc. The result was 15:8 in favor of that reported.

Because there are only subtle differences in the dimensions of the two centered antiprisms, based entirely on the z parameter of Zr2, a refinement with this parameter fixed at the ideal value (z=3/4) was tried. This resulted in 0.1% greater R indices, while parameters applying to the mixed Fe-Sn sites changed by $2\sigma$ or less. However, the average of Fo-Fc for the reflections that were violations in the ideal I4/mcm was about 15% higher.

Another relevant observation was that the z parameter of Zr2 had a standard deviation about ten times that of the other positional parameters. Coupling of the z parameter refinement with the multiplicities of Fe, Sn sites was not the cause. The implication is that the Zr2 atoms were slightly disordered along c-direction. Spacegroup I4, a subgroup of I422 in the lower Laue class, was also explored to see whether the two-fold axes perpendicular to $\vec{c}$ in the latter were responsible. In fact, standard deviations of all z parameters were now large, and the thermal parameters of Fe2, Sn3 became very anisotropic.

With these results, we concluded that the original refinement in the space group I422 was the right one, and that the behavior of the Zr2 atoms was probably a reflection of the random occupancies of the centers of the Zr2 antiprisms by Sn and Fe atoms of somewhat different sizes.

**$Zr_6Sn_2Fe$**

Some regular hexagonal plate crystals obtained after annealing an arc-melted button of the composition $Zr_6Sn_{1.8}Fe_{1.0}$ (see Results) were sealed in glass capillaries. Oscillation photographs showed most of these to be single. Random reflections located and tuned by the diffractometer gave an hexagonal unit cell, and two octants of reflection data collected on this basis indicated Laue symmetry 6/mmm with no systematic absences. Among the five possible space groups, $P\bar{6}2m$ was selected since the powder pattern had already been identified as that of a $Zr_6Al_2Co$-type material (above). The corresponding atom positions were used for the initial model. Refinement with isotropic thermal parameters yielded R=7 %, $R_w$=9 %. However, further refinement did not give much improvement in the residuals until a secondary extinction correction was applied which gave convergence at R=2.6%, $R_w$=2.9%. The refined composition $Zr_3Zr_{2.99(2)}Sn_{1.98(1)}Fe_{1.00(1)}$ indicated the absence of substitutional defects, and so the atoms were returned to unit occupancy. The largest residual electron density, 1.9 $e/Å^3$, was close to Zr1. The other possible enantiomer gave residuals that were 0.6 - 0.8% higher.

The refined parameters and important bond lengths for the three structures studied are listed in Table 2 and 3. More crystal and refinement data, the anisotropic displacement parameters, and the structure factor data are available as supplementary material.

Table 2. Positional parameters and multiplicities of atoms

| | occup[a] | sym | x | y | z | Biso, Å$^2$ |
|---|---|---|---|---|---|---|
| | | $Zr_5Sb_{2.55}Fe_{0.45}$ ($W_5Si_3$-type) | | | | |
| Zr1 | 1 | m | 0 | 1/2 | 1/4 | 0.47(2) |
| Zr2 | 1 | $\bar{4}2m$ | 0.07675(4) | 0.21593(5) | 0 | 0.51(2) |
| Sb2 | 1 | mm | 0.16302(3) | x + 1/2 | 0 | 0.47(1) |
| Sb1 | 0.55(1) | 42 | 0 | 0 | 1/4 | 0.72(2) |
| Fe | 0.45(1) | | | | | |
| | | $Zr_5Sn_{2.3}Fe_{0.7}$ ($W_5Si_3$ derivative) | | | | |
| Zr1 | 1.000(4) | 222 | 0 | 1/2 | 0 | 0.6(1) |
| Zr2 | 1 | 1 | 0.07552(4) | 0.21043(4) | 0.7482(4) | 0.79(2) |
| Sn2[b] | 1.009(3) | 2 | 0.16375(3) | x + 1/2 | 3/4 | 0.57(1) |
| Sn1 | 0.09(2) | 42 | 0 | 0 | 0 | 0.7(2) |
| Fe1 | 0.91(2) | | | | | |
| Sn3 | 0.48(2) | 42 | 0 | 0 | 1/2 | 0.8(1) |
| $Fe_2$ | 0.52(2) | | | | | |
| | | $Zr_6Sn_2Fe$ ($Zr_6Al_2Co$-type) | | | | |
| Zr1 | 1 | mm | 0.3929(2) | 0 | 0 | 0.63(6) |
| Zr2 | 0.996(8) | mm | 0.7548(1) | 0 | 1/2 | 0.50(5) |
| Sn | 0.990(6) | $\bar{6}$ | 1/3 | 2/3 | 1/2 | 0.64(2) |
| Fe | 1.00(1) | $\bar{6}m2$ | 0 | 0 | 0 | 0.75(6) |

[a]The mixed atom populations and the compound's crystal compositions are based on the assumption that there are no vacancies in the lattices (see text).

[b]Standard coordinates would be 0.33625(3), x + 1/2, 1/4.

Table 3. Important distances lengths(Å) in $Zr_5Sb_{2.55}Fe_{0.45}$, $Zr_5Sn_{2.3}Fe_{0.7}$ and $Zr_6Sn_2Fe$

| | $Zr_5Sb_{2.55}Fe_{0.45}$ | $Zr_5Sn_{2.3}Fe_{0.7}$ | $Zr_6Sn_2Fe$[c] |
|---|---|---|---|
| Zr1 - Zr1 | 2.7675(7) | 2.7397(3) | |
| Zr2 - Zr2 | 3.5866(9) | 3.5338(7) | |
| Zr2 - Zr2(□-□) | 3.2471(9) | 3.231(4) | |
| | | 3.205(4)[a] | |
| | 3.5219(9) | 3.484(4) | |
| | | 3.460(4)[a] | |
| Zr2 - Zr2(interchain) | 3.245(1) | 3.383(1) | |
| Zr1 - Zr2(interchain) | 3.5383(6) | 3.618(1) | |
| | | 3.611(1) | |
| Zr2 - Sb1, Sn1, Fe | 2.8891(6) | 2.853(1) | |
| Zr2 - Sn3, Fe2 | | 2.846(1) | |
| Zr1 - Sb2, Sn2 | 2.9025(6) | 2.9282(4) | |
| Zr2 - Sb1, Sn1 | 2.9389(7)[b] | 2.9605(6)[b] | |
| | 2.9725(6)[b] | 3.0213(5)[b] | |
| | 3.2195(8) | 3.227(2) | |
| Zr1 - Sn | | | 3.0094(4) |
| Zr2 - Sn | | | 3.0678(8) |
| Zr1 - Zr1 | | | 4.2491(8) |
| Zr1 - Zr2 | | | 3.369(1) |
| | | | 3.2464(8)[d] |
| Zr2 - Zr2 | | | 3.384(2) |
| Zr1 - Fe | | | 3.130(1) |
| Zr2 - Fe | | | 2.6182(9) |

[a]Around the more nearly equally populated Fe2-Sn3 site.

[b]Normal to c.

[c]All atoms have a like-atom repeat at 3.4863(5) Å($\vec{c}$).

[d]Within tricapped trigonal prism.

# RESULTS AND DISCUSSION

## Antimony System

Attempts to prepare the iron analogue of the stable $Zr_5Sb_3Co$, where interstitial cobalt is bound within an $Mn_5Si_3$-type structure,[2] regularly gave $ZrFe_2$ plus a phase with the $Mn_5Si_3$ structure and a composition near $Zr_5Sb_{3.3}Fe_{0.3}$ that presumably reflects a mixed Sb-Fe occupancy of the interstitial position. Reduction of the antimony content in an effort to obtain a simpler product like $Zr_5Sb_3Fe_x$ led instead to a tetragonal phase. EDX analyses and a single crystal structural study showed this was ~$Zr_5Sn_{2.5}Fe_{0.5}$ in a $W_5Si_3$-type structure with iron substituting for some antimony (below). This result led to the synthetic and analytical studies to determine the phase characteristics of the new material, Table 4. Reactions with the composition $Zr_5Sb_{2.5}Fe_{0.5}$ were found to yield a pure phase with $W_5Si_3$-structure both before and after an annealing treatment, and SEM-EDX analyses also showed that both samples consisted of homogeneous single phases. Some (0.1-0.2 %) lattice parameter shrinkage was observed on annealing, but such effects are common[2,6,7] and presumably reflect improved ordering.

The next four reactions, Table 4, were designed to diagnose phase stability on variation of the iron content while the Zr:Sb ratio was held near 5:2.5. Increased iron led to the appearance of $ZrFe_2$ and, now that the sample was antimony-richer than $Zr_5Sb_{2.5}Fe_{0.5}$, to a $Mn_5Si_3$-type phase near ~$Zr_5Sb_{3.2}Fe_{0.2}$ in addition to the major phase, viz.

Table 4. Formation of the $W_5Si_3$-type phase in the Zr-Sb-Fe system

| rxn | composition[a] | conditions[b] | results[c] (Zr:Sb:Fe) |
|---|---|---|---|
| 1 | 5:2.47:0.5 | AM | W |
| | | AN | W[d] |
| 2 | 5:2.55:0.67 | AM | W + M(trace) + $ZrFe_2$(trace) |
| | | AN | W + M + $ZrFe_2$ |
| 3 | 5:2.53:0.67 | AM | W + $ZrFe_2$ |
| 4 | 5:2.51:0.62 | AM | W + $ZrFe_2$(trace) |
| | | AN | W + M(trace) + $ZrFe_2$ |
| 5 | 5:2.5:0.33 | AM | W + Y |
| | | AN | W + Y |
| 6 | 5:2.67:0.5 | AM | W + M |
| | | AN | W + M |
| 7 | 5:2:0.42 | AM | W + Z[e] + β-Zr(Sb) |

[a]Loaded compositions; the analytical composition for some of the samples are given in the text.

[b]AM: arc-melting; AN: annealing of the previous arc-melted sample at 1200°C for 3d.

[c]Phases were identified by both EDX measurements and powder patterns. W: $W_5Si_3$-type; M: $Mn_5Si_3$-type with a composition near $Zr_5Sb_{3.3}Fe_{0.3}$(lower limit); Y: $Y_5Bi_3$-type; Z: $Zr_6Al_2Co$-type.

[d]$Zr_5Sb_{2.58}Fe_{0.53}$ by SEM; a=11.0885(3), c=5.5420(3) Å.

[e]a=7.706(1), c=3.773(1) Å.

"$11Zr_5Sb_{2.5}Fe_{0.67}$"$\longrightarrow 10Zr_5Sb_{2.5}Fe_{0.5} + 0.8Zr_5Sb_{3.2}Fe_{0.2} + 1.1ZrFe_2$. With a smaller amount of iron, a $Y_5Bi_3$-type phase also appeared, as observed before for binary antimony-limited compositions near $Zr_5Sb_3$.[13]

The last two reactions, Table 4, were run with varying amounts of antimony. An excess gives the $Mn_5Si_3$-type phase seen before, and a deficiency produces a hexagonal $Zr_6Al_2Co$-type phase (below) plus zirconium. EDX analyses of the most antimony-deficient sample gave $\sim Zr_6Sb_{2.3}Fe_{0.7}$ for the $Zr_6Al_2Co$-type portion and $\sim Zr_5Sb_{2.42}Fe_{0.53}$ for the $W_5Si_3$-type phase. We conclude that the $W_5Si_3$-type phase in this system has a narrow composition range at ~1200°C, from $\sim Zr_5Sb_{2.40}Fe_{0.60}$ (rxn 3) with a=11.083(1), c=5.540(1) Å to $\sim Zr_5Sb_{2.55}Fe_{0.44}$ (rxn 6) and a=11.107(1), c=5.554(1) Å. The sums of the antimony and iron contents were always close to 0.60 per zirconium, implying that there are no vacancies in the structure.

On the basis of these observations, analogous phases were studied in which other transition metal atoms (T) substitute for iron in $Zr_5Sb_{2.5}T_{0.5}$ phases, Table 5. All the iron group elements and their fifth period congeners Ru and Rh form the $W_5Si_3$ phase with almost the same feature, that is, with a composition near $Zr_5Sb_{2.5}T_{0.5}$ apparently necessary for stability. The phase compositions determined by EDX methods varied modestly on annealing, mainly for the $Mn_5Si_3$-type examples, and these implied mixed Sb-T populations in both the $Mn_5Si_3$ interstitial site and in the cobalt site in $Zr_6Al_2Co$-type examples as well. The $Mn_5Si_3$ examples appear only with higher antimony concentrations.

Table 5. Products in $Zr_5Sb_{2.5}T_{0.5}$ syntheses (T=Co, Ni, Ru and Rh)[a]

| rxn | conditions[b] | | products | | |
|---|---|---|---|---|---|
| | (°C, d) | Zr:Sb:T[c] | phase[d](%) | a | c |
| Co | AM | 5:2.55:0.37 | W (80) | 11.095(2) | 5.541(1) |
| | | 6:2.34:0.69 | Z (20) | 7.741(1) | 3.686(1) |
| | AN, 1100, 30 | 5:2.5:0.35 | W | 11.100(1) | 5.540(1) |
| | | | Z (trace) | | |
| Ni | AM | 5:2.45:0.43 | W (65) | 11.100(2) | 5.527(1) |
| | | 5:3.3:0.3 | M (25) | 8.463(1) | 5.772(1) |
| | | 6:2.44:0.65 | Z (10) | 7.69(1) | 3.78(1) |
| | AN, 1200, 30 | 5:2.55:0.4 | W (85) | 11.093(2) | 5.524(1) |
| | | 6:2.35:0.7 | Z (10) | 7.689(5) | 3.792(5) |
| | | | M (trace) | | |
| Ru | AM | | W (60) | 11.089(3) | 5.575(2) |
| | | | M (40) | 8.468(4) | 5.818(4) |
| Rh | AM | 5:2.45:0.65 | W (40) | 11.091(2) | 5.549(1) |
| | | 5:3.1:0.14 | M (60) | 8.479(1) | 5.787(2) |
| | AN, 1100, 30 | 5:2.5:0.55 | W (70) | 11.107(2) | 5.563(1) |
| | | 5:3.26:0.3 | M (30) | 8.592(1) | 5.855(1) |

[a]All reactions were loaded as $Zr_5Sb_{2.5}T_{0.5}$.

[b]AM: arc-melting; AN: annealing of the previously arc-melted samples.

[c]Compositions of corresponding phases as determined by EDX.

[d]Abbreviations and cell types W: $W_5Si_3$, tetragonal; M: $Mn_5Si_3$, Z: $Zr_6Al_2Co$, both hexagonal. Cell dimensions are in Å.

A tetragonal $W_5Si_3$-type structure with a composition $Zr_5Sb_{2.55(1)}Fe_{0.45(1)}$ was refined from single crystal X-ray data. All of the Sb-Fe mixing occurs on the main group element (Sb1) site that centers square antiprisms of zirconium. The X-ray analysis assumed there were no vacancies at this point, in accord with the SEM-EDX results. A convenient geometric description of the structure starts with antiprisms (Zr2) that share opposite square faces to generate infinite chains $^1_\infty[Zr_{8/2}(Sb_xFe_{1-x})Sb_{8/2}]$. One of these is highlighted in Figure 1 in a projection down the short c axis. The twist angle between the squares is actually 39.1° rather than the ideal 45°. The structure also contains parallel, linear chains of zirconium with a very short repeat (2.77 Å = c/2) that lie within shared $^1_\infty[ZrSb_{4/2}]$ tetrahedra centered on the side faces of the cell in this view. The two chains are not as independent as this description suggests, however; the same antimony atoms envelope both chains, those in the tetrahedra also bridging pairs of edges of the zirconium antiprisms (Figure 1, dashed lines). Side views of the two chains are shown in Figure 2 with these interconnections omitted. Other short Zr-Zr separations in this material will be noted later in a comparison of structures.

## Tin in $W_5Si_3$-Like Phases

Tin analogues of the foregoing antimony phases are closely related but with some contrasts; only iron seems to form a $W_5Si_3$-like phase, this has a higher iron content, and a lower crystal symmetry yields two different populations for the antiprismatic chain-centering Sn-Fe atoms.

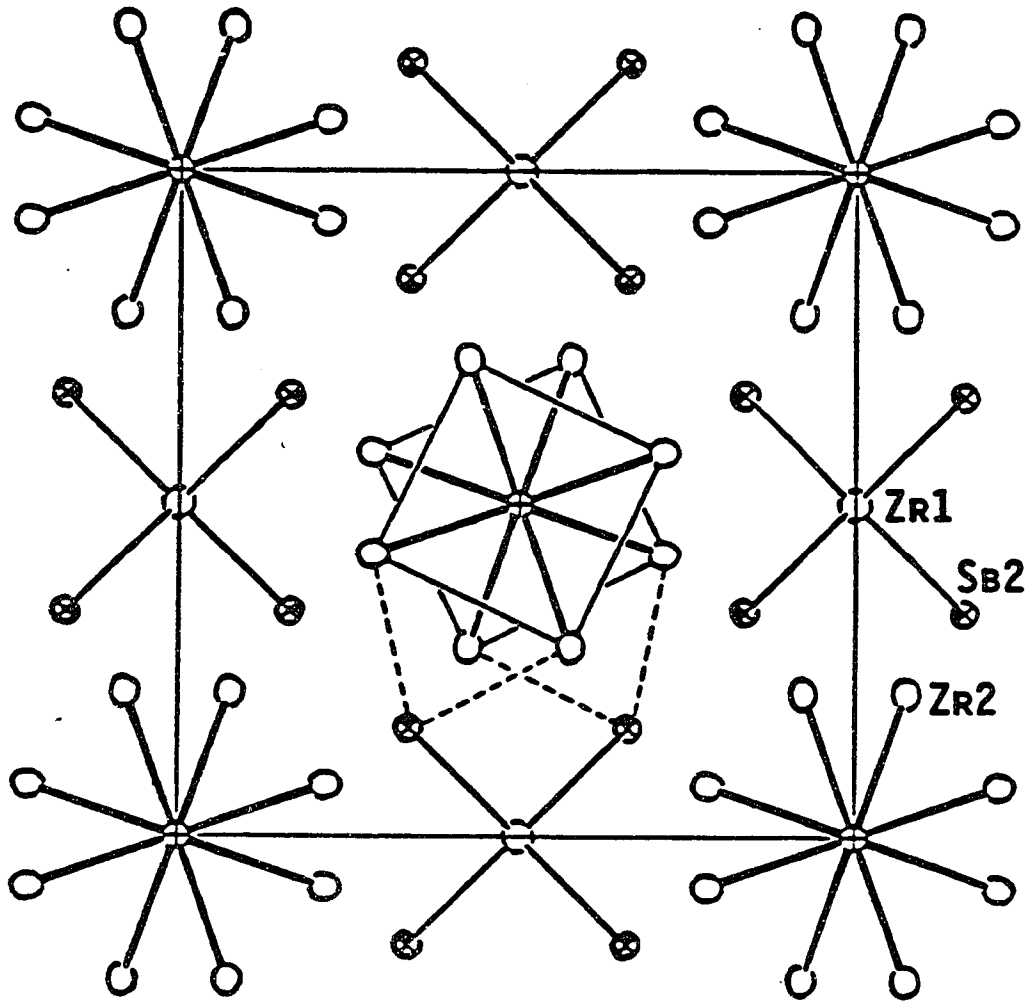


Figure 1. Projection of the tetragonal structure of $Zr_5Sb_{2.55}Fe_{0.45}$ down the short c axis. The Zr2 (◯) antiprism about the $Sb_{2.55}Fe_{0.45}$ site (⊕) in the center of the cell and the tetrahedra of Sb2 (◔) about Zr1 are emphasized. Other short Zr2-Zr2 and Zr1-Zr2 separations are shown (see text). Dashed lines illustrate the commononality of antimony to both chains (97 % probability ellipsoid).

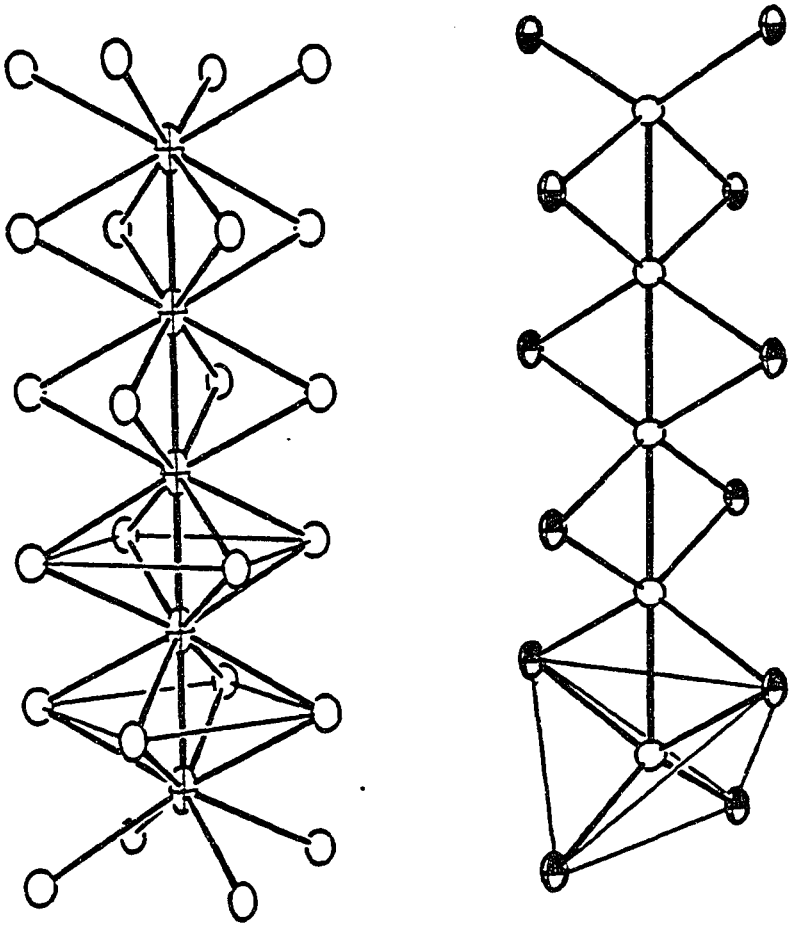

Figure 2. Side view illustrating the geometric essence of the chains of $(Sb,Fe)Zr_{8/2}$ and $Sb_{4/2}Zr$ (right) in $Zr_5Sb_{2.55}Fe_{0.45}$. One antiprism and one tetrahedron are lightly outlined (97 %).

As-cast samples are invariably composed of $Mn_5Si_3$-type phases and $ZrFe_2$, Table 6, and only after annealing do $W_5Si_3$-type phases appear. The optimal yields of the $W_5Si_3$ example, 80-90 %, were achieved for compositions $Zr_5Sn_{2+x}Fe_{1-x}$, $0 < x < 0.28$, judging from the intensity distributions in the powder patterns (Table 6) and the X-ray analysis. This range was also supported by (unconstrained) EDX results of $\sim Zr_5Sn_{1.95}Fe_{1.05}$ and $\sim Zr_5Sn_{2.25}Fe_{0.75}$ for this portion of annealed compositions $Zr_6Sns_{1.8}Fe_{1.2}$ and $Zr_6Sn_2Fe$ (both primarily $Zr_6Al_2Co$-type products, below). Analogous reactions with cobalt gave only $Zr_6Al_2Co$- and $Mn_5Si_3$-type phases upon annealing.

The refined $W_5Si_3$-like structure for this sample is iron-richer than found with antimony, $Zr_5Sn_{2.28(2)}Fe_{0.72(2)}$ and near the inferred lower limit for iron (above). The acentric space group I422 lacks all mirror planes normal to the four-fold axis present in the parent $W_5Si_3$ (I4/mcm, Figure 1) although the two independent, centered Fe-Sn sites in adjacent antiprisms retain 42 symmetry. The shared faces of the antiprisms are still the same size but these are no longer equally spaced, although their alternate displacements in $\vec{c}$ are only 0.020 Å. More importantly, the two mixed Sn-Fe populations refine to distinctly different values, 91(2) % and 52(2) % iron (assuming no vacancies). Surprisingly, the latter occurs in the slightly smaller antiprism although the refined Zr-Sn, Fe distances differ by only 0.007 Å (5σ). The violations of the systematic absences for an ideal $W_5Si_3$ arrangement come solely from the unfixed z-coordinate of Zr2 and the unequal atomic distributions of the mixed Sn and Fe. The latter appear to contribute

Table 6. Formation of $W_5Si_3$-type phases in Zr-Sn-T systems, T=Fe, Co

| rxn | composition[a] (Zr:Sn:T) | conditions[b] (°C, d) | results[c] |
|---|---|---|---|
| Fe | 5:2.5:0.5 | AM | M + $ZrFe_2$ |
| | | AN, 1000, 7 | W + M |
| | 5:2.25;0.75 | AM | M + $ZrFe_2$ |
| | | AN, 1050, 7 | W (a=11.1663(9), c=5.4747(8)) + M (trace) + $ZrFe_2$ (trace) |
| | 5:2.0:1.0 | AM | M + $ZrFe_2$ |
| | | AN, 1000, 7 | W (a=11.160(1), c=5.4719(8)) + Z (trace) + $ZrFe_2$ (trace) |
| | 5:2.0:1.0 | AM,AN,1350, 8 | W ($Zr_5Sn_{2.18}Fe_{0.77}$;[d] a=11.1763(7), c=5.4794(6)) + $ZrFe_2$ (<2%) |
| Co | 5:2.0:1.0 | AM | M + impurity |
| | | AN, 1000, 10 | Z (40%) + M (60%) |

[a]Loaded composition.

[b]AM: arc-melting; AN: annealing of the previously arc-melted sample.

[c]W: $W_5Si_3$-type; M: $Mn_5Si_3$-type; Y: $Y_5Bi_3$-type; Z: $Zr_6Al_2Co$-type. Trace is <5%. Dimensions in Angstroms.

[d]Average EDX result.

significantly more to the observations than the deviation of z from 3/4, which may be an artifact of the refinement.

There appears to be no precedent for a $W_5Si_3$-like structure with this lower symmetry, possibly because it generally cannot be distinguished from a $W_5Si_3$-type by powder pattern means. The strongest additional line calculated for the Guinier pattern is only 0.4 % of Imax. Previously reported analogues of both structures involve only mixed main-group elements, e.g., $Co_5Si_2B$, $Fe_5Si_2B$,[14] $Ni_5Si_2B$,[15] and $Nb_5Sn_2Si$,[16] although the binary $\beta$-$Ti_3Sb$ also exhibits the same disposition, $Ti_5Sb_2Ti$.[17] The second and third actually exhibit a Fe or Ni deficiency within the tetrahedral chains, e.g., $Fe_4Fe_{0.86}Si_2B$. All have been studied by powder or single crystal film methods.

Some rationale for the formation of the $W_5Si_3$-like phase on substitution of iron in $Zr_5Sb_3$ or $Zr_5Sn_3$ can be obtained from Pettifor's structure maps.[18,19] Pettifor assigned Mendeleev numbers[20] in such a way that elements in one group have successive numbers, and he then defined structural fields on this basis. In the $A_5B_3$ binary map, the point corresponding to $Zr_5Sb_3$ falls in the $Mn_5Si_3$-type region, as it should, but the substitution of iron or any other of the transition elements tried in this study for antimony would move the point toward the $W_5Si_3$ region. Since no boundary between these two structure types was established in the map, it is not clear what amount of substitution is needed to form a $W_5Si_3$-type structure. The same expectation holds for $Zr_5Sn_3$, which also forms in $Mn_5Si_3$-type structure. However, why a cobalt example does not always form cannot be answered with this map.

Of course, the stability of $ZrFe_2$ also plays an important role in determining the composition of the $W_5Si_3$-type products.

## $Zr_6Al_2Co$-Type Phases

A new phase was seen in compositions near $Zr_5Sn_2Fe$, and its powder pattern was found to be in good agreement with that for a $Zr_6Al_2Co$-type phase. Several compositions around this were studied in an effort to clarify the system, Table 7. As-cast samples contained only a $Mn_5Si_3$-type phase and $ZrFe_2$, but annealing at 1000°C for seven days was sufficient to produce the pattern of what was presumed to be the peritectically decomposing tin-iron analog, $Zr_6Sn_2Fe$. However, not a single sample prepared in this way was single phase. Even reactions with the stoichiometry determined by the single crystal structural analysis (below) showed ~15% of a $W_5Si_3$-type phase (and possible $ZrFe_2$) in the powder pattern. Incomplete equilibration is evident, perhaps because of a gross composition inhomogeneity produced by the arc-melting.[6] Nonetheless, the very brittle, annealed $Zr_6Sn_{1.8}Fe_{1.0}$ product yielded single crystals, and the structure was refined as the expected $Zr_6Al_2Co$-type. The lattice parameters of this phase do not change with loaded composition. This and the stoichiometric result of the structure refinement, $Zr_6Sn_{1.99(1)}Fe_{1.00(1)}$, indicate a line phase without vacancies near 1050°C.

The analogous cobalt compound also forms; however, no further attempts were made to elucidate the composition width or the details of the structure. $Zr_6Al_2Co$-type phases are also formed with antimony

Table 7. Characteristics of $Zr_6Al_2Co$-Type phases in Zr-Sn-T systems, T=Fe, Co

| | composition[a] (Zr:Sn:T) | conditions[b] | (°C, d) | results[c] |
|---|---|---|---|---|
| Fe | 6:1.8:1.2 | AM | | M + $ZrFe_2$ (10%) + impurity (10%) |
| | | AN | 1000, 8 | Z + $ZrFe_2$ (5%) + W (10%) + M (2%) |
| Fe | 6:2.0:1.0 | AM | | M + $ZrFe_2$ (10%) + impurity (10%) |
| | | AN | 1000, 7 | Z + W (15%) |
| Fe | 6:1.8:1.0 | AM,AN | 1050, 7 | Z + W (<5%); very brittle |
| Co | 6:2.0:1.0 | AM,AN | 1000, 10 | Z (a=7.9450(8), c=3.4993(7) Å) |
| | | | | + M (15%) + β-Zr (<3%) |
| | | GRST | 1000, 9 | Z (a=7.9386(6), c=3.5102(7) Å) |
| | | | | + M (15%) |

[a]Loaded composition.

[b]AM: arc-melting; AN: annealing of the previously arc-melted sample; GRST: previous sample was ground, pelleted and sintered.

[c]W: $W_5Si_3$-type; M: $Mn_5Si_3$-type; Z: $Zr_6Al_2Co$-type.

instead of tin, namely, as a minor component in as-cast samples of the composition $Zr_5Sb_{2.5}T_{0.5}$ with T=Fe, Co, Ni, Ru (Tables 4, 5). Antimony evidently again substitutes for some of the T element since the compositions determined by EDX analyses corresponded to a general formula near $Zr_6Sb_{2.3}T_{0.7}$.

The structure of $Zr_6Sn_2Fe$ is shown in Figures 3 and 4 in views along and normal to the hexagonal c axis, respectively. The result can be assembled starting with trigonal prism $(Zr2)_6Fe$ at the origin together with a larger pair of $(Zr1)_6Sn$ trigonal prisms centered on 1/3,2/3,1/2, etc. (Figure 3). The tin-centered prisms also share all edges parallel to $\vec{c}$ to generate a network in the ab plane. Each type of prismatic unit also shares opposite triangular faces with like units to generate confacial chains parallel to $\vec{c}$, viz., $[(Zr2)_{6/2}Fe][(Zr1)_{6/4}Sn)]_2$, Figure 4. Finally, such a high concentration of centered (Fe, Sn) atoms relative to zirconium leads to a secondary condensation between the two types of prismatic units such that zirconium atoms in each prism also cap rectangular faces in the other. These interactions, shown with dashed lines in Figure 3, lead to a classic tricapped trigonal prismatic environment for both Sn and Fe. The Fe-Zr distances in the $FeZr_6$ prisms seem particularly short, 2.619(1) Å, relative to 2.853(1) Å for the 91 % Fe site in $Zr_5Sn_{2.3}Fe_{0.7}$ (above). However, similar results are found for iron within bicapped trigonal prisms in $Zr_3Fe$, where d(Zr-Fe) is 2.63 and 3.03 Å to prismatic and capping zirconium, respectively.[21] On the other hand, roughly octahedral $Zr_6Fe$ units in the more oxidized

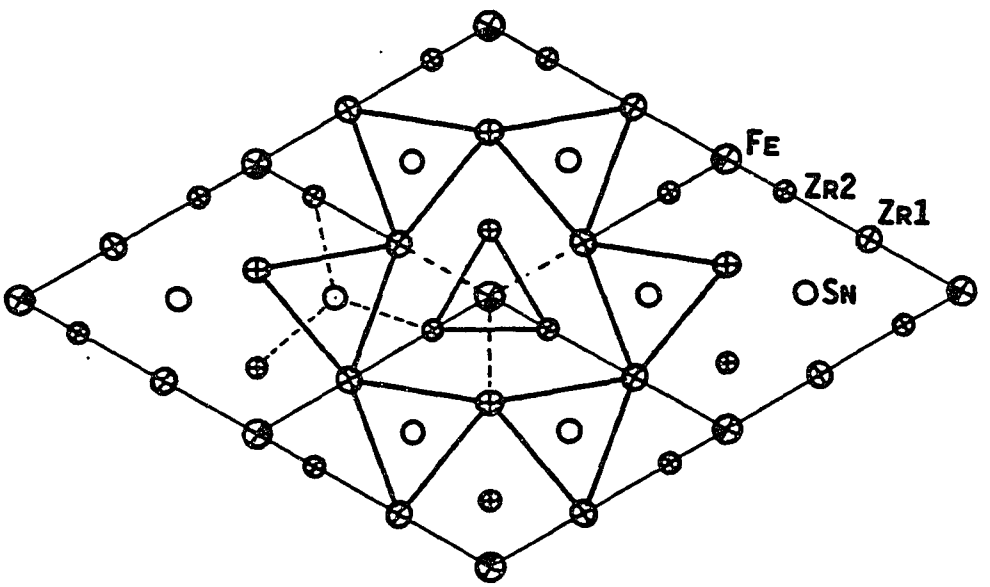


Figure 3. Projection of the hexagonal structure $Zr_6Sn_2Fe$ along the short (3.49 Å) c axis. A portion of the zirconium (⊕) trigonal prisms centered by tin (○) or iron (◐) are emphasized. The two types of prisms differ in elevation by c/2. One set of the prism face-capping interconnections between different kinds of trigonal prisms is shown dashed (99.5 % ellipsoids).

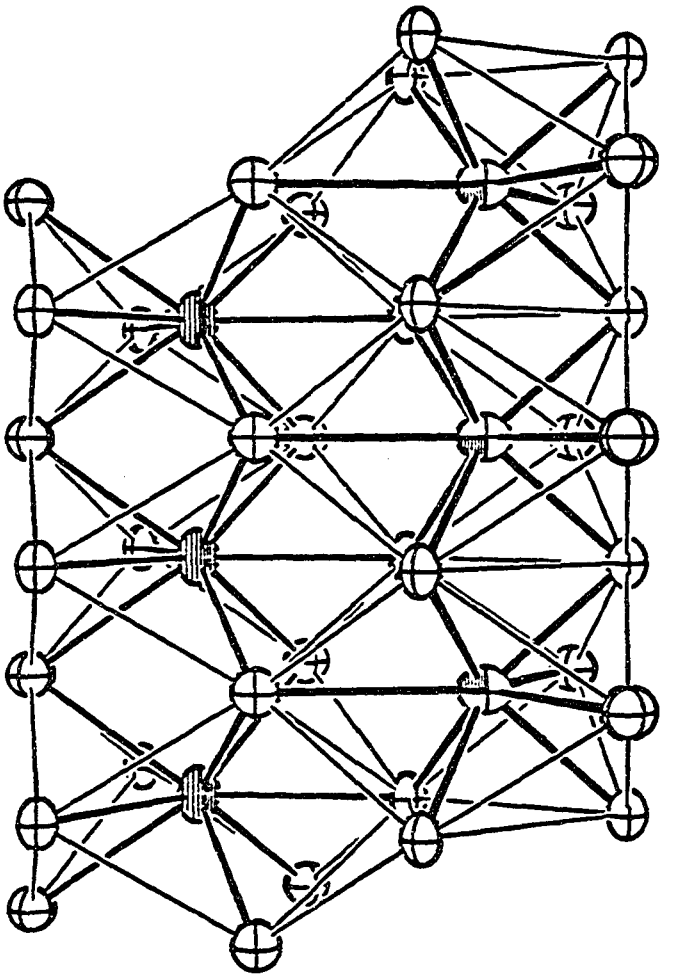

Figure 4. Side view of the pair of interconnected trigonal prismatic chains shown in Figure 3. The tin-centered chain is on the left and the iron-based portion is on the right with the nine Zr-Fe interactions given heavier emphasis. Iron is partially and tin wholly shaded (99.5%).

$Cs_{0.6}Zr_6I_{14}Fe$ have $\bar{d}$(Zr-Fe) as short as 2.48 Å,[22] suggesting there is a good deal more in electronic effects in these compounds than meets the eye!

Except for $Zr_6Al_2Co$ analogues with T=Fe, Ni,[9] there are only a couple of other examples of this structure type, $Ni_6Si_2B$[23] and (anti-) $\beta$-$K_2UF_6$.[24,25] The newly identified $Zr_6Sn_2Fe$ has been found by powder pattern comparison to be identical to the $\theta$-phase reported by Tanner and Levinson[26] in a study of a portion of the Zr-Sn-Fe system. They judged this to be a line phase with a composition near $Zr_6Sn_{1.7}Fe_{1.2}$. The same phase has also been identified by powder X-ray methods as a precipitate after irradiation of $\beta$-Zircaloy-4 with nitrogen ions.[27,28]

There is nothing particularly notable about any other of the Zr-Sb, -Sn, -Fe distances in the structures reported here relative to those in several $Mn_5Si_3$-type examples that have recently been studied for the same or similar elements.[2,4,6,13,29] On the other hand, Zr-Zr bonding and some geometric aspects among these three types do provide some interesting variations and comparisons.

## General Comparison

It is not clear why the foregoing $W_5Si_3$-like phases need two such chemically distinct elements centered in the antiprisms and in almost fixed ratio in each instance in order to stabilize these, but the effect is presumably electronic. Among binary zirconium compounds, the $W_5Si_3$ structure is known only for $Zr_5Al_3$, while this arrangement is distinctly more common with the electron-poorer rare-earth elements or with Ti, Nb

and Ta when either group is combined with Ga or, for the former, In and Tl.[10] Involvement of silicon, germanium or tin as the main-group element (Ma) evidently again provides $W_5Si_3$-type phases only with earlier or later transition elements, namely from group 5 or 6 with Si or Ge or for La, Ce, Pr with Sn.[10] The sparsity of $Zr_5Ma_3$ examples with the $W_5Si_3$ structure must arise because of the greater stability of the $Mn_5Si_3$-type compounds formed between Zr (Hf, Ti) and many of these main group elements, either as binary phases or in ternaries $Zr_5Ma_3Z$ with interstitial Z. $Zr_5Al_3$ also exists as a binary phase with this structure.[30] The conversion to a $W_5Si_3$-like product $Zr_5Ma_{3-x}T_x$ with Ma=Sb, Sn, x ~ 0.5, and T = Fe, Co ... thus appear to be quite specific.

The most interesting structural comparison is between the $Mn_5Si_3$-and $W_5Si_3$-types. The former contain parallel confacial $Mn_{6/2}Si_{6/2}$ trigonal antiprismatic chains and, again, linear manganese chains. These share the same Si atoms which give the second type of manganese a twisted antiprismatic environment. Interchain interactions are relatively long, 3.49 - 3.54 Å in the known binaries $Zr_5Sb_3$[13] and $Zr_5Sn_3$,[6] but still somewhat shorter than Zr-Zr separations within the "octahedral" chains; however, extended Hückel MO calculations on $Zr_5Sb_3$ indicate the interchain "bonds" have relatively low overlap populations.[2] The linear chains in these two phases are evidently bonded, with repeat distances around 2.90 Å [d1(Zr)=2.918 Å]. The alternative $W_5Si_3$ structure appears to form in generally electron-richer systems, e.g., $Nb_5Ga_3$, $Nb_5Ge_3$ and $Mo_5Ge_3$ either alone or with a $Mn_5Si_3$ form as well.[10] (Exceptions include $Zr_5Al_3$ (dimorphic) and a number of rare-earth metal examples

like $La_5Sn_3$.) The electronic factors involved in the structural differentiation are unknown and worthy of study.

The most interesting feature of the $Mn_5Si_3$-type phases formed by zirconium (and rare-earth metals) is their avidity to bond interstitially a wide variety of a third element Z, generally those elements to the right of Fe in the periodic table. These occur in the center of every metal octahedron, obviously gaining strong Zr-Z interactions with small loss of Zr-Zr bonding.[2-4] The alternative with iron (and some neighboring elements T) is to form the zirconium-richer $Zr_5Ma_2(Ma_xT_{1-x})$ described here, where the added elements is an integral part of the $W_5Si_3$ structure, that is, centered in the antiprismatic chain. The change from a $Mn_5Si_3$- to a $W_5Si_3$-type phase is accompanied by not only an increase in coordination number of the centered (T,Z) element from six to eight but also significantly closer Zr-Zr separations, namely, 3.20 - 3.24 Å and 3.24 - 3.38 Å within and between the square antiprismatic chains, respectively, and 2.74-2.77 Å along the linear chains in the compounds described here. A countervailing factor is the decrease in the number of zirconium near neighbors about Sb or Sn from five to four, largely in the environment of the linear zirconium string.

The next step to $Zr_6Sn_2Fe$ represents an obviously efficient way of achieving efficient bonding with nine-coordinate tin and iron. This as well as the substituted $W_5Si_3$-type phases appear to have considerably narrower electronic requirements than do the wide variety of compounds with a $Mn_5Si_3(Z)$-type structure.

## REFERENCES


1. The Ames Laboratory-DOE is operated for the U. S. Department of Energy by Iowa State University under Contract No. W-7405-Eng-82. This research was supported by the Office of Basic Energy Sciences, Materials Sciences Division, Washington, D. C.
2. Garcia, E.; Corbett, J. D. Inorg. Chem. 1988, 27, 2907; 1990, 29, 3274.
3. Corbett, J. D.; Garcia, E.; Kwon, Y-U.; Guloy, A. Pure & Appl. Chem. 1990, 62, 103.
4. Kwon, Y.-U.; Corbett, J. D., Department of Chemistry, Iowa State University, Ames, IA, unpublished research, 1990.
5. Sevov, S. C.; Corbett, J. D., Department of Chemistry, Iowa State University, Ames, IA, unpublished research, 1990.
6. Kwon, Y.-U.; Corbett, J. D. Chem. Mater. 1990, 2, 27.
7. Kwon, Y.-U.; Rzeznik, M. A.; Guloy, A.; Corbett, J. D. Chem. Mater. 1990, 2, 546.
8. Werner, P. E. TREOR-4. "Trial and Error Program for Indexing of Unknown Powder Patterns...", Department of Structural Chemistry, Arrhenius Laboratory, University of Stockholm, Sweden, 1984.
9. Krypyakevich, P. I.; Burnashova, V. V.; Markiv, V. Ya. Dopovidi Akad. Nauk. Ukrain. Ser. A. 1970, 32, 828.
10. Villars, P.; Calvert, L. D. "Pearson's Handbook of Crystallographic Data for Intermetallic Phases"; Amer. Soc. Metals: Metals Park, Ohio, 1985; Vol. 1, pp. 506, 559, 580.

11. TEXSAN, Version 5.0, Molecular Structure Corporation, The Woodlands, Texas, 1989.

12. Sheldrick, G. M., Universität Göttingen, FRG, 1986.

13. Garcia, E.; Corbett, J. D. Inorg. Chem. 1988, 27, 2353.

14. Aronsson, B.; Lundgren, G. Acta Chem. Scand. 1959, 13, 433.

15. Uraz, A. A.; Rundqvist, S. Acta Chem. Scand. 1970, 24, 1843.

16. Horyn, R.; Lukaszewicz, K. Bull. Acad. Polon. Sci., Ser. Sci. Chim. 1970, 18, 59.

17. Kjekshus, A.; Gronvold, F.; Thorbjornsen, J. Acta Chem. Scand. 1962, 16, 1493.

18. Pettifor, D. G. J. Phys. C: Solid State Phys. 1986, 19, 283.

19. Pettifor, D. G. Mater. Sci. Technol. 1988, 4, 675.

20. Pettifor, D. G. New Scientist 1986, May 29, p. 48.

21. Buschow, K. H. J. J. Less-Common Met. 1981, 79, 243.

22. Hughbanks, T.; Rosenthal, G.; Corbett, J. D. J. Am. Chem. Soc. 1988, 110, 1511.

23. Rundqvist, S.; Jellinek, F. Acta Chem. Scand. 1959, 13, 425.

24. Zachariasen, W. H. Acta Crystallogr. 1948, 1, 265.

25. Wells, A. F. Structural Inorganic Chemistry, 5th ed.; Clarendon Press: Oxford, 1984; p. 1262.

26. Tanner, L. E.; Levinson, D. W. Trans. Am. Soc. Met. 1960, 52, 1115.

27. Yang, T. Y.; Yu, G. P.; Chen, L. J. J. Nucl. Mat. 1987, 150, 67.

28. The reported[26] composition of the θ phase was incorrectly quoted in reference 27 in terms of weight fractions of the components.

29. Garcia, E.; Corbett, J. D. J. Solid State Chem. 1988, 73, 452.

30. Kim, S.-J.; Kematick, R. J.; Yi, S. S.; Franzen, H. F. J. Less-Common Met. 1988, 137, 55.

# FUTURE WORK

The research on the A15 phases is not complete and needs further study: the atomic ordering in $Zr_4Sn$ implied by the superlattice reflections may require an electron microscopic study, and the A15 phase in zirconium-lead system also requires further study of the stoichiometry and structure. Synthetic difficulties were the major obstacle in studying the Zr-Pb system, and a new approach would need to be devised. Some of the interstitial phases like $Zr_5Pb_3Z$, Z = Al, Sb and Te, and $Zr_5Sn_3Al$ may need repeat reactions to confirm the stoichiometries. The unattempted interstitials B-O in $Zr_5Pb_3$ host also need to be tried.

A preliminary study on the interstitial chemistry of $Zr_5In_3Z$ system yielded some promising results. The host has a lower number of conduction electrons and, therefore, the effect of the electron count on the interstitial chemistry can be further studied in addition to those of $Zr_5Sn_3$ and $Zr_5Sb_3$ hosts. However, this system is much different from the others because there is no $Zr_5In_3$ binary compound at all. A third interstitial element like Al, Ga, and Cu stabilizes the compound in a $Mn_5Si_3$-type structure.[34] This system may have an advantage of not having self-interstitial mixing. However, the zirconium-indium system itself has been poorly studied; the complete range is not covered even in the most recent phase diagram.[35] The reported binary phases ($Zr_3In$,[36] $Zr_2In$, ZrIn, $ZrIn_2$, and $ZrIn_3$[37]) were re-investigated in this study, but none of them was reproduced except one phase, $ZrIn_3$. Arc-

melting and annealing reactions at 1000°C of various compositions resulted in very suspicious powder patterns. A phase diagram study is recommended before starting anything.

The possibility of magnetic ordering of iron atoms in the $Zr_5Sn_{2+x}Fe_{1-x}$ seems very high because the iron-iron distance along the chain direction is only 2.7 Å and the separation between neighboring chains is 7-8 Å. Moreover, one of the solid solution extremes corresponds to $Zr_5Sn_2Fe$ stoichiometry in which the chains are all filled by iron atoms. A preliminary study of magnetic property done on $Zr_5Sn_{2.3}Fe_{0.7}$ sample showed that the signal was dominated by that of impurity $ZrFe_2$. However, there was an evidence of field dependent ordering at ~300°K. A synthesis has to be designed to eliminate the $ZrFe_2$ impurity in order to study this system's magnetic properties.

## REFERENCES


1. Schemel, J. H. "ASTM Manual on Zirconium and Hafnium"; ASTM-STP-639, 1977; p.20.
2. Saller, H. A. In "Nuclear Engineering Handbook"; Etherington, E. Ed.; McGraw-Hill: New York, 1958; Chapter 10.
3. Etherington, H.; Dalzell, R. C.; Lillie, D. W. In "Metallurgy of Zirconium"; Lustman, B.; Kerze, Jr., F. Ed.; McGraw-Hill: New York, 1955; Chapter 1.
4. Woo, O. T.; Carpenter, G. J. C. J. Nucl. Mater. 1988, 159, 397.
5. Yang, T. Y.; Yu, G. P.; Chen, L. J. J. Nucl. Mater. 1987, 150, 67.
6. McPherson, D. J.; Hansen, M. Trans. Amer. Soc. Met. 1953, 45, 915.
7. Rossteutscher, W.; Schubert, K. Z. Metallkde. 1965, 56, 813.
8. Williams, C. D.; Ells, C. E.; Dixon, P. R. Canad. Metal. Quart. 1972, 11, 257.
9. Conne, M. D.; Dorner, S.; Lupton, D. F. J. Nucl. Mater. 1986, 141-143, 369.
10. Nowotny, H.; Schachner, H. Monatsh. Chem. 1953, 84, 169.
11. Gran, G.; Andersson, S. Acta Chem. Scand. 1960, 14, 956.
12. Aronsson, B. Acta Chem. Scand. 1960, 14, 1414.
13. Kieffer, R.; Benesovsky, F.; Lux, B. Planseeberichte Pulvermetallurgie 1956, 4, 30.
14. Parthé, E.; Reiger, W. J. Dental Res. 1968, 47, 829.
15. Garcia, E.; Corbett, J. D. Inorg. Chem. 1988, 27, 2907.
16. Garcia, E.; Corbett, J. D. Inorg. Chem. 1990, 29, 3274.

17. Abriata, J. P.; Bolcich, J. C.; Arias, D. Bull. Alloy Phase Diag. 1983, 4, 147.

18. Holmber, B.; Dagerhamm, T. Acta Crystallogr. 1961, 15, 919.

19. Garcia, E., Ph.D. Dissertation, Iowa State University, Ames, Iowa, 1987.

20. Schäfer, H. "Chemical Transport Reactions" (English Translation), Academic Press: New York, 1965.

21. Emel'yanov, V. S.; Bystrov, P. D.; Evstyukhin, A. I. J. Atomic Energy U.S.S.R.,1 1956, No. 1, 43.

22. Hönle, W.; von Schnering, H. G.; Z. Kristallogr. 1980, 153, 339.

23. Clark, C. M.; Smith, D. K.; Johnson, G. J. "A FORTRAN IV Program for Calculating X-Ray Diffraction Patterns - Version V", Department of Geoscience, The Pennsylvania University: University Park, PA, 1973.

24. Werner, P. E. "TREOR-4 Trial and Error Program for Indexing of Unknown Powder Patterns", Department of Structural Chemistry, Arrhneus Laboratory, University of Stockholm: S-106 91 Stockholm, Sweden, 1984; p. 20.

25. Rietveld, H. M. J. Appl. Crystallogr. 1969, 2, 65.

26. TEXSAN: Single Crystal Structure Analysis Software, Version 5.0, Molecular Structure Corporation, The Woodlands, TX, 1989.

27. SDP User's Guide, Enraf-Nonius, Delft, Holland and B. A. Frenz & Associate, Inc., College State, TX, 1988.

28. Lapp, R. L.; Jacobson, R. A., U.S. Department of Energy Report IS-4708, Iowa State University, Ames, Iowa, 1979.

29. Powell, D. R.; Jacobson, R. A., U.S. Department of Energy Report IS-4737, Iowa State University, Ames, Iowa, 1980.

30. Karcher, B. A., Ph.D. Dissertation, Iowa State University, Ames, Iowa, 1984.

31. Sheldrick, G. M.; SHELXS-86, Programs for Structure Determination, Universität Göttingen, Germany, 1986.

32. International Tables for X-Ray Crystallography; Kynoch Press: Birmingham, England, 1968, Vol. III.

33. Walker, N.; Stuart, D. Acta Crystallogr. 1983, A39, 159.

34. Bularzik, J.; Kwon, Y.-U.; Corbett, J. D., Department of Chemistry, Iowa State University, Ames, IA, unpublished research, 1988.

35. Schunk, F. A. "Constitution of Binary Alloys"; 2nd ed.; McGraw-Hill: New York, 1969, p. 457.

36. Anderko, K. Z. Metallkd. 1958, 49, 165.

37. Raman, A.; Schubert, K. Z. Metallkd. 1965, 56, 44.

## ACKNOWLEDGEMENTS

The author wishes to thank Professor John D. Corbett for his guidance and encouragement; the lively lessons on chemistry and science from him is especially acknowledged.

Dr. Lee M. Daniels and Professor Robert A. Jacobson and his group members are thanked for the X-ray single crystal analysis facilities and many helpful discussions. Thanks are due to Professor Hugo F. Franzen for the arc-melting and induction furnaces and the powder diffractometer for Rietveld analysis.

The author also thanks Slavi C. Sevov for the operation of SEM/EDX instruments and his helpful discussions with the data interpretations; Arnold M. Guloy for the operations of the high-temperature furnace. Other group members, in the past and present, and Shirley Standley will be remembered for the warm and friendly atmosphere in the group.

Special thanks are to the author's parents who have raised and supported him. The author regrets that his grandmother is not thanked alive; however, her devotion to the author, especially during his childhood, will be remembered with thanks.

Finally, the author's wife Kyungseo Kim Kwon and his children O'chon and O'kyung are deeply thanked for their love and understanding.